Fabrication of Electrospun Fibrous Meshes and 3D Porous Titanium Scaffolds for Tissue Engineering

A Dissertation
Presented to
The Academic Faculty

by

Xiaokun Wang

In Partial Fulfillment
of the Requirements for the Degree
Doctor of Philosophy in the
Department of Biomedical Engineering
College of Engineering

Peking University/Georgia Institute of Techonology/EmoryUniversity
May, 2013

Fabrication of Electrospun Fibrous Meshes and 3D Porous Titanium Scaffolds for Tissue Engineering

Approved by:

Dr. Haifeng Chen, Advisor
Department of Biomedical Engineering
Peking University

Dr. Barbara D. Boyan Coadvisor
Department of Biomedical Engineering
Georgia Institute of Technology

Dr. Ying Luo
Department of Biomedical Engineering
Peking University

Dr. Zigang Ge
Department of Biomedical Engineering
Peking University

Dr. Jianzhong Xi
Department of Biomedical Engineering
Peking University

Dr. Xin Zhang
Peking University Third Hospital

Date Approved: May 2013

ACKNOWLEDGEMENTS

First, I would like to thank my advisors Dr. Haifeng Chen, Dr. Barbara D. Boyan and Dr. Zvi Schwartz. In 2007, I came to Dr. Haifeng Chen's lab and started my journey of biomedical engineering. In my first four years of PhD study, Dr. Chen has exposed me to many different perspectives of being a good researcher, like how to think and work independently, and be creative. When the GaTech/PKU/Emory joint program first started, Dr. Chen was so supportive. Thanks to his support and reference, I successfully went through the application and got enrolled in the program, which gave me the incredible experiences in the later life of my PhD. In 2011, I came to my second campus, Georgia Institute of Technology, joined Boyan/Schwartz lab for the final step of my PhD. It was a completely different environment. The support and encouragements from Dr. Boyan and Dr. Schwartz have given me more confidence on making further achievements in my research. Boyan/Schwartz lab is a highly collaborative lab filled with clinicians, engineers, chemists, and biologists. When I arrived, I would say that I was strictly a material engineer. Upon applying the many biological techniques in Boyan lab to my materials, I started to grasp the biological concepts. Besides the research, I also learned how to get organized on my research, how to properly interpret the data, thoroughly critique a paper, and more importantly, how to make a presentation and give a talk. For a student aiming for academia, Dr. Boyan is my role model, as a successful academic professor, a productive industry collaborator, an energetic team leader and a considerable mentor. I wish one day I could be like her, an outstanding researcher and an incredible stylist. Dr. Schwartz is the person who was involved in the design of the last experiment conducted in this thesis. I would also like to thank my thesis committee members. Dr. Luo, Dr. Ge, Dr. Xi, Dr. Zhang. I remembered when I did my thesis proposal, they had to stay up till 10:30pm with me because of the time difference.

I would also like to thank the members of Chen lab Boyan/Schwartz lab. They have been really helpful throughout the years. I would like to thank Song Yun, Yujing Yin, Ling Yin, Shize Liu, Yiqun Cong, they were with me when I was in Dr. Chen's lab, we set up the whole lab and share the precious moments together. Also thank Dr. Yingfang Ao's lab in Peking University Third Hospital. Dr. Zhenxing Shao and Dr. Jingxian Zhu, they helped me for most of the cell experiments in specific aim 1 and 2. Also I want to thank the members in Dr. Changyong Wang's lab in Academy of Military Medical Sciences, Miss Tong Hao who helped me in the alginate project. And I would like to thank Dr. Rolando Gittens in Boyan/Schwartz lab, the most important collaborator and a true friend. I would like to thank Jiaxuan Chen and Qingfen Pan, thank you so much for helping me in the beginning when I had difficulties communicating with people. Reyhaan Chaudhri, Alice Cheng and Shirae Leslie, thank you so much for editing "Xiaokun style" papers for me. Ms. Brentis Henderson, Shannon Sullivan, Sharon Hyzy in Atlanta, and Jialei Luo in Beijing have made the administration process and lab work so much easier. All of the Boyan laboratory graduate students have made my life here more enjoyable: Reyhaan Chaudhri, Chris Lee, Khairat El-Baradie, Chris Hermann, Rolando Gittens, Junghwa Park, Maryam Doroudi, Shirae Leslie, Qingfen Pan, Erin Hewitt, James Wade, Alice Cheng, Marcus Walker, and Henry Mei. Last but not least, I would like to thank Dr. Cheng Zhu and Dr. Shiyi Chen for setting up this great program. I would also like to thank my parents. They have always been there to support, motivate and comfort me. Without their help, I would not get to where I am today.

Table of Contents

List of Tables

List of Figures

Summary

Tissue and organ repair has been the ultimate goal of the surgery repair method. Tissue engineering is a multidisciplinary field that is rapidly emerging as a promising new approach for repair and regeneration of damaged tissue. In this approach, scaffolds which allow cells to invade the construct and guide the cells grow into specific tissue play a pivotal role. Therefore designing scaffolds favorable to cellular growth and maturation is of great importance. Electrospinning has gained popularity recently as a simple and versatile method to produce fibrous structures from polymers and ceramic precursors with nano- to microscale dimensions. These electrospun fibers have been extensively applied to create nanofiber scaffolds for cardiovascular, urologic and bone tissue engineering applications. Specifically for bone and cartilage tissue engineering, polymeric materials have some attractive properties such as the biodegradability. However, it is often necessary to functionalize the polymeric scaffold surfaces by grafting peptide (such as RGD) or bioactive ceramics (such as hydroxyapatite) to achieve better mechanical properties, better cell attachment or better biocompatibility. Ceramic scaffolds and implant coatings, such as hydroxyapatite and silica-based bioglass have also been considered as bone graft substitutes for bone repair because of their bioactivity and, in some cases, tunable resorbability. Commonly there is no need to functionalize ceramic surfaces with peptide to enhance the biocompatibility, and the physical parameters of ceramic scaffolds, such as surface structures and crystallizations can affect cell responses. Besides tissue engineering scaffolds, for clinical application, especially for load-bearing artificial implants, metallic materials such as titanium are the most commonly used material. Osseointegration refers to the direct structural and functional connection between living bone and the surface of a load-bearing artificial implant. To achieve better osseointegration between bone and the implant surface, rough surfaces have become current standard of clinical implants. Compared to rough surfaces, three dimensional porous

structures can provide enhanced fixation with bone by allowing tissue to grow into the pores. In this study, pre-3D electrospun polymer and ceramic scaffolds with peptide conjugation and 3D titanium scaffolds with different surface morphology were fabricated to testify the osteoblast and mensechymal stem cell attachment and differentiation. The ***overall goal*** of this thesis is to determine if the peptide functionalization of polymeric scaffolds and physical parameters of ceramic and metallic scaffold can promote osteoblast maturation and mesenchymal stem cell differentiation *in vitro* to achieve an optimal scaffold design for greater osseointegration. This overall goal was evaluated in **three specific aims**: (1) to determine if functionalized electrospun polymer meshes perform better than non-functionalized meshes with respect to mesenchymal stem cell (MSC) specific attachment; (2) to determine if crystallization, surface microstructure or nanostructure of electrospun ceramic scaffolds affects osteoblast maturation; (3) to determine if surface texture within 3D microenvironment affects osteoblast differentiation. The experimental approach to complete the study is to develop pre-3D electrospun meshes and 3D porous scaffolds and access differentiation of mensechymal stem cells and osteoblasts in vitro. The results of the studies showed with functionalization of MSC-specific peptide, polymer scaffolds behaved with higher biocompatibility and MSC affinity. For the ceramic and metallic scaffolds, microstructures and nanostructures can synergistically promote osteoblast maturation and 3D micro-environment with micro-roughness is an promising design for osteoblast maturation and MSC differentiation in vitro compared to 2D surfaces.

Chapter 1. Introduction

1.1 Biodegradable Polymers

Biodegradable polymers are those which degrade *in vitro* and *in vivo* into products that can be digested by metabolites or can be the products of metabolites. There are two kinds of biodegradable polymers, natural-derived polymer and synthetic polymer. Natural-derived polymer, such as collagen, has great biocompatibility and as structurally, they closely mimic native cellular environments. However, disadvantages such as the possibility of causing immunity reaction, unstable resources and relatively high cost, are also obvious. Synthetic polymers, on the other hand, offers attractive advantages, like high reproducibility, highly controllable molecular weight, controllable degradation time and good mechanical properties. Poly(glacolic-lactic acid) (PLGA) and poly(caprolactone) (PCL) are most commonly used biodegradable polymers in bone and cartilage tissue engineering.

1.2 Electrospinning

There are several methods to fabricate ECM-like porous structures, such as template [1], self-assemble [2,3], phase separation [4,5], salt-leaching [6] and electrospinning [6-8]. Electrospinning is a relatively easy and fast process to produce nanofibers. Although the first patent on electrospinning technique was published as early as in 1934[9], this technique has not been well established until recent times [10-12]. Technically, electrospinning is a process that uses a strong electric field to draw a polymer fluid into fine linear fiber [13,14]. The basic electrospinning set up is shown in **Figure 1-1**, which consists of a nozzle, a high voltage power supply, a container for polymer fluid and an electrode collector. When a viscous fluid is charged with a high voltage, the electrostatic force draws the fluid into liquid jet. Because of the interaction between the jet and external electric field and charge repulsion inside the jet, the charged jet undergoes a bending or whipping instability to stretch it thinner.

Solvent evaporation from the filaments results in solid fibers. In most cases, the as-spun fibers deposit randomly on the electrode collector forming a non-woven nanofiber mat.

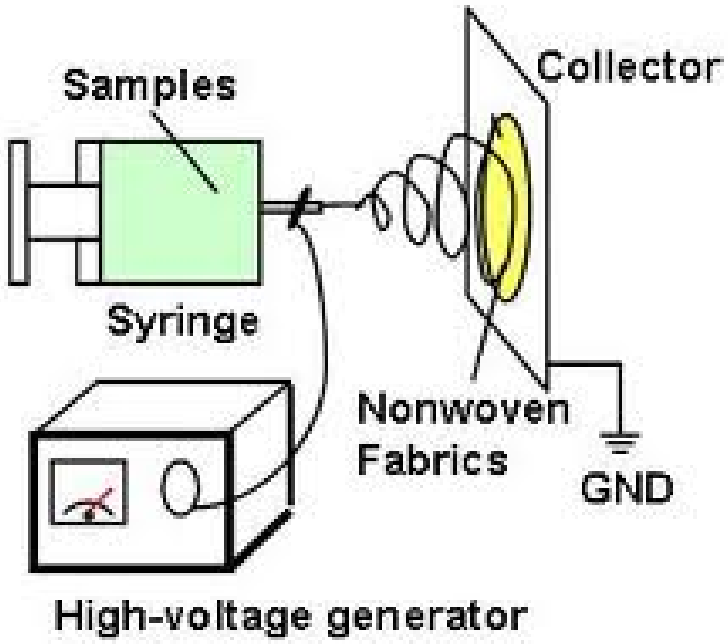

Figure 1-1. Setup of electrospinning www.zeably.com/Electrospinning

Previous studies have been made to apply electrospun fibrous scaffolds to bone tissue engineering [15,16]. Most of the electrospun scaffolds are made of polymers or composite, and some studies are also focused on ceramic scaffolds [17,18]. Electrospun scaffolds have also been made using a composite of synthetic and natural polymers to take advantage of the mechanical properties of the former and the biological performance of the latter [19,20]. An attractive property of organic polymers is that they can be resorbed by the body and fully replaced by the native tissue [15,16]. These organic polymers can also provide surfaces for cell attachment and growth, but it is often necessary to be functionalized, specifically for bone applications, with osteogenic molecules such as hydroxyapatite [21,22] and growth factors like bone morphogenic proteins [23] to promote cell differentiation. Electrospun fibrous scaffolds are widely used for soft tissue and hard tissue engineering. C.M Vaz *et al.* [24] fabricated PCL/PLA bilayer tube-shaped scaffold and cultured 3T3 fiberblast cells. Cell

s can spread and proliferate well on the fibrous scaffold. The results showed the potential of electrospun scaffold for blood vessel engineering. For hard tissue application, polymers together with ceramic nanoparticles form composite materials, which have been used the most. H. Yoshimoto *et al.* [16] used pure PCL fiber meshes as mesenchymal stem cell scaffolds. 4 weeks after culture in osteogenic media, mineralization and type I collagen were observed. Lihong Lao *et al.* [25] use PLGA as polymer matrix and nanosized hydroxyapatite were used as ceramic filler to enhance mechanical property and osteogenic property. Similar method is used by Chunmei Li *et al.* [23], they fabricated silk fibroin fiber scaffolds containing bone morphogenetic protein 2 and nanoparticles of hydroxyapatite for bone formation from human marrow-derived mesenchymal stem cells. In my first study, we constructed polycaprolactone (PCL) electrospun meshes by optimizing the polymer solution concentration. PCL electrospun fibers were further modified by mixing with HA nanoparticle or conjugating with functional peptide to promote the biocompatibility of PCL fibers. The peptide is considered as MSCs-homing peptide, which was identified by phage display by Dr. Shao in Peking University Third Hospital. The peptide was covalently conjugated to PCL meshes to construct a "MSCs-homing device" for bone tissue engineering repair.

1.3 Titania and Silica-based Bioceramics

Ceramic scaffolds have been considered as bone graft substitutes for bone repair because of their excellent biocompatible and bioactive properties, with calcium-based chemistries such as hydroxyapatite [18] and β-tricalcium phosphate [26] commonly used because of their bioactivity and, in some cases, tunable resorbability [27]. Studies using solid substrate surfaces show that cell differentiation is sensitive to microscale and nanoscale topography [28–30]. When osteoblasts or mesenchymal stem cells are cultured on titanium substrates, which have an inherent TiO_2 ceramic layer on the surface, they exhibit enhanced osteoblastic differentiation, particularly if the surface has both microscale and nanoscale features [31–33].

It is well known that titanium makes a practical implant material because of its good mechanical properties and biocompatible oxide layer, titania. Although not bioresorbable, TiO_2 could serve as an attractive substrate for bone tissue engineering due to its good biological performance. Similar to titania, silica-containing bioglass products also have beneficial osteoconductive functions. In general, the titania-silica binary materials are widely studied as implant coating [34-36], and the fibrous titania-silica ceramic are mainly used in the field of catalyst and fuel cell area [37-39]. Some researches has showed electrospun silica nanofibers have the osteoconductive potentials and the effects of surface structure on MG63 osteoblast-like cells were also discussed [15]. In fact, surface roughness not only is affected by the fiber diameter, but also by the degree of crystallization and morphology of the fibers. Previous study showed different content of silica in the titania-silica binary materials has influence on crystal phase of titania-silica nanoparticals [39]. With the existence of silica, the degree of crystal of titania particles significantly decreased under the same sinter temperature. The purpose of my second study was to assess the contributions of nanofiber dimensions and microscale pattern on cell response. To do this, pure TiO_2 and silica-titania binary nanofiber meshes were fabricated using electrospinning to have different surface microroughness and nanofiber diameters.

1.4 Porous Metals

Most materials used for implants in dental and orthopedic applications are metallic, commonly Ti and its alloys, because of their mechanical properties (*e.g.,* weight-to-strength ratio) and good biological performance. Bone integration of metal implants is critical for successful bone regeneration and healing in dental and orthopedic applications. To enhance the bone integration, microroughness has become standard feature required for advanced osteogenic responses, also nanofeatured titanium surfaces increased ALP activity and the upregulated gene expression of the bone-related proteins. Comparing to the surface

modification, 3D porous Ti scaffold (**Figure 1-2**) allows for bone to grow into the component providing enhanced fixation and produces a system which enables stresses to be transferred from the implant to the bone.

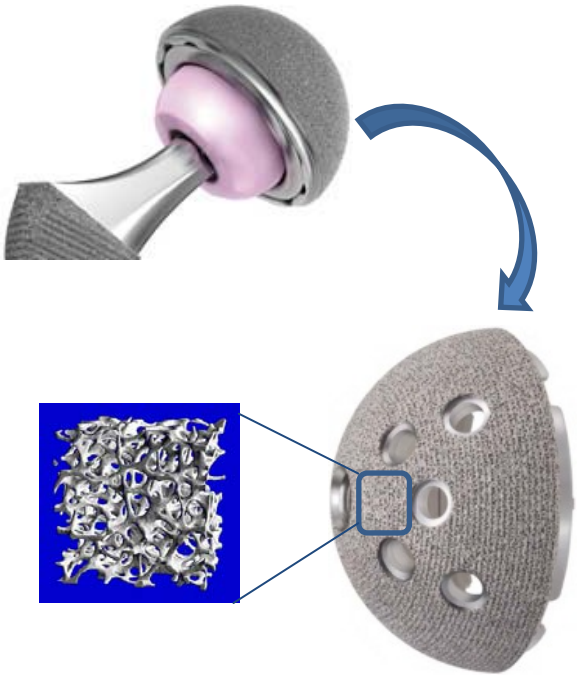

Figure 1-2. Commercially available trabecular bone implant. Zimmer Technology

Numerous investigations into porous materials initiated in the early 1970s, including polymers, ceramics and metals. Although ceramics have great biocompatibility as we mentioned before, the disadvantages such as poor mechanical properties limit the applications of porous ceramic materials for load bearing implants. Porous metals are still required by orthopaedic load bearing applications. Porous metal fabrication started in 1930's, and biomedical application of porous metal started in the late 1960's and early 70's. Gakabte *et al*. [40] pioneered the development of fiber-metal leading to its clinical use as a porous coating in hip and knee arthroplasty. In the last two decades, a variety of porous coatings and materials have also been used to obtain biological fixation of bone with metal implants in load-bearing implants. The most common metallic materials include sintered Ti and CoCrMo alloy beads, diffusion-bonded Ti, fiber metal and plasma-sprayed Ti [40-43]. Recently, a new series of highly porous metals have been developed and applied in orthopeadic surgery, such

as porous tantalum and titanium foams made by different techniques [44].

Clinical and histological evidence from retrieved implants clearly demonstrate that these porous surfaces enhance bone tissue in-growth and are effective in supplementing the stability of the implant by biological fixation [45]. Boblyn *et al.* [46] used highly porous tantalum as implants and carried in vivo study in dogs to characterize the mechanical property and bone ingrowth between bone and porous implants. And the results show the filling of the pores of the implants with new bone increased from 13% at two week to 42~53% at 4 weeks. V.K. Balla *et al.* [47] also used porous tantalum structures to study the in vitro biological properties. Human fetal osteoblast cell line was used for the cell viability and proliferation assay. Although there are some studies as we mentioned previously are focused on the fabrication of porous metal implants and the influence of the implants on cells, the mechanism of and detailed behavior including the osteodifferentiation marker expression of osteoblast or mesenchymal stem cells on 3D porous scaffold is not well investigated. In the part 3 of my thesis, we will systematically study the osteoblast cell and mesenchymal stem cell responses on 3D titanium scaffolds.

1.5 Thesis Objective

The decade from 2001 to 2011 has been termed the ‘‘bone and joint decade’’, because it has been recognized that musculoskeletal injuries are the most reported health condition in the USA, with an associated cost close to 8% of the US gross domestic product in lost wages and healthcare-related costs [48]. More than 25% of musculoskeletal injuries involve bone fractures, with many of these fractures not being able to heal by themselves, thus requiring some type of bone void filler that can promote bone regeneration and reduce the healing time for the patient. With an aging population in developed countries and statistics showing, for example, that one in every two women over 50 years old will suffer an osteoporotic bone fracture [49], there is a pressing need to find reliable bone repair materials. Tissue

engineering offers a promising approach for repair and regeneration of damaged human tissue. A common methodology for bone tissue engineering is the fabrication of three-dimensional (3-D) porous scaffolds using biodegradable polymers, biocompatible ceramics or metals.

The overall goal of this thesis is to understand if the surface chemical functionalization of polymeric scaffolds and physical parameters of ceramic and metallic scaffolds can promote osteoblast maturation and mesenchymal stem cell differentiation *in vitro* to achieve an optimal scaffold design for greater osseointegration. The thesis includes three aims. The first aim is to determine if functionalized electrospun polymer meshes perform better than non-functionalized meshes with respect to mesenchymal stem cell (MSC) specific attachment. In this aim, we hypothesize functionalized bioactive PCL fiber meshes with MSC-adhesion specific peptide will promote attachment and spreading of MSCs *in vitro* and extracting MSCs *in vivo*. To investigate this hypothesis, electrospinning of polymer solution was established and a peptide sequence (E7) with seven amino acids which has specific affinity to bone marrow-derived MSCs was covalently conjugated onto polycaprolactone (PCL) electrospun meshes to construct a 'MSCs-homing device' for in situ cartilage regeneration [50]. The effectiveness of covalently conjugation was characterized and in vivo and in vitro studies were carried on cartilage regeneration.

The second aim is to determine if crystallization, surface microstructure or nanostructure of electrospun ceramic scaffolds affects osteoblast maturation. In this aim, we hypothesize that nanofiber morphology and micropatterns of ceramic meshes can synergistically promote osteoblast maturation and MSC differentiation. Electrospun titania and titania-silica fiber meshes were fabricated by electrospinning and the factors which may influence the fiber morphology were optimized. MG63 osteoblast-like cells and MSCs were seeded on the different fibrous meshes, and were assayed for cell number, cell differentiation markers as well as local growth factors to evaluate the osteogenic effects of the different ceramic meshes.

In the first two studies, we focused on the electrospinning fibrous meshes. Although the electrospun fiber meshes are considered "3D" in terms of interconnected porous structures, the pores are still too small for cells to migrate into the pores. So we continued to study the real 3D structure, with pores large enough for cells to migrate. Based on the results of my previous two studies, the third aim is to determine if surface texture within 3D microenvironment affects osteoblast differentiation. In this aim, we hypothesize that 3D porous Ti structures with enhanced surface roughness are optimal for osteoblast maturation and MSC differentiation in vitro comparing to 2D surfaces. 3D titanium scaffolds with pore size of 150μm were made from titanium meshes. MG63 cells, human osteoblast cells and MSCs were seeded onto the scaffolds and assayed for cell number, cell differentiation markers as well as local growth factors to evaluate the osteogenic effects.

In all, this thesis evaluated the effects of functionalized and bioactive scaffolds with different chemical or physical parameters on osteoblast maturation and MSC osteo-differentiation *in vitro* and created some favorable designs for tissue engineering scaffolds.

1.6 References

1. Matsusaki, M., H. Yoshida, and M. Akashi, The construction of 3D-engineered tissues composed of cells and extracellular matrices by hydrogel template approach. Biomaterials, 2007. **28**(17): p. 2729-2737.
2. Gelain, F., D. Bottai, A. Vescovi, and S. Zhang, Designer Self-Assembling Peptide Nanofiber Scaffolds for Adult Mouse Neural Stem Cell 3-Dimensional Cultures. PLoS ONE, 2006. **1**(1): p. e119.
3. Sieminski, A., A. Was, G. Kim, H. Gong, and R. Kamm, The Stiffness of Three-dimensional Ionic Self-assembling Peptide Gels Affects the Extent of Capillary-like Network Formation. Cell Biochemistry and Biophysics, 2007. **49**(2): p. 73-83.
4. Cai, Q., J. Yang, J. Bei, and S. Wang, A novel porous cells scaffold made of polylactide–dextran blend by combining phase-separation and particle-leaching techniques. Biomaterials, 2002. **23**(23): p. 4483-4492.
5. Hua, F.J., T.G. Park, and D.S. Lee, A facile preparation of highly interconnected macroporous poly(d,l-lactic acid-co-glycolic acid) (PLGA) scaffolds by liquid–liquid phase separation of a PLGA–dioxane–water ternary system. Polymer, 2003. **44**(6): p. 1911-1920.
6. Kim, T.G., H.J. Chung, and T.G. Park, Macroporous and nanofibrous hyaluronic acid/collagen hybrid scaffold fabricated by concurrent electrospinning and deposition/leaching of salt particles. Acta Biomaterialia, 2008. **4**(6): p. 1611-1619.
7. Il Keun Kwon, Satoru Kidoaki, Takehisa Matsuda, Electrospun nano- to microfiber fabrics made of biodegradable copolyesters: structural characteristics, mechanical properties and cell adhesion potential, Biomaterials, 2005;26(18):3929-2939
8. F. Yang, R. Murugan, S. Wang, S. Ramakrishna. Electrospinning of nano/micro scale poly(L-lactic acid) aligned fibers and their potential in neural tissue engineering, Biomaterials, 2005, 26(15):2603-2610
9. Formhals A. US Patent 1,975,504, 1934.
10. Bognitzki, M., W. Czado, T. Frese, A. Schaper, M. Hellwig, M. Steinhart, A. Greiner, and J.H. Wendorff, Nanostructured Fibers via Electrospinning. Advanced Materials, 2001. **13**(1): p. 70-72.
11. Huang ZM, Zhang YZ, Kotaki M, Ramakrishna S. A review on polymer nanofibers by electrospinning and their applications in nanocomposites. Compos Sci Technol 2003;63:2223–53.
12. Yu, J.H., S.V. Fridrikh, and G.C. Rutledge, Production of Submicrometer Diameter Fibers by Two-Fluid Electrospinning. Advanced Materials, 2004. **16**(17): p. 1562-1566.
13. Zong, X., K. Kim, D. Fang, S. Ran, B.S. Hsiao, and B. Chu, Structure and process relationship of electrospun bioabsorbable nanofiber membranes. Polymer, 2002. **43**(16): p. 4403-4412.
14. Shin, Y.M., M.M. Hohman, M.P. Brenner, and G.C. Rutledge, Experimental characterization of electrospinning: the electrically forced jet and instabilities. Polymer, 2001. **42**(25): p. 09955-09967.

15. Bhattarai, S.R., N. Bhattarai, H.K. Yi, P.H. Hwang, D.I. Cha, and H.Y. Kim, Novel biodegradable electrospun membrane: scaffold for tissue engineering. Biomaterials, 2004. **25**(13): p. 2595-2602.
16. Yoshimoto, H., Y.M. Shin, H. Terai, and J.P. Vacanti, A biodegradable nanofiber scaffold by electrospinning and its potential for bone tissue engineering. Biomaterials, 2003. **24**(12): p. 2077-2082.
17. Sakai, S., Y. Yamada, T. Yamaguchi, and K. Kawakami, Prospective use of electrospun ultra-fine silicate fibers for bone tissue engineering. Biotechnology Journal, 2006. **1**(9): p. 958-962.
18. Wu, Y., L.L. Hench, J. Du, K.-L. Choy, and J. Guo, Preparation of Hydroxyapatite Fibers by Electrospinning Technique. Journal of the American Ceramic Society, 2004. **87**(10): p. 1988-1991.
19. Venugopal, J.R., S. Low, A.T. Choon, A.B. Kumar, and S. Ramakrishna, Nanobioengineered Electrospun Composite Nanofibers and Osteoblasts for Bone Regeneration. Artificial Organs, 2008. **32**(5): p. 388-397.
20. Wutticharoenmongkol, P., N. Sanchavanakit, P. Pavasant, and P. Supaphol, Preparation and Characterization of Novel Bone Scaffolds Based on Electrospun Polycaprolactone Fibers Filled with Nanoparticles. Macromolecular Bioscience, 2006. **6**(1): p. 70-77.
21. Sui, G., X. Yang, F. Mei, X. Hu, G. Chen, X. Deng, and S. Ryu, Poly-L-lactic acid/hydroxyapatite hybrid membrane for bone tissue regeneration. Journal of Biomedical Materials Research Part A, 2007. **82A**(2): p. 445-454.
22. Venugopal, J., S. Low, A. Choon, T. Sampath Kumar, and S. Ramakrishna, Mineralization of osteoblasts with electrospun collagen/hydroxyapatite nanofibers. Journal of Materials Science: Materials in Medicine, 2008. **19**(5): p. 2039-2046.
23. Li, C., C. Vepari, H.-J. Jin, H.J. Kim, and D.L. Kaplan, Electrospun silk-BMP-2 scaffolds for bone tissue engineering. Biomaterials, 2006. **27**(16): p. 3115-3124.
24. Vaz, C.M., S. van Tuijl, C.V.C. Bouten, and F.P.T. Baaijens, Design of scaffolds for blood vessel tissue engineering using a multi-layering electrospinning technique. Acta Biomaterialia, 2005. **1**(5): p. 575-582.
25. Lao, L., Y. Wang, Y. Zhu, Y. Zhang, and C. Gao, Poly(lactide-co-glycolide)/hydroxyapatite nanofibrous scaffolds fabricated by electrospinning for bone tissue engineering. Journal of Materials Science: Materials in Medicine, 2011. **22**(8): p. 1873-1884.
26. Kasten, P., R. Luginbühl, M. van Griensven, T. Barkhausen, C. Krettek, M. Bohner, and U. Bosch, Comparison of human bone marrow stromal cells seeded on calcium-deficient hydroxyapatite, β-tricalcium phosphate and demineralized bone matrix. Biomaterials, 2003. **24**(15): p. 2593-2603.
27. Matsushita, N., H. Terai, T. Okada, K. Nozaki, H. Inoue, S. Miyamoto, and K. Takaoka, A new bone-inducing biodegradable porous β-tricalcium phosphate. Journal of Biomedical Materials Research Part A, 2004. **70A**(3): p. 450-458.
28. Yim, E.K.F., S.W. Pang, and K.W. Leong, Synthetic nanostructures inducing differentiation of human mesenchymal stem cells into neuronal lineage. Experimental Cell Research, 2007. **313**(9): p. 1820-1829.

29. Charest, J.L., A.J. García, and W.P. King, Myoblast alignment and differentiation on cell culture substrates with microscale topography and model chemistries. Biomaterials, 2007. **28**(13): p. 2202-2210.
30. Zinger, O., K. Anselme, A. Denzer, P. Habersetzer, M. Wieland, J. Jeanfils, P. Hardouin, and D. Landolt, Time-dependent morphology and adhesion of osteoblastic cells on titanium model surfaces featuring scale-resolved topography. Biomaterials, 2004. **25**(14): p. 2695-2711.
31. Martin, J.Y., Z. Schwartz, T.W. Hummert, D.M. Schraub, J. Simpson, J. Lankford, D.D. Dean, D.L. Cochran, and B.D. Boyan, Effect of titanium surface roughness on proliferation, differentiation, and protein synthesis of human osteoblast-like cells (MG63). Journal of Biomedical Materials Research, 1995. **29**(3): p. 389-401.
32. Lincks, J., B.D. Boyan, C.R. Blanchard, C.H. Lohmann, Y. Liu, D.L. Cochran, D.D. Dean, and Z. Schwartz, Response of MG63 osteoblast-like cells to titanium and titanium alloy is dependent on surface roughness and composition. Biomaterials, 1998. **19**(23): p. 2219-2232.
33. Bucci-Sabattini, V., C. Cassinelli, P.G. Coelho, A. Minnici, A. Trani, and D.M.D. Ehrenfest, Effect of titanium implant surface nanoroughness and calcium phosphate low impregnation on bone cell activity in vitro. Oral Surgery, Oral Medicine, Oral Pathology, Oral Radiology, and Endodontology, 2010. **109**(2): p. 217-224.
34. Young-Mi Kang a, Kyoung-Hwa Kim b, Yang-Jo Seol b, Sang-Hoon Rhee Evaluations of osteogenic and osteoconductive properties of a non-woven silica gel fabric made by the electrospinning method, Acta Biomaterialia 2009, 5: 462-469
35. Li P., Ohtsuki C., Kokubo T., Nakanishi K., Soga N., Groot K. The role of hydrated silica, titania, and alumina in inducing apatite on implants. Journal of Biomedical Materials Research 1994, 28, 1: 7-15
36. Dieudonn S.C., Dolder J., Ruijter J.E., Paldan H., Peltola T., van't Hof M.A., Happonen R.P., Jansen J.A. Osteoblast differentiation of bone marrow stromal cells cultured on silica gel and sol–gel-derived titania. Biomaterials. 2002, 23,14: 3041-3051
37. Kim P., Kim H., Joo J., Kim W., Song I.K., Yi J. Preparation and application of nanoporous carbon templated by silica particle for use as a catalyst support for direct methanol fuel cell. Journal of Power Sources 2005, 145, 2: 139-146
38. Ann M. Diskin, Robert H. Cunningham, R.Mark Ormerod The oxidative chemistry of methane over supported nickel catalysts. Catalysis Today. 1998, 46:147-154
39. Baglio V., Blasi A., AricòA. S., Antonucci V., Antonucci P.L., Trakanprapai C. , Esposito V., Licoccia S., and Traversa E. Composite Mesoporous Titania Nafion-Based Membranes for Direct Methanol Fuel Cell Operation at High TemperatureJ. Electrochem. Soc., 2005, 152, 7: A1373-A1377
40. Chang H., Kim S.H., Jang H.D., Cho S.W., Effect of SiO2 nanoparticles on the phase transformation of TiO2 in micron-sized porous TiO2–SiO2 mixed particles. Materials Letters. 2011, 65: 3272–3274 [57] Galante, J. and W. Rostoker, Fiber metal composites in the fixation of skeletal prosthesis. Journal of Biomedical Materials Research, 1973. 7(3): p. 43-61.

41. Georgette, F.S. and J.A. Davidson, The effect of HIPing on the fatigue and tensile strength of a cast, porous-coated Co Cr Mo alloy. Journal of Biomedical Materials Research, 1986. 20(8): p. 1229-1248.
42. He, P., J.C. Feng, B.G. Zhang, and Y.Y. Qian, Microstructure and strength of diffusion-bonded joints of TiAl base alloy to steel. Materials Characterization, 2002. 48(5): p. 401-406.
43. Zheng, X., M. Huang, and C. Ding, Bond strength of plasma-sprayed hydroxyapatite/Ti composite coatings. Biomaterials, 2000. 21(8): p. 841-849.
44. Levine, B., A New Era in Porous Metals: Applications in Orthopaedics. Advanced Engineering Materials, 2008. 10(9): p. 788-792.
45. Clemow, A.J.T., A.M. Weinstein, J.J. Klawitter, J. Koeneman, and J. Anderson, Interface mechanics of porous titanium implants. Journal of Biomedical Materials Research, 1981. 15(1): p. 73-82.
46. Bobyn, J.D., G.J. Stackpool, S.A. Hacking, M. Tanzer, and J.J. Krygier, Characteristics of bone ingrowth and interface mechanics of a new porous tantalum biomaterial. Journal of Bone & Joint Surgery, British Volume, 1999. 81-B(5): p. 907-914.
47. Balla, V.K., S. Bodhak, S. Bose, and A. Bandyopadhyay, Porous tantalum structures for bone implants: Fabrication, mechanical and in vitro biological properties. Acta Biomaterialia, 2010. 6(8): p. 3349-3359.
48. Jacobs JJ, Andersson GBJ, Bell JE, Weinstein SL, Dormans JP, Gnatz SM, et al. The burden of musculoskeletal diseases in the United States. Rosemont, IL: AAOS; 2008.
49. Agrawal CM, Attawia M, Borden MD, Boyan BD, Bruder SP, Bucholz RW, et al. Bone graft substitutes. Rosemont, IL: ASTM–AAOS; 2003.
50. Shao, Z., X. Zhang, Y. Pi, X. Wang**,** Z. Jia, J. Zhu, L. Dai, W. Chen, L. Yin, H. Chen, C. Zhou, and Y. Ao, A MSC Homing Device Fabricated by Polycaprolactone Electrospun Mesh Conjugated with a MSC affinity, Biomaterials, 2012. **33**(12): p. 3375-3387

Chapter 2. Fabrication of Hydroxyapatite Nanoparticles and Functional Peptide Modified Polycaprolactone Electrospun Meshes and Thermal Polymerized Alginate Hydrogels

2.1 Fabrication of Pure PCL, PCL/HA Composite and Functional Peptide Modified Nanofibers

2.1.1 Introduction

Tissue engineering has been considered as a successful approach in multiple clinical applications [1-4]. There are three major components which are crucial for tissue engineering, including the development of a biocompatible scaffold, living cells, and/or bioactive molecules. These parameters form a construct system that promotes tissues repair and regeneration [5].Biodegradable polymers are considered to be an ideal choice for scaffolds. For bone repair and regeneration, PCL, which has been approved by the United States Food and Drug Administration (FDA) in many medical applications, has been widely used for biomaterial and biomedical applications because of its slow degradability, good biocompatibility, and superior rheological and viscoelastic properties [6, 7]. The design and preparation of nanoscale fine structures have attracted great attention because of their potential unique properties and applications. The electrospinning technique has been reported to be a simple and versatile method to produce fibrous structure with nanoscale to microscale dimensions from synthetic and natural polymers [8-13]. This technique allows for the production of polymer fibers with diameters varying from 3 nm to greater than 5μm. Potential applications of electrospinning include filtration membranes, catalytic nanofibers, fiber-based sensors, and tissue engineering scaffolds [14-22]. One attractive feature of electrospinning is the simplicity and inexpensive nature of the setup; the typical electrospinning setup consists of a syringe pump, a high voltage source, and a collector. During the electrospinning process, a polymer solution is held at a needle tip by surface tension. The application of an electric

field using the high-voltage source causes charge to be induced within the polymer, resulting in charge repulsion within the solution. This electrostatic force opposes the surface tension; eventually, the charge repulsion overcomes the surface tension, causing the initiation of a jet. As this jet travels, the solvent evaporates and an appropriate collector can be used to capture the polymer fiber. There are different parameters which influence electrospinning process, as-prepared fiber diameter and morphology, including voltage, solution concentration, solvent polarity, feeding rate, tip-collector distance and collector morphology. In this study, we focused on the influences of solution concentration, solvent polarity and collector morphology on the electrospun polymer fiber morphology.

Electrospinning technique was first applied to polymer fiber fabrication, and the biodegradable fibers are widely used as tissue engineering scaffolds. However, pure polymer fibers are not favorable for cells to attach or differentiate, so functionalization by bioglass or peptide is needed. Hydroxyapatite (HA) is among the family of calcium phosphate-based bioceramics [23, 24]. Due to its nontoxicity, bioactivity and osteoconductivity, and similarity of its chemical and crystalline structures as the nature bone minerals [25, 26], the HA particles are also frequently applied solely or as a major component of the bone repair biomaterials. The nano-sized HA can improve the mechanical properties and support calcium and phosphate delivery after implantation as well. Therefore, incorporation of the nano-HA into polymer matrix is assumed to mimic the nature bone structure as well as enhance cell growth and response [27, 28]. Together with the advantages of synthetic biopolymers, compounding of the biopolymers and HA is one of the supreme methods for obtaining bone tissue engineering scaffolds [29-33].

In addition to the polymer/bioceramic composite, the use of adhesive peptides to modify polymer scaffolds is also a major method to promote the biocompatibility of pure polymer scaffolds. Arginine-glycine-aspartic acid (RGD), a peptide derived from fibronectin in the

extracellular matrix (ECM), is best known for cell adhesion on synthetic material surfaces [34-36]. However, this peptide lacks specificity for the general existence of fibronetin in all cells. In this study, a seven amino-acid peptide was identified by phage-display, which has the specific affinity to mensechymal stem cells (MSCs). MSCs are multi-potential cells that can differentiate into bone, cartilage, fat, muscle, marrow stroma, and other tissue types when induced by the appropriate biological cues in vitro and in vivo. MSCs are considered to be the first choice for repairing the site of tissue damage [37-45]. However, due to the complicated environment in vivo, the inability to target MSCs in tissues of interest with high specificity has become a barrier for stem cell therapies [46-49]. The low efficiency and engraftment problems of MSCs become more acute in endogenous stem cell-based therapies [50]. In this study, hydroxyapatite nanocrystals were used as filler and different surfactant were used to optimize the distribution of HA particles. Beside HA nanoparticles, the microstructures of the PCL meshes were controlled by adjusting the solvent composition and collector morphology and PCL meshes were modified with the affinity peptide of MSCs and MSC attachment and early stage proliferation were also investigated.

2.1.2 Materials and Methods

PCL was obtained from Polysciences incorporation. Hydroxyapatite nanoparticles with diameter of 200nm were obtained from Alfa Aesar. Methylene dichloride and cetyltrimethyl ammonium bromide were provided by Beijing Chemical (Beijing, China).

Fabrication of the PCL meshes

PCL was dissolved in 1ml methylene dichloride to form 0.08~0.30 g/ml concentration. In the typical electrospinning setup, 1ml PCL solution with different concentrations were loaded in glass syringe, the feeding speed is 0.4ml/h, the collection distance was 10cm and the applied voltage was 8kV. The electrospun fibers were collected on the flat plate.

For the composite fiber fabrication, 0.05g Span-80 or CTAB powder was added in 2ml methylene dichloride, followed by adding 0.5g HA power in the solution. The suspension was sonicated for 15min to disperse the hydroxyapatite, into which 4.0 g PCL was added. The mixture was further magnetically stirred for 15 min, followed by ultrasonication for another 15 min to obtain the well-mixed PCL/HA suspension with a PCL concentration of 20%. And the mixture was electrospun using typical procedure described before. The fiber morphology was observed by SEM (Hitachi S-4800).

Based on the different applications, three different types of PCL meshes are being fabricated using electrospinning in this study. Thick, non-woven PCL fibrous meshes were prepared from a 0.2g/ml PCL solution. In a typical procedure, 2 g of PCL (MW 43,000 to 50,000) was dissolved in 10 mL of CH_2Cl_2. After stirring for 3 h until PCL was completely dissolved, 1 mL of the solution was loaded into a glass syringe with a blunt-ended stainless steel needle. The feeding rate, collection distance, and applied voltage were controlled at 0.5 mL/h, 10 cm, and 8 kV, respectively. The electrospun fibers were collected on a flat plate covered by aluminum foil. For the lattice-patterned PCL meshes used in the study of cell adhesion, the same PCL solution was used for electrospinning, whereas the copper mesh was used as a collector for the PCL fiber mesh to have a lattice pattern. In addition, aligned fibers with low porous density and thin fiber diameter were fabricated by using CF_3OH as solvent and rolling tube, with the rotation speed of 2000rps, as the collector.

Peptide conjugation with PCL meshes and characteristics

All peptides were provided by Peking University Third Hospital. To briefly describe the synthesis of the peptide, a specific peptide was marked as E7, which was identified in the hMSC-affinity clones and designed by Institute of Sports Medicine, Peking University Third Hospital. A peptide with the same amino acids as E7 but different sequences was used as the negative control and marked as M7. The commonly used cell affinity peptide, comprising

three amino acids RGD (arginine, glycine, and aspartic acid), was used as the positive control. All the peptides were designed to have an extra cysteine linked to the carboxyl (C) terminus of all peptides to facilitate PCL polymer conjugation and fluorescein- 5-isothiocyanate (FITC) (Fanbo Biochemicals Co., Ltd., Beijing, China) labeling. Peptides were stored in -20℃ and dissolved in DMSO to yield a 2 mg/mL concentration before usage.

The PCL meshes were immersed into a 10% w/v solution of 1,6-hexanediamine (Sigma, St. Louis, MO, USA) prepared in isopropanol at 37℃ for 1 h. After the exposure, the PCL meshes were thoroughly washed in ultrapure water and dried under vacuum at room temperature. For the conjugation of E7 (EPLQLKM), M7 (MLKPLEQ), and RGD peptides to the surface of the aminated PCL meshes, the aminated PCL meshes were washed thrice with activation buffer (0.1 M PBS containing 0.15 M NaCl, pH 7.2) before treatment, and sulfosuccinimidyl-4-(N-maleimidomethyl)cyclohexane-1-carboxylate (sulfo-SMCC) (Thermo FisherScientific Inc., Rockford, IL, USA) was used as a crosslinker. A total of 500 mL (2 mg/ mL) sulfo-SMCC solution was added onto the aminated PCL meshes, incubated for 1 h at room temperature, and washed with conjugation buffer (activation buffer containing 0.1 M EDTA, pH 7.0). The peptides were dissolved in conjugation buffer at a concentration of 0.1 mM. Up to 500 mL of the peptide solution was applied onto the sulfo-SMCC-treated PCL scaffold and incubated overnight at 4 ℃. The peptide conjugated PCL meshes were thoroughly washed thrice with ultrapure water, and dried under vacuum at room temperature. After the conjugation, the meshes were observed under a scanning electron microscope (SEM) and a confocal microscope. The peptide surface density/amount and the homogeneity of the immobilized peptides on the PCL meshes were measured by high performance liquid chromatography (HPLC) [51]. Briefly, every three meshes from E7, M7, and RGD group were weighed using an analytical balance, respectively, and hydrolyzed in a 6 N HCl aqueous solution at 100℃ for 24 h. Subsequently, 2,4-dinitroflurobenzene (DNFB, Sigma, St. Louis,

MO, USA) was used for pre-column derivation. HPLC analysis was performed using an LC-20A liquid chromatograph (SHIMADZU, Shimadzu, Japan) and an Inertsil ODS-4 (4.6 mm - 150 mm, 5 mm) column (GL Science, Tokyo, Japan) following a previously described protocol with modifications. All amino acid monomers used as a standard were purchased from Sigma (St. Louis, MO, USA) and Amrsco (Solon, OH, USA). The SEM, Confocal Microscope and HPLC analysis was done by experts in Peking University Medical School.

2.1.3 Results

Electrospun pure PCL fibers obtained from different solution concentration were shown in **Figure 2-1**. At lowest concentration 0.08g/ml (**Figure 2-1**a,b), no fiber was formed, only beads were observed under SEM. As concentration increasing, more fibers and fewer beads were observed. When the concentrations reached 0.20g/ml and 0.30g/ml (**Figure 2-1**c-f), fibers were formed and relatively thicker fibers were formed with 0.03g/ml solutions (**Figure 2-1**e, f). The three-dimensional fibrous mesh consists of fibers with diameters ranging from 500nm to 2μm and the fibers were randomly oriented and interconnected voids were present (**Figure 2-1**c, e).

PCL/HA composite with different types of surfactant were fabricated. The fibrous mesh had a randomly interconnected and highly porous structure. The fibers were evenly distributed in general. Pure PCL fibers were electrospun as control (**Figure 2-2**a). Without surfactant, HA nanoparticles formed clusters (**Figure 2-2**b), with nonionic surfactant Span-80 (**Figure 2-2**c), HA became more evenly distributed, but smaller clusters can still be observed in the fibers. However, with ionic surfactant CTAB (**Figure 2-2**d), HA nanoparticles have uniform distribution and higher density in the fibers.

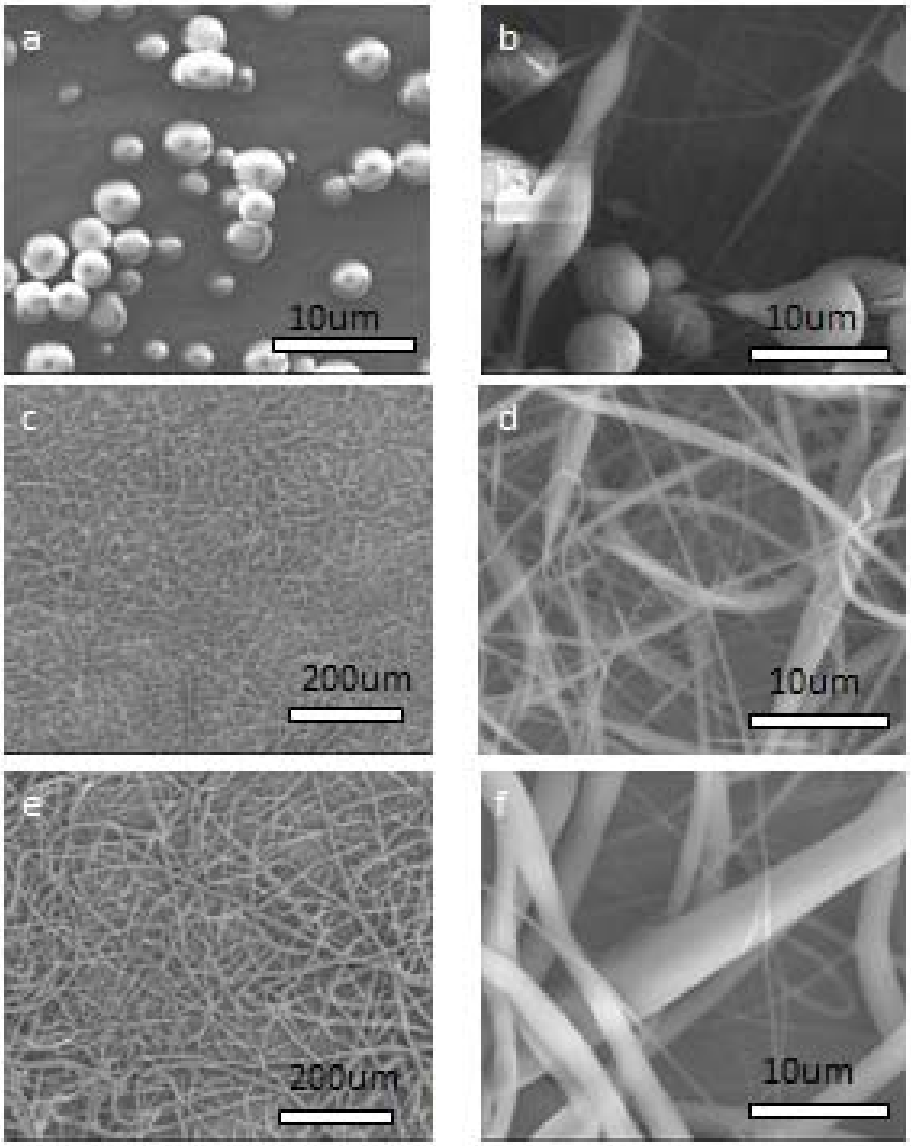

Figure 2-1. SEM images of electrospun PCL fibers with different concentrations. (a,b) 0.08g/ml, (c,d) 0.20g/ml, (e,f) 0.30g/ml

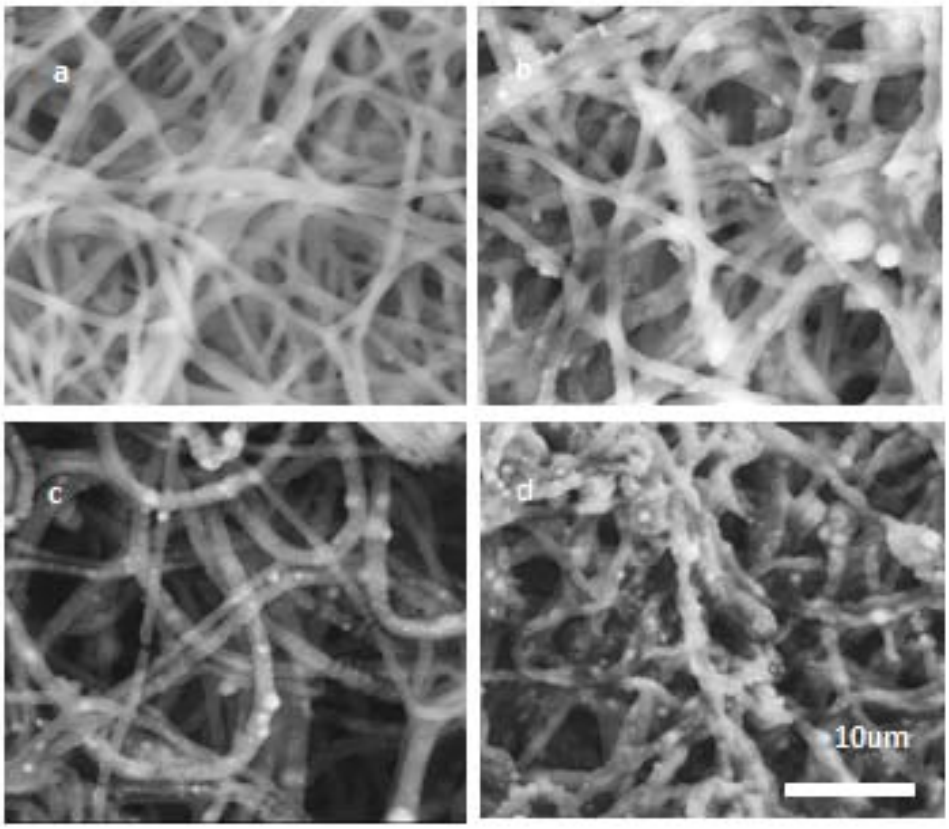

Figure 2-2. SEM images of pure PCL and PCL/HA composite electrospun fibers, (a) pure PCL fibers, (b) PCL/HA composite without surfactant addition, (c) PCL/HA composite with span-80 addition, (d) PCL/HA composite with CTAB addition.

Characterization of peptide-conjugated PCL meshes

The chemical reaction of the conjugation was shown in **Fig 2-3**A. After conjugation, the PCL fibers showed a homogeneous green fluorescence because the peptides were pre-labeled with FITC (**Fig. 2-3**B), indicating a homogeneous conjugation of the peptides on the PCL surface. SEM images revealed the different mesh morphology with different collectors and solvents. With copper meshes as collector, the electrospun meshes tended to copy the pattern of the copper meshes (**Fig. 2-3** C-F); the aluminum foil made randomly distributed fibers (**Fig. 2-3** G-J), and rolling tube collector made aligned, low porous density fibers (**Fig.2-3** K-N). No significant differences between the peptide-conjugated PCL meshes and pure PCL meshes on the morphology of the meshes (**Fig. 2-3**C to N). HPLC-based amino acid analysis was conducted to evaluate the peptide surface density/amount and the homogeneity of the immobilized peptides on the PCL meshes. Based on the spectrum of the standard amino acid monomers (**Fig. 2-4**A), the amino acids in E7- and M7-conjugated PCL meshes were identified (**Fig. 2-4**B), which showed consistency with the correspondent peptide sequences. All the peptide-conjugated PCL meshes were analyzed using the same protocol. A quantitative analysis was also conducted based on the calculation of the "peak-area" of every amino acid. At the same initial concentration, E7, M7, and RGD had similar conjugated efficiencies (**Fig. 2-4**C), especially at 0.1 nM. This result indicates that the method to conjugate peptides with PCL meshes is stable and valid. The peptides at 0.1 nM concentration was used in subsequent experiments for conjugation.

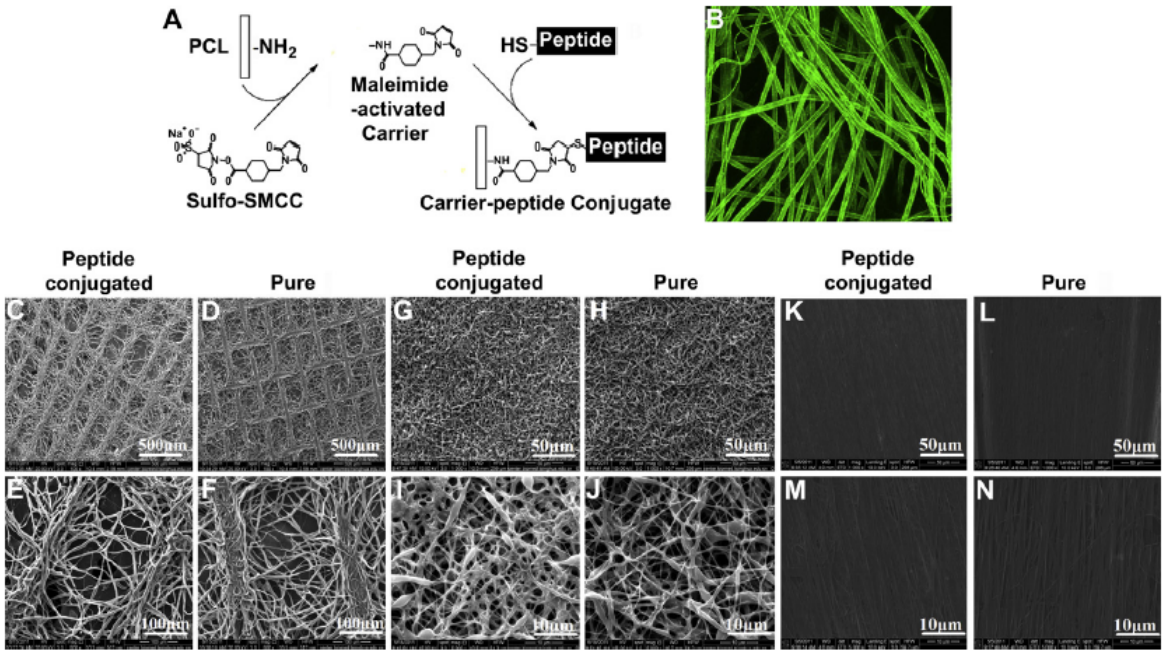

Figure 2-3. FITC-labeled peptides were covalently conjugated with PCL meshes, and were characterized via SEM. Sulfo-SMCC was used as a crosslinker between the FITC labeled peptides and the PCL electrospun fibers (A). After conjugation, homogeneous green fluorescence on PCL fibers was visualized under a confocal microscope (B). The structure of peptide-conjugated and pure PCL meshes with lattice (C to F), thick non-woven (G to J), and lower porosity (K-N) were examined via SEM.
Image Published: Shao, Z., X. Zhang, Y. Pi, **X. Wang,** Z. Jia, J. Zhu, L. Dai, W. Chen, L. Yin, H. Chen, C. Zhou, and Y. Ao, Biomaterials, 2012. **33**(12): p. 3375-3387

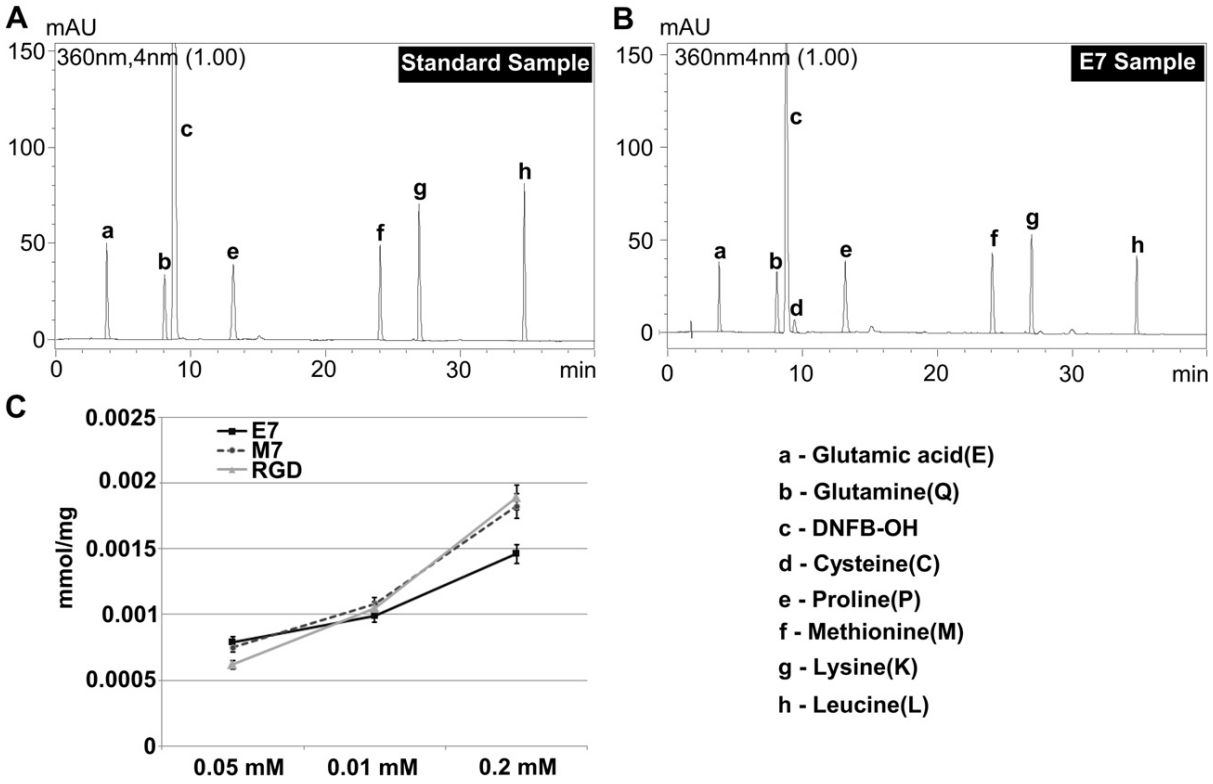

Figure 2-4. The peptide surface density/amount and homogeneity of the immobilized peptides on PCL meshes was evaluated via HPLC. The amino acids in the E7- and M7-conjugated PCL mesh samples were identified (B) According to the spectrum of the standard amino acid monomers (A). A quantitative analysis was conducted based on the calculation of the "peak-area" of every amino acid for E7, M7, or RGD to indicate the conjugation efficiency (C).
Image Published: Shao, Z., X. Zhang, Y. Pi, **X. Wang,** Z. Jia, J. Zhu, L. Dai, W. Chen, L. Yin, H. Chen, C. Zhou, and Y. Ao, Biomaterials, 2012. **33**(12): p. 3375-3387

2.1.4 Discussion

Previous studies have proved that solution viscosity (as controlled by changing the polymer concentration) is one of the biggest determiners of fiber size and morphology when spinning polymeric fibers. The relationship between the polymer viscosity and/or concentration on fibers obtained from electrospinning has been studied in a number of systems, including poly(DL-lactic acid) (PDLA), poly(lactic-co-glycolic acid) (PLGA), poly(ethylene oxide) (PEO),[52,53] poly(vinyl alcohol) (PVA), poly(methyl methacrylate) (PMMA), polystyrene, poly(L-lactic acid) (PLLA), gelatin, dextran, and collagen type I-PEO [52-56]. Similar to our results, at low polymer concentrations, defects in the form of beads and droplets have been observed [56]; the process under these conditions was characteristic of electrospraying rather than spinning. Additionally, the presence of junctions and bundles has been seen, indicating that the fibers were still wet when reaching the collector. Increasing the solution viscosity by increasing polymer concentration yielded uniform fibers with few beads and junctions. Polymers and bioceramics such as tricalcium phosphate and HA are osteoconductive and can be electrospun to form continuous nanofibers with defined patterns. Uniform random nanofibers of PCL/HA were obtained by the electrospinning process. The segregation of HA powder was reduced and a good dispersion of HA particles within the polymer matrix was obtained during this study by adding surfactant to the solvent. At the same concentration of HA, there was a considerate agglomeration of HA particles and broken fiber formation in the non-surfactant group. The non-ionic surfactant with the hydrophilic PEG chain improved the stability of the suspension. And the optimal performance of a composite material was achieved when the small particles are uniformly dispersed throughout the polymer and interact strongly with the organic matrix with the addition of ionic surfactant CTAB.

There are several parameters which can influence the electrospinning process, like concentration, solvent polarity, collector morphology, voltage, collecting distance and

feeding rate. In this study, to better observe the MSC behavior on PCL meshes with or without peptide modification, solvent polarity and collector morphology were chosen to manipulate the electrospun meshes. The results we got were consistent with previous study, as the higher polarity solvent CF_3OH produced thinner fiber diameter and at the early stage of collection, the electrospun fibers tended to copy the pattern of the collector [57]. These PCL meshes with different morphology provided a better observation of MSC response on the peptide-conjugated PCL meshes [58]. In the present study, E7 was covalently conjugated onto the PCL electrospun meshes to establish an MSC attracting matrix for both *in vitro* and *in vivo* [58].

2.1.5 Conclusion

In this study, the electrospinning system was set up and the concentration of polymer solution was optimized. PCL/HA composite fibrous meshes were also fabricated via electrospining and the ionic surfactant was robust for stabilizing PCL/HA suspension to achieve evenly distributed composite fibers. An MSC-homing peptide (E7) identified through phage display was conjugated with PCL electrospun meshes. The E7-conjugated PCL electrospun meshes have shown promoted cell attachment and proliferation compared to pure PCL meshes [58]. In addition, in vitro and in vivo study [58] by Dr. Shao in Peking university third hospital showed E7 has specificity toward MSCs compared with the RGD-conjugated PCL electrospun meshes. This study provides a promising way to improve MSC-based tissue engineering repair.

2.2 Characterization of Thermal Polymerizable Alginate-GMA Hydrogel for in situ Cell Encapsulation

2.2.1 Introduction

Hydrogels derived from organic materials such as polysaccharides, are promising materials for tissue-engineered scaffolds and have attracted many interests in the field of tissue engineering. Natural materials have many desirable characteristics such as their three-dimensional porous structure, biodegradability, good water absorption, and tissue-like elastic properties [59-65]. These properties make hydrogels ideal candidates for creating environments where cells and tissues can grow [66]. Alginate is an anionic polysaccharide produced by brown algae that is widely used in pharmaceutical and biomedical applications. Ionic cross-linked alginate, such as calcium alginate is highly characterized and has been used for multiple tissue engineering applications [67-72]. While this ionic cross-linked alginate cannot gelate *in situ*, the alginate solution required treatment by calcium solution *in vitro* before the cross-linked hydrogel applied *in vivo*.

Recently, synthesis of a polysaccharide modified with thermal cross-linkable or photo cross-linkable groups, such as an acrylic or a methacrylic group, may provide an alternative method for hydrogel formation [73-80]. Most of these works focused on photo cross-linking, which utilizes ultraviolet light to initiate a free radical polymerization reaction, forming covalent cross-links through the acrylate or methacrylate groups [81,82]. These free radical-cross-linked hydrogels allow macromonomers to gelate *in situ* and enables the hydrogels to form different shapes to better match the implantation site [83]. Although these photo cross-linked hydrogels have many useful properties and have been used as cell carriers for several tissue engineering applications including for cartilage, bone, nerve, and liver [84-94], one concern with the photo cross-linking process is the potential damage to the cells encapsulated in the macromonomers. More importantly, since we cannot use the UV photo cross-linking process

in vivo, this limits the use of those hydrogels as injectable hydrogels, and therefore limits their therapeutic application.

In this study, thermal polymerizable alginate-GMA macromonomers were synthesized. Thermal initiator was used to avoid UV irradiation, which is harmful to the cells and human, and allows the macromonomers to polymerize at physiological temperature. The mild reaction conditions enable cell and protein encapsulation as well as *in vivo* gelation. The properties of alginate-GMA were investigated extensively, including gelation time, swelling ratio and porosity. Cell viability and proliferation were assessed using the human endothelial cell lines HUVEC and L929 in preliminary tests for the potential application of alginate-GMA as an injectable hydrogel for use in tissue engineering.

2.2.2 Materials and methods

Sodium alginic acid (Sigma Aldrich), glycidyl methacrylate (GMA)(Fluka), NaOH (Beijing Chemical Works), ammonium persulfate (APS), N', N', N', N'-tetramethylethylendiamine (TEMED)(Sigma Aldrich). H-DMEM (GIBCO), FBS (MDgenics Inc), penicillin, streptomycin, Haematoxylin Eosin, propidium iodide and calcein-AM and MTT (Sigma Aldrich).

Synthesis of AA-GMA macromonomers

Briefly, 2g of sodium alginic acid was dissolved in distilled water to make a 0.02g/ml solution of alginate. 5.68g GMA was added to the alginate solution and thoroughly mixed with stirring. 5M NaOH was added to adjust the pH to 10. The reaction was conducted at 60℃ and N_2 protection for 4 hours. The solution was precipitated with an excess of ethanol. The product was thoroughly washed by ethanol 5-6 times and freeze dried under a vacuum.

Thermal polymerization of AA-GMA

To prepare the hydrogels, AA-GMA macromonomers were dissolved in distilled water at concentrations of 0.03g/ml to 0.07g/ml, 5% (w/w of AA-GMA) of APS and TEMED were

added to the solution. The solution formed hydrogels in a water bath at 37℃ in 5 to 20 minutes.

^{1}H NMR

Sodium alginic acid and AA-GMA samples were dissolved in D_2O at a concentration of 0.005g/ml. ^{1}HNMR spectra was recorded with a 400MHz Bruker AV400 NMR spectrometer. The percentage of double bonds was calculated using the formula below (Haa represents H atoms in the alginate backbone, Ha represents H atoms in the methyl group of GMA):

$$\%DM = \frac{Ha/3}{(Haa-1)/6} * 100\%$$

Formula 1[34]

Surface morphology

The surface morphology of freeze-dried thermal cross-linked AA-GMA hydrogels were characterized with a Quanta 200FEG scanning electron microscope operated at 20kV.

Swelling assay

A weighed amount of dry thermal cross-linked AA-GMA hydrogel was placed in an excess volume of 1X PBS for 24-120 hours. The surface of the hydrogel was blotted with tissue paper before the wet weight was measured. The equilibrium swelling ratio (q) was calculated as the ratio of the wet weight to the dry weight.

$$q = W_w/W_d$$

***In vivo* inflammatory effects**

Male Sprague-Dawley (SD) rats weighing about 250g were used. One hundred microliters of 0.05 g/ml macromonomer solution with a pre-measured amount of APS and TEMED was injected into inner side of each leg. Each week after injection, animals were euthanized and surrounding tissues were histologically processed using Haematoxylin-Eosin stains [95].

Cell encapsulation and cell viability assay

The human endothelial cell line HUVEC was used. Cells were cultured in DMEM with 10% fetal bovine serum (FBS) and 1% penicillin/streptomycin at 37℃ in 5% CO_2 at 100% humidity. Different amounts of AA-GMA with APS and TEMED were dissolved in 1.5ml growth media. 1 x 10^6 cells in growth media were added to the solution and mixed evenly. 0.5ml of this mixture was then added in 24-well cell culture plates and placed in incubator to let the polymerization occur. After 24 hours, hydrogels with cells were transferred into 6-well plates and immersed in culture media.

Cell viability and morphology were characterized at 24, 48, 72, 96 hours after seeding. For the cell viability assay, cell-loaded gels were stained with calcein-AM and propidium iodide (PI) for 20 minutes at 37℃. All live cells were labeled with calcein-AM and dead cells with PI. Cells were imaged using a fluorescence microscope (OLYMPUS IX71). To analyze cell growth, the number of cells in an $8mm^2$ area was counted in 5 images from each sample. Due to the 3D structure, it was necessary to exclude cells outside of the focal plane, so the brightness threshold was set to eliminate the background light. This part of work was completed with the help with Tong Hao in Dr. Changyong Wang's lab in Academy of Military Medical Sciences.

2.2.3 Results and Discussion

Synthesis and characterization of AA-GMA macromonomers and hydrogels

The thermal polymerized AA-GMA macromonomers were synthesized through reaction of the epoxy group of GMA with the hydroxyl group of alginate under an alkaline condition. The structure of the AA-GMA macromonomer, shown in **Figure 2-5**, was confirmed by ^1H NMR spectroscopy in D_2O (**Figure 2-6**). The methacryloyl group of GMA was effectively attached to the available –OH groups of alginate via open-ring reaction of epoxy group [37]. Compared with the spectrum of alginate (**Figure 2-5** A), six new resonance peaks from the AA-GMA macromonomer appeared. This indicates that six different species of H appeared

after the reaction, and this illustrates the mechanism of reaction as shown in **Figure 2-5**. From the ^{1}H NMR spectra of the AA-GMA macromonomers, the %DM is determined by using the Formula 1 shown before, and under these reaction condition, the %DM is about 25%.

Three groups of hydrogels were made with three concentrations of marcomonomer solutions and are listed in **Table 2-1**. The polymerization time was determined by a rheometer. The AA-GMA macromonomer underwent a free radical polymerization under thermal condition with the addition of initiator. According to Table 2-1, AA-GMA solutions of lower concentration have longer polymerization times, while AA-GMA solution of higher concentration has shorter polymerization times. This shows that through controlling the macromonomer concentration, we can control the polymerization time to meet different needs.

SEM was used to characterize the morphology of the freeze-dried cross-linked AA-GMA hydrogel. As shown in **Figure 2-7**, the freeze-dried hydrogel has porous structure with pore size about 50-150μm, which increased with deceasing gel content.

Swelling property influences the solute diffusion rate, the surface properties of the hydrogel and the mass transport properties through the scaffold. **Figure 2-8** shows the swelling property of AA-GMA hydrogels with different gel concentrations. Basically, the swelling ratio increased with decreasing macromonomer content in the gel. This results mainly because hydrogels with lower macromonomer concentrations have larger pore sizes, resulting in faster transport of water through the gel. Moreover, hydrogels with larger pores can retain more water compared to hydrogels with smaller pores.

***In vivo* inflammatory assay**

Male SD rats were injected with 0.1ml of 0.04g/ml AA-GMA macromonomer PBS solution with initiator for each leg. Each week the rats were euthanized and we found the AA-GMA

macromonomer solution had formed a hydrogel in the muscle and the gel was clearly distinguishable. **Figure 2-9** shows the inflammatory function of AA-GMA hydrogels *in vivo* in two weeks. All stained sections of the smears of AA-GMA hydrogels showed no dense collection of neutrophils and macrophages in two weeks. These observations show the AA-GMA hydrogel has a mild inflammatory effect, indicating good biocompatibility of the AA-GMA hydrogel.

Cell encapsulation

To evaluate the potential use of AA-GMA hydrogel as *in situ* cell matrices for tissue engineering applications, the human endothelial cell line (HUVEC) was used. This cell type may have a particular application in vascular grafting or promoting endothelialization of implants. Previous studies also indicated that methacrylated polysaccharide was cytocompatible [37]. For cell encapsulation, three different concentrations (0.03, 0.05, 0.07g/ml) of AA-GMA macromonomer were used. Cell viability was observed after thermal-encapsulation. **Figure 2-10** shows the cell viability of the three groups from 24 to 96 hours after seeding. Live cells were labeled by Calcein-AM, and dead cells were labeled by PI. After 24 to 96 hours in culture, three groups of encapsulated HUVECs all exhibited a high percentage of viability. There was no significant difference between the high concentration groups and low concentration groups while the higher concentration group had a little adverse effect in the first 24 hours (more red-labeled cells observed) (**Figure 2-10** A, B, C), after 24 hours, the cells started proliferate and the viability in 96h showed no differences among the three groups (**Figure 2-10** D) Even when the higher concentration was used, few dead cells were observed, showing that AA-GMA hydrogels have good cytocompatibility. Since the cells were directly mixed with the reaction mixture during in situ gelation, it is possible that free radicals generated during the polymerization may have adverse effects on cell viability in the first 24h [22], This adverse effect may fade away with the disappearance

of free radical. **Figure 2-11** shows cell growth in the 0.05g/ml AA-GMA group. **Figure 2-11** A and B shows that the density of green fluorescence increases over time, which suggests an increase in cell proliferation in the hydrogels. **Figure 2-11** C shows that there are no significant changes in cell viability and **Figure 2-11** D shows that cell number increased during the 96 hour culture time. Both of the results illustrate that the 3D porous structure allows cell migration and nutrients transportation. Unlike the ionic hydrogel, which are usually pre-manufactured before application, such as alginate microbeads, this novel hydrogel can polymerize under physiological temperature, these observation demonstrate the hydrogel can not only be pre-manufactured to any structures, but also can be a promising injectable hydrogel for *in situ* gelation for tissue engineering.

Table 2-1. Thermalpolymerized AA-GMA hydrogels investigated (0.5ml aqueous solution)

Sample no.	*AA-GMA (g)*	*AA-GMA concentration (g/ml)*	*APS (g)*	*TEMED (µl)*	*Gelation Time (min)*
1	0.015	0.03	0.0015	1	22
2	0.025	0.05	0.0025	2	12
3	0.030	0.06	0.0030	3	8
4	0.035	0.07	0.0035	3	5

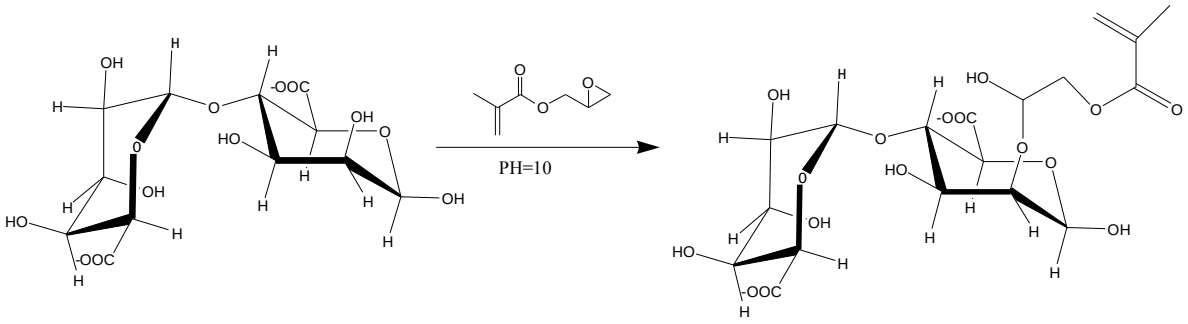

Figure 2-5. Reaction Scheme of the macronomomer AA-GMA

A

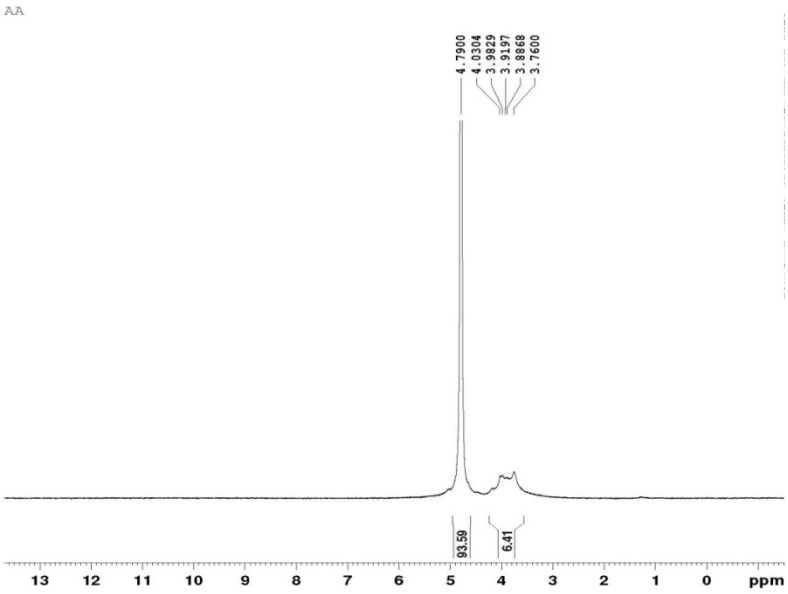

B

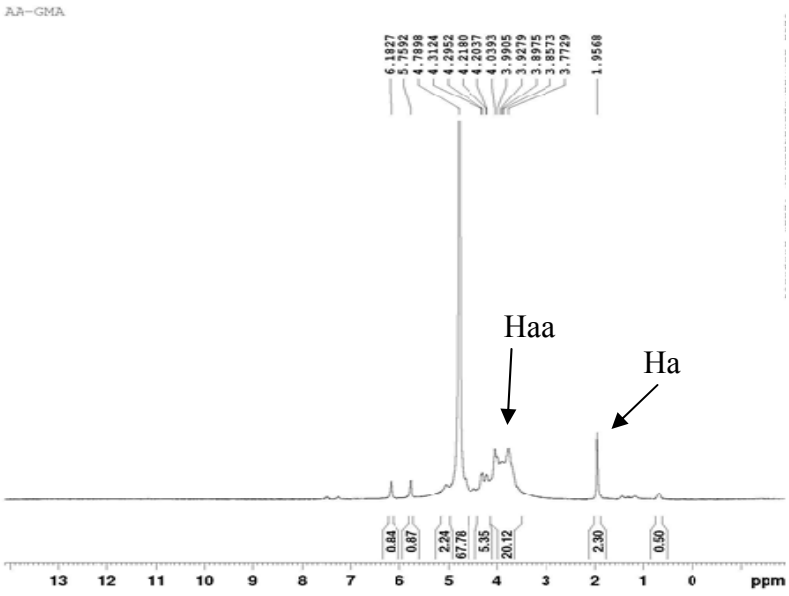

Figure 2-6. H NMR spectra of (A) Sodium alginic acid and (B) the AA-GMA macromonomer

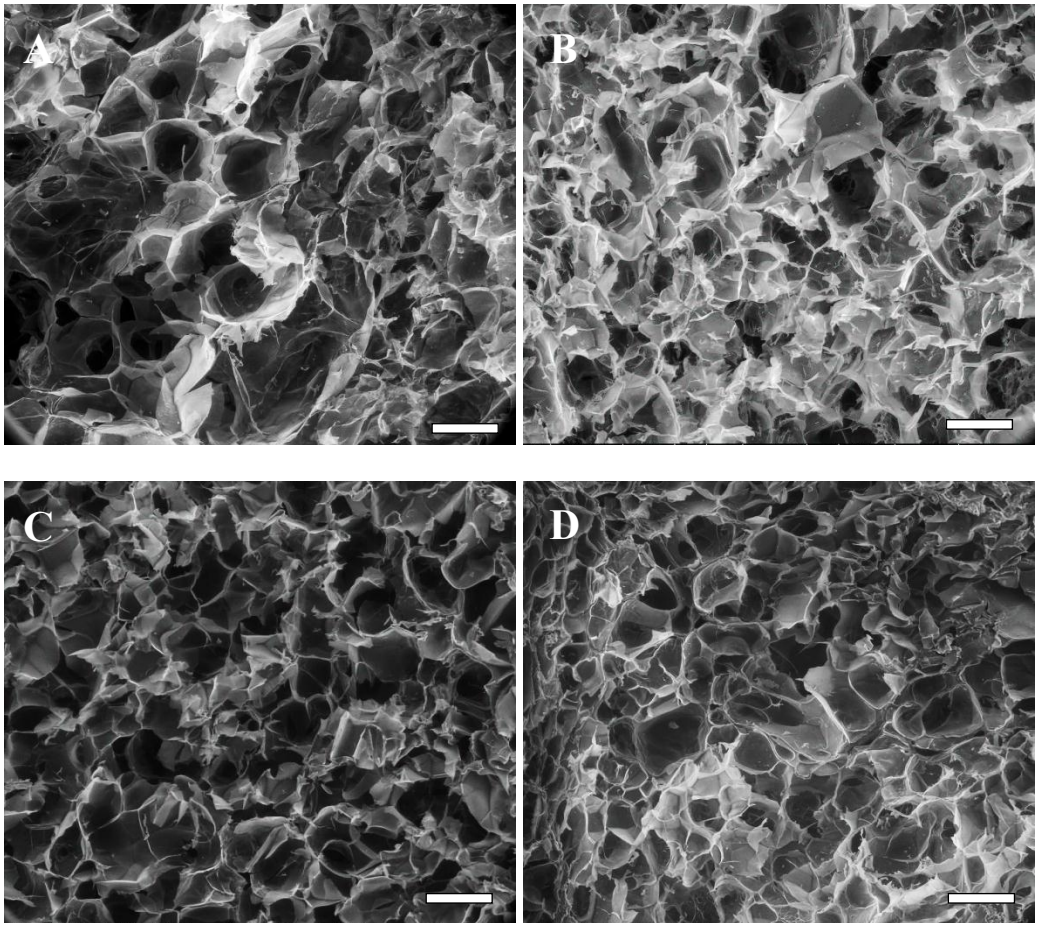

Figure 2-7. SEM images of the (A) 0.03g/ml AA-GMA, (B) 0.05g/ml AA-GMA, (C) 0.06g/ml AA-GMA, (D) 0.07g/ml AA-GMA freeze-dried hydrogen. The bar is 100μm.

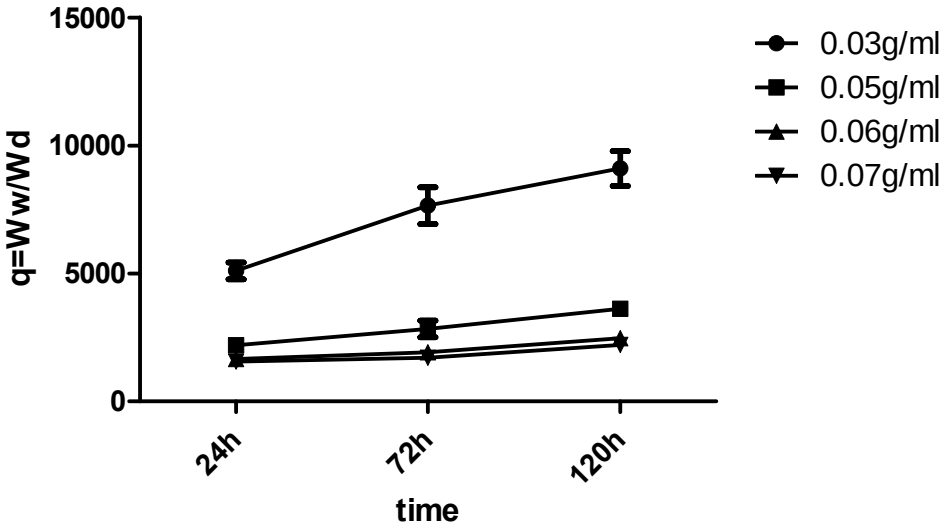

Figure 2-8. Swelling Ratio of AA-GMA hydrogel of different concentration

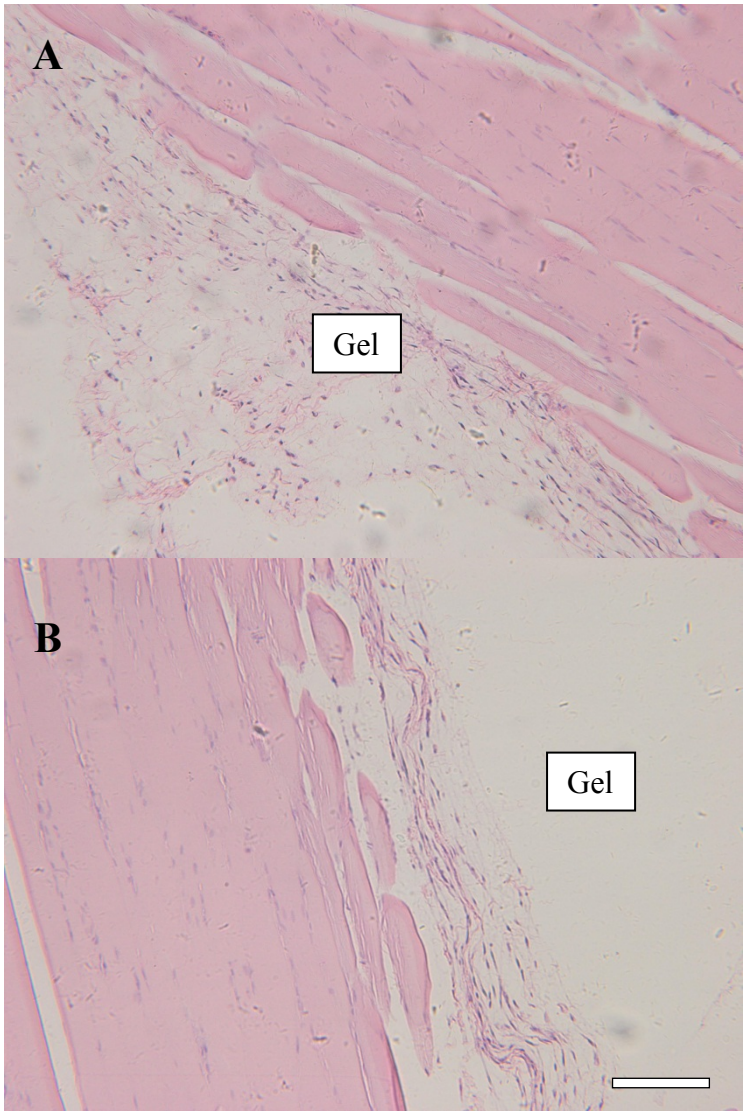

Figure 2-9. Representative hematoxylin-eosin stained sample of polyAA-GMA hydrogel with subjacent muscle. (A) Hydrogels removed 1 week after injection, (B) 2 weeks after injection. The bar is 100μm

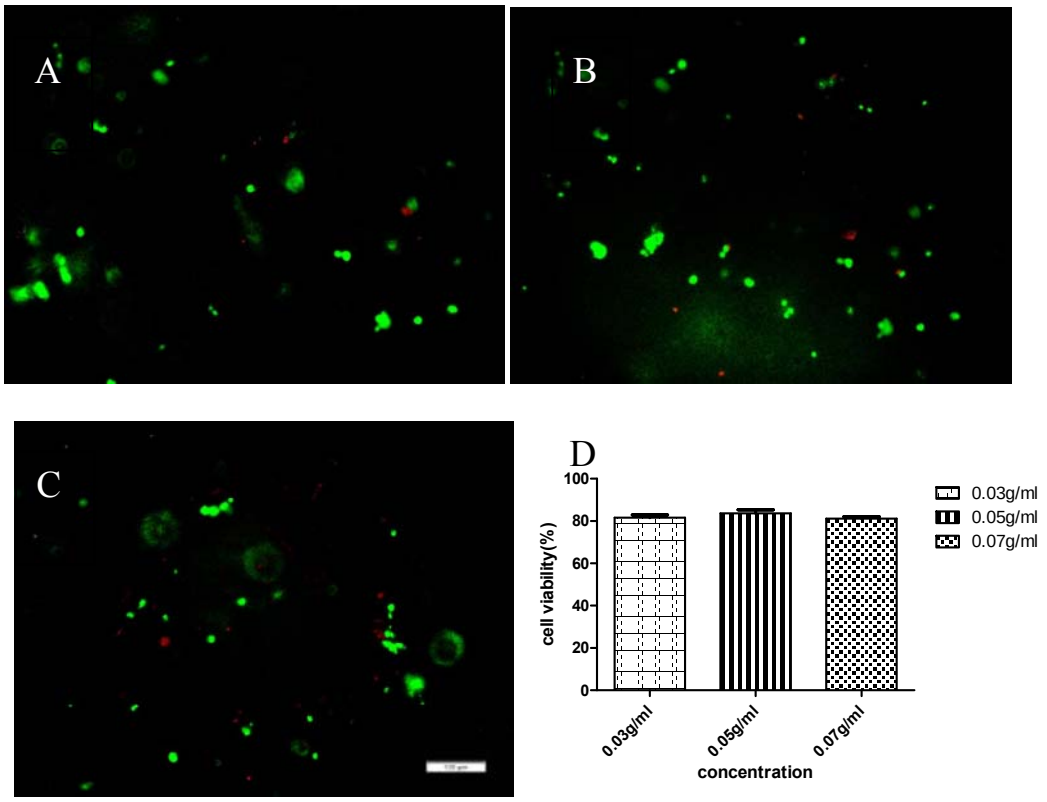

Figure 2-10. Cell viability of HUEVCs encapsulated in AA-GMA hydrogels at the (A) 0.03g/ml for 24h; (B)0.05g/ml for 24h; (C) 0.07g/ml for 24h; The bar is 100μm. (D) live/dead assay, the histogram refers to the percentage of live cells in the different groups in 96h.

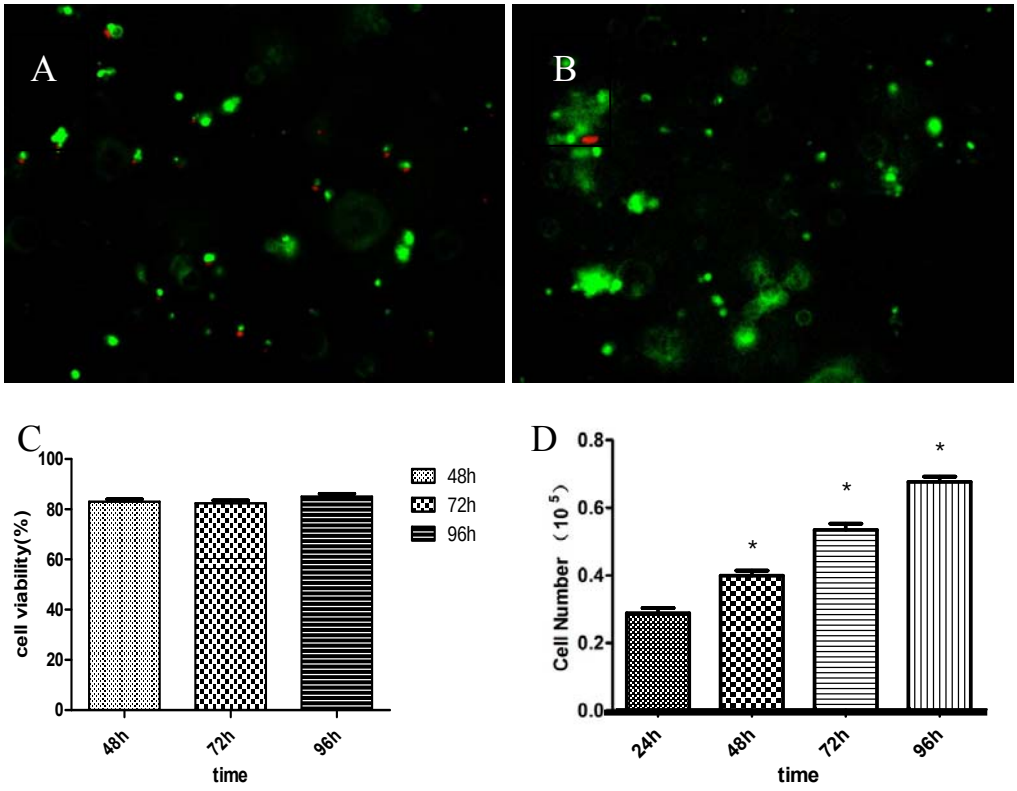

Figure 2-11. Cell growth of HUEVCs encapsulated in AA-GMA hydrogels at the (A) 0.05g/ml for 24h; (B) 0.05g/ml for 96h (C) Cell viability in 0.05g/ml hydrogels during 96h. (D) Cell number in 0.05g/ml hydrogels during 96h. ($*10^3$) * Vs 24h $P < 0.05$ using one way ANOVA analysis.

2.2.4 Conclusion

Alginate was modified with glycidyl methacrylate (GMA) to produce an alginate-GMA (AA-GMA) macromonomer, which polymerized at physiological temperature when using APS as an initiator and TEMED as a catalyst. AA-GMA hydrogels exhibited a three-dimensional porous structure with an average pore size ranging from 50-150μm, and the pore size increased with deceasing macromonomer gel content. Muscle injection *in vivo* showed the AA-GMA solution mixed with initiator could form a hydrogel *in situ* and exhibited a mild inflammatory response. Human endothelial cells (HUVECs) were encapsulated in the AA-GMA hydrogels *in situ* at body temperature. Cell viability remained good at low and high macromonomer concentrations and cells proliferated well in the hydrogels. These promising results show a potential use of AA-GMA hydrogels for *in situ* tissue engineering scaffold applications.

2.3 References

1. Cheng, N.C., et al., Genipin-crosslinked Cartilage-derived Matrix as a Scaffold for Human Adipose-derived Stem Cell Chondrogenesis. Tissue Eng Part A, 2012.
2. Lim, K.T., et al., Enhanced Osteogenesis of Human Alveolar Bone-Derived Mesenchymal Stem Cells for Tooth Tissue Engineering Using Fluid Shear Stress in a Rocking Culture Method. Tissue Eng Part C Methods, 2012.
3. Chen, W., et al., Human embryonic stem cell-derived mesenchymal stem cell seeding on calcium phosphate cement-chitosan-RGD scaffold for bone repair. Tissue Eng Part A, 2012.
4. Diekman, B.O., et al., Cartilage tissue engineering using differentiated and purified induced pluripotent stem cells. Proc Natl Acad Sci U S A, 2012.
5. Jayasuriya, A.C. and C. Shah, Controlled release of insulin-like growth factor-1 and bone marrow stromal cell function of bone-like mineral layer-coated poly(lactic-co-glycolic acid) scaffolds. J Tissue Eng Regen Med, 2008. 2(1): p. 43-9.
6. Chou, C.L., et al. ,Micrometer scale guidance of mesenchymal stem cells to form structurally oriented cartilage extracellular matrix. Tissue Eng Part A, 2012.
7. Lim, K.T., et al., Enhanced Osteogenesis of Human Alveolar Bone-Derived Mesenchymal Stem Cells for Tooth Tissue Engineering Using Fluid Shear Stress in a Rocking Culture Method. Tissue Eng Part C Methods, 2012.
8. Park, S.H., et al., Development of dual scale scaffolds via direct polymer melt deposition and electrospinning for applications in tissue regeneration. Acta Biomater, 2008. 4(5): p. 1198-207
9. Tong, H.W. and M. Wang, Electrospinning of aligned biodegradable polymer fibers and composite fibers for tissue engineering applications. J Nanosci Nanotechnol, 2007. 7(11): p. 3834-40.
10. Dosunmu, O.O., et al., Electrospinning of polymer nanofibres from multiple jets on a porous tubular surface. Nanotechnology, 2006. 17(4): p. 1123-7.
11. Zhang, H., et al., Electrospinning preparation of uniaxially aligned ternary terbium complex/polymer composite fibers and considerably improved photostability. J Nanosci Nanotechnol, 2010. 10(3): p. 2070-6.
12. Wang, Y., et al., Electrospinning of polymer nanofibers with ordered patterns and architectures. J Nanosci Nanotechnol, 2010. 10(3): p. 1699-706.
13. Rajesh, K.P. and T.S. Natarajan, Electrospun polymer nanofibrous membrane for filtration. J Nanosci Nanotechnol, 2009. 9(9): p. 5402-5.
14. Buttiker, R., et al., Membranes for specific adsorption: immobilizing molecularly imprinted polymer microspheres using electrospun nanofibers. Chimia (Aarau), 2011. 65(3): p. 182-6.
15. Kang, H., et al., A novel catalyst based on electrospun silver-doped silica fibers with ribbon morphology. J Colloid Interface Sci, 2010. 341(2): p. 303-10.
16. Formo, E., et al., Functionalization of electrospun TiO2 nanofibers with Pt nanoparticles and nanowires for catalytic applications. Nano Letters, 2008. 8(2): p. 668-72.

17. Kumar, P.R., et al., Nanofibers: effective generation by electrospinning and their applications. J Nanosci Nanotechnol, 2012. 12(1): p. 1-25.
18. Zhang, H., et al., Oxygen sensing properties of Cu(I) complex/polystyrene composite nanofibers prepared by electrospinning. J Nanosci Nanotechnol, 2011. 11(11): p. 9840-5.
19. Jin, G., et al., Tissue engineered plant extracts as nanofibrous wound dressing. Biomaterials, 2012.
20. Nguyen, T.H., et al., A novel fibrous scaffold composed of electrospun porous poly({varepsilon}-caprolactone) fibers for bone tissue engineering. Journal of Biomaterials Applications, 2012.
21. Yang, W., et al., In vivo bone generation via the endochondral pathway on three-dimensional electrospun fibers. Acta Biomater, 2012.
22. Liu, H., et al., An in vitro evaluation of the Ca/P ratio for the cytocompatibility of nano-to-micron particulate calcium phosphates for bone regeneration. Acta Biomater, 2008. 4(5): p. 1472-9.
23. Kon, M., et al., Development of calcium phosphate based functional gradient bioceramics. Biomaterials, 1995. 16(9): p. 709-14.
24. Shikinami, Y. and M. Okuno, Bioresorbable devices made of forged composites of hydroxyapatite (HA) particles and poly L-lactide (PLLA). Part II: practical properties of miniscrews and miniplates. Biomaterials, 2001. 22(23): p. 3197-211.
25. Kuroda, K. and M. Okido, Hydroxyapatite coating of titanium implants using hydroprocessing and evaluation of their osteoconductivity. Bioinorg Chem Appl, 2012. 2012: p. 730693.
26. Verma, D., K.S. Katti, and D.R. Katti, Osteoblast adhesion, proliferation and growth on polyelectrolyte complex-hydroxyapatite nanocomposites. Philos Transact A Math Phys Eng Sci, 2010. 368(1917): p. 2083-97.
27. Addison, W.N. and M.D. McKee, Inositol hexakisphosphate inhibits mineralization of MC3T3-E1 osteoblast cultures. Bone, 2010. 46(4): p. 1100-7.
28. Liu, L., et al., Three-dimensional dynamic culture of pre-osteoblasts seeded in HA-CS/Col/nHAP composite scaffolds and treated with alpha-ZAL. Acta Biochim Biophys Sin (Shanghai), 2012. 44(8): p. 669-77.
29. Hunter, K.T. and T. Ma, In vitro evaluation of hydroxyapatite-chitosan-gelatin composite membrane in guided tissue regeneration. J Biomed Mater Res A, 2012.
30. Jin, H.H., et al., In vivo evaluation of porous hydroxyapatite/chitosan-alginate composite scaffolds for bone tissue engineering. Int J Biol Macromol, 2012. 51(5): p. 1079-85.
31. Venkatesan, J., et al., Chitosan-amylopectin/hydroxyapatite and chitosan-chondroitin sulphate/hydroxyapatite composite scaffolds for bone tissue engineering. Int J Biol Macromol, 2012. 51(5): p. 1033-42.
32. Li, A.D., et al., Electrospun Chitosan-graft-PLGA nanofibres with significantly enhanced hydrophilicity and improved mechanical property. Colloids Surf B Biointerfaces, 2012. 102C: p. 674-681.
33. Schneider, T., et al., Influence of fiber orientation in electrospun polymer scaffolds on viability, adhesion and differentiation of articular chondrocytes. Clin Hemorheol Microcirc, 2012.

34. Reagan, M.R., et al., Stem Cell Implants for Cancer Therapy: TRAIL-Expressing Mesenchymal Stem Cells Target Cancer Cells In Situ. J Breast Cancer, 2012. 15(3): p. 273-82.
35. Tsai, C.C., et al., Benefits of hypoxic culture on bone marrow multipotent stromal cells. Am J Blood Res, 2012. 2(3): p. 148-59.
36. Horwitz EM, Le Blanc K, Dominici M, Mueller I, Slaper-Cortenbach I, Marini FC, et al. Clarification of the nomenclature for MSC: the International Society for cellular therapy position statement. Cytotherapy 2005;7(5):393-5.
37. Dominici M, Le Blanc K, Mueller I, Slaper-Cortenbach I, Marini F, Krause D, et al. Minimal criteria for defining multipotent mesenchymal stromal cells. The International Society for Cellular Therapy position statement. Cytotherapy 2006;8(4):315-7.
38. Pittenger MF. Multilineage potential of adult human mesenchymal stem cells. Science 1999;284(5411):143-7.
39. Prockop DJ. Marrow stromal cells as stem cells for nonhematopoietic tissues. Science 1997;276(5309):71-4.
40. Vinatier C, Mrugala D, Jorgensen C, Guicheux J, Noel D. Cartilage engineering: a crucial combination of cells, biomaterials and biofactors. Trends Biotechnol 2009;27(5):307-14.
41. Li W-J, Tuli R, Huang X, Laquerriere P, Tuan RS. Multilineage differentiation of human mesenchymal stem cells in a three-dimensional nanofibrous scaffold. Biomaterials 2005;26(25):5158-66.
42. Karp JM, Leng Teo GS. Mesenchymal stem cell homing: the devil is in the details. Cell Stem Cell 2009;4(3):206-16.
43. Caplan Arnold I, Correa D. The MSC: an injury drugstore. Cell Stem Cell 2011; 9(1):11-5.
44. Meyerrose T, Olson S, Pontow S, Kalomoiris S, Jung Y, Annett G, et al. Mesenchymal stem cells for the sustained in vivo delivery of bioactive factors. Adv Drug Deliv Rev 2010; 62(12):1167-74.
45. Pittenger MF. Multilineage potential of adult human mesenchymal stem cells. Science 1999;284(5411):143-7.
46. Prockop DJ. Marrow stromal cells as stem cells for nonhematopoietic tissues. Science 1997;276(5309):71-4.
47. Lim, K.T., et al., Enhanced Osteogenesis of Human Alveolar Bone-Derived Mesenchymal Stem Cells for Tooth Tissue Engineering Using Fluid Shear Stress in a Rocking Culture Method. Tissue Eng Part C Methods, 2012.
48. Chen, W., et al., Human embryonic stem cell-derived mesenchymal stem cell seeding on calcium phosphate cement-chitosan-RGD scaffold for bone repair. Tissue Eng Part A, 2012.
49. Diekman, B.O., et al., Cartilage tissue engineering using differentiated and purified induced pluripotent stem cells. Proc Natl Acad Sci U S A, 2012.
50. Tan, Q., et al., Comparison of potentials of stem cells isolated from tendon and bone marrow for musculoskeletal tissue engineering. Tissue Eng Part A, 2012. 18(7-8): p. 840-51.

51. Cardwell, R.D., L.A. Dahlgren, and A.S. Goldstein, Electrospun fibre diameter, not alignment, affects mesenchymal stem cell differentiation into the tendon/ligament lineage. J Tissue Eng Regen Med, 2012.
52. Wang, S., et al., Fabrication and properties of the electrospun polylactide/silk fibroin-gelatin composite tubular scaffold. Biomacromolecules, 2009. 10(8): p. 2240-4.
53. Jiang, H., et al., Optimization and characterization of dextran membranes prepared by electrospinning. Biomacromolecules, 2004. 5(2): p. 326-33.
54. Dong, H. and W.E. Jones, Jr., Preparation of submicron polypyrrole/poly(methyl methacrylate) coaxial fibers and conversion to polypyrrole tubes and carbon tubes. Langmuir, 2006. 22(26): p. 11384-7.
55. Dong, C., et al., Preparation of PVA/PEI ultra-fine fibers and their composite membrane with PLA by electrospinning. J Biomater Sci Polym Ed, 2006. 17(6): p. 631-43.
56. Khajavi, R. and R. Damerchely, Effect of polyvinyl alcohol concentration in spinning dope on diameter, beads and HHS of produced nanofibers. Pak J Biol Sci, 2007. 10(2): p. 314-7.
57. Zhang, W.J., et al., Affinity peptide developed by phage display selection for targeting gastric cancer. World J Gastroenterol, 2012. 18(17): p. 2053-60
58. Shao, Z., X. Zhang, Y. Pi, X. Wang, Z. Jia, J. Zhu, L. Dai, W. Chen, L. Yin, H. Chen, C. Zhou, and Y. Ao, A MSC Homing Device Fabricated by Polycaprolactone Electrospun Mesh Conjugated with a MSC affinity, Biomaterials, 2012. 33(12): p. 3375-3387
59. Lee YM, Kim SS, Kim SH, Synthesis and properties of poly (ethylene glycol) macoromer/beta-Chitosan hydrogels. Journal of Materials Science: Materials in Medicine 1997:8: 537-541
60. Jia X, Burdick JA, Kobler J, Clifton RJ, Rosowski JJ, Zeitels SM, et al. Synthesis and characterization of in situ cross-linkable hyaluronic acid-based hydrogels with potential application for vocal fold regeneration. Macromolecules 2004:37:3239–48.
61. Yin W, Su R, Qi W, He Z. A casein-polysaccharide hybrid hydrogel cross-linked by transglutaminase for drug delivery. Journal of Materials Science, 2011
62. Choi CH, Jung JH, Rhee YW, Kim DP, Shim SE, Lee CS. Generation of monodisperse alginate microspheres and in situ encapsulation of cells in microfluidic device. Biomed Microdevices 2007:9:855–862
63. Li X, Liu T, Song K, Yao L, Ge D, Bao C, Ma X, Cui Z. Cultureof neural stem cells in calcium alginate beads. BiotechnolProg 2006:22:1683–1689.
64. Jin R, Hiemstra C, Zhong Z, Feijen J. Enzyme-mediated fast in situ formation of hydrogels from dextran–tyramine conjugates. Biomaterials 2007:28:2791–800.
65. Partap S, Muthutantri A, Rehman IU, Davis GR, Darr JA. Preparation and Characterization of controlled porosity alginate hydrogels made via a simultaneous micelle templating and internal gelation process. Journal of Materials Science, 2007, 10, 3501-3507.
66. Cai X, Lin Y, Ou G, Luo E, Man Y, Yuan Q, Gong P Ectopic osteogenesis and chondrogenesis of bone marrow stromal stem cells in alginate system. Cell BiolInt 2007:31:776–783

67. Barralet, JE, Wang L, Lawson M, Triffitt JT, Copper PR, Shelton RM. Comparison of bone marrow cell growth on 2D and 3D alginate hydrogels. Journal of Materials Science: Materials in Medicine. 2005:16:515-519
68. Wu MH, Pan WC. Development of microfluidic alginate microbead generator tunable by pulsed airflow injection for the microencapsulation of cells. MicrofluidNanofluid 2010:8:823–835
69. Rafat M, Li F, Fagerholm P, Lagali NS, Watsky MA, Munger R, et al. PEG-stabilized carbodiimidecrosslinked collagen–chitosan hydrogels for corneal tissue engineering. Biomaterials 2008:29:3960–72.
70. Hong Y, Song H, Gong Y, Mao Z, Gao C, Shen J. Covalently crosslinked chitosan hydrogel: properties of in vitro degradation and chondrocyte encapsulation. ActaBiomater 2007:3:23–31.
71. K. A. Smeds, and M. W. Grinstaff. Photocrosslinkable polysaccharides for in situ hydrogel formation. J. Biomed. Mater. Res. 2010:54:115–121.
72. Song P, Zhang Y, Kuang J. Preparation and characterization of hydrophobically modified phlyacrylamide hydrogels by grafting glycidyl methacrylate. Journal of Materials Science, 2007, 42, 8, 2775-2781
73. Baer AE, Wang JY, Kraus VB, Setton LA, Collagen geneexpression and mechanical properties of intervertebral disccell-alginate cultures. J Orthop Res 2001:19:2–10.
74. Bryant S, Chowdhury T, Lee D, Bader D, Anseth K. Crosslinkingdensity influences chondrocyte metabolism in dynamicallyloaded photocrosslinked poly(ethylene glycol) hydrogels. Ann Biomed Eng 2004:32:407–417.
75. Iwasaki N, Yamane ST, Majima T, Kasahara Y, Minami A, Harada K, et al. Feasibility of polysaccharide hybrid materials for scaffolds in cartilage tissue engineering: evaluation of chondrocyte adhesion to polyion complex fibers prepared from alginate and chitosan. Biomacromolecules 2004:5:828–33.
76. Lin XK, Chen L, Zhao YP, Dong ZZ, Synthesis and characterization of thermaoresponsive shape-memory poly(stearyl acrylate-co-acrylamide)hydrogels. Journal of Materials Science, 2010, 45, 2703-2707
77. Elisseeff J, Anseth K, Sims D, McIntosh W, Randolph M, Yaremchuk M, Langer R. Transdermal photopolymerization of poly(ethylene oxide)-based injectable hydrogels for tissueengineeredcartilage. Plast Reconstr Surg 1999:104:1014–1022.
78. Li Q, Williams CG, Sun C, Wang J, Leong K, and Elisseeff JH. Photocrosslinkable polysaccharides based on chondroitin sulfate. J. Biomed. Mater. Res. A. 2004:68A:28–33.
79. Dadsetan M, Szatkowski JP, Yaszemski MJ, and Lu LC. Characterization of photo-cross-linked oligo[poly(ethylene glycol) fumarate] hydrogels for cartilage tissue engineering. Biomacromolecules. 2007:8:1702–1709.
80. Tiwari A, Grailer JJ, SrikanthPilla, Steeber DA, and Gong S. Biodegradable hydrogels based on novel photopolymerizable guar gum–methacrylate macromonomers for in situ fabrication of tissue engineering scaffolds. ActaBiomaterialia 2009:5: 3441–3452
81. Burdick J, Chung C, Jia X, Randolph M, Langer R. Controlleddegradation and mechanical behavior of photopolymerizedhyaluronic acid networks. Biomacromolecules 2005:6:386–391.

82. Alice I. Chou,1 Steven B. Nicoll. Characterization of photocrosslinked alginate hydrogels for nucleus pulposus cell encapsulation. J Biomed Mater Res 2009:91A: 187–194.
83. Singh V, Tiwari A, Sanghi R. Studies on K2S2O8/ascorbic acid initiated synthesis of Ipomoea dasyspermaseed gum-g-poly(acrylonitrile): a potential industrial gum. J
84. Tan RW, Niu XF, Gan SL, Feng QL. Preparation and characterization of an injectable composite. Journal of Materials Science: Materials in Medicine. 2009:20:1245-1253.
85. Gerecht S, Burdick JA, Ferreira LS, Townsend SA, Langer R, and Vunjak-Novakovic G. Hyaluronic acid hydrogen for controlled self-renewal and differentiation of human embryonic stem cells. Proc. Natl. Acad. Sci. U. S. A. 2007:104:11298–11303.
86. Murua A, Portero A, Orive G, Hernandez RM, Castro MD, Pedraz JL. Cell microencapsulation technology: towards clinical application. J Control Release 2008:132:76–83
87. Salinas CN, Cole BB, Kasko AM, and Anseth KS. Chondrogenic differentiation potential of human mesenchymal stem cells photoencapsulated within poly(ethylene glycol)-arginine- glycine-aspartic acid-serine thiol-methacrylate mixed-mode networks. Tissue Eng. 2007:13:1025–1034.
88. Hwang NS, Varghese S, Zhang Z, and Elisseeff J. Chondrogenic differentiation of human embryonic stem cell-derived cells in arginine-glycine-aspartate modified hydrogels. Tissue Eng. 2006:12:2695–2706.
89. Reza A, Nicoll S. Hydrostatic pressure differentially regulatesouter and inner annulus fibrosus cell matrix production in 3d scaffolds. Ann Biomed Eng 2008:36:204–213.
90. Han J, Wang K, Yang D, Nie J. Photopolymerization of methacrylated chitosan/PNIPAAm hybrid dual-sensitive hydrogels as carrier for drug delivery. Int J BiolMacromol 2009:44:229–35.
91. Bencherif SA, Srinivasan A, Horkay F, Hollinger JO, Matyjaszewski K, Washburn NR. Influence of the degree of methacrylation on hyaluronic acid hydrogels properties. Biomaterials 2008:29:1739–49.
92. Benoit DSW, Durney AR, and Anseth KS. Manipulations in hydrogel degradation behavior enhance osteoblast function and mineralized tissue formation. Tissue Eng. 2006:12:1663–1673.
93. Madhumathi K, Binulal NS, Nagahama H, Tamura H, Shalumon KT, Selvamurugan N, et al. Preparation and characterization of novel b-chitin–hydroxyapatite composite membranes for tissue engineering applications. Int J BiolMacromol, 2009:44:1–5.
94. Chenite A, Chaput C,Wang D, Combes C, Buschmann BD, Hoemann CD, Leroux JC, Atkinson BL, Binette F, Selmani A. Novel injectable neutral solutions of chitosan form biodegradable gels in situ. Biomaterials, 2000:21:2155-2161
95. Berger J, Reist M, Mayer JM, Felt O, Peppas NA, Gurny R. Structure and interactions in covalently and ionically crosslinked chitosan hydrogels for biomedical applications. Eur J Pharm Biopharm, 2004: 57:19–34

Chapter 3. Fabrication of Electrospun titania-based nanofiber meshes and evaluations of the morphology and osteogenic potential

3.1 Fabrication and Characterization of Titania-Based Nanofiber Meshes

Electrospun ceramic nanofibers are made by starting polymer solution containing precursors of ceramics followed by high temperature pyrolysis. Numerous electrospun ceramic nanofibers, including silica (SiO_2) and titania (TiO_2) nanofibers, have been fabricated and studied. Electrospun TiO_2 nanofibers have been studied with particular interest because of well-studied precursors and wide applications. In this study, pure titania fibers and titania-silica fibers with different Ti/Si ratio are fabricated and the morphology of electrospun titania-based fibers are characterized.

3.1.1 Methods

The titania and silica/titania fibrous meshes were prepared from titanium(Ⅳ) isopropoxide(TiP), tetraethyl orthosilicate(TEOS), poly(vinyl pyrrolidone)(PVP, M_w≈1 300 000) and acetic acid. In a typical procedure, 0.5ml of TiP was mixed with 0.5ml ethanol and 0.5ml acetic acid. After 10min stirring, the sol was added to 1.5ml 6% and 10%PVP ethanol solution, followed by magnetic stirring for 30min.The starting solution of titania-silica fibers were made of sol containing 0.25ml of TiP, 0.25ml TEOS mixed with 0.5ml ethanol and 0.5ml acetic acid. Then the sol was added to 1.5ml 10%PVP ethanol solution. In the electrospinning set up, the collection distance was 10cm and the applied voltage was 8kV. The electrospun fibers were collected on the flat plate. Finally, the PVP was removed from these fibers by heating them in air at 700℃ for 3h.

Sample topography and cell morphology were examined by scanning electron microscopy (Hitachi S-4800) using a 15 kV accelerating voltage. Fiber diameter distribution was evaluated by image analysis software (ImageJ, NIH software) from three images of at least

two different samples. Fiber diameter was evaluated from at least 150 fibers at 16,000X magnification.

The chemical composition of the scaffolds was examined by XPS(Axis Ultra by Kratos Analytical Ltd.), of at least two different samples with 3 spots per sample. Additionally, crystal structure x-ray diffraction (XRD) was investigated by RAPID-S (Rigaku Denkico Ltd.)

3.1.2 Results

Figure 3-1 shows the SEM images of electrospun fibers. These images reveal that fibers have diameters varying from around 100nm to 300nm. Under lower magnification (**Figure 3-1**a,c,e), fibers in each group were evenly distributed in general, and higher magnification images (**Figure 3-1**b,d,f) revealed more detailed structures of the fiber. Comparing **Figure 3-1**b and **Figure 3-1**d, it is observed that the average diameter of fibers increases with the increasing starting polymer concentration. Also, even using the same concentration of starting polymer, pure titania meshes have thicker fibers than titania-silica50/50 hybrid meshes (**Figure 3-1**d, f). Besides the diameter, the existence of silica also has influences on fiber surface morphology. Figure 1d shows pure titania fibers have the formation of titania crystal clusters and the silica-titania50/50 fibers (**Figure 3-1**f) have smoother surfaces.

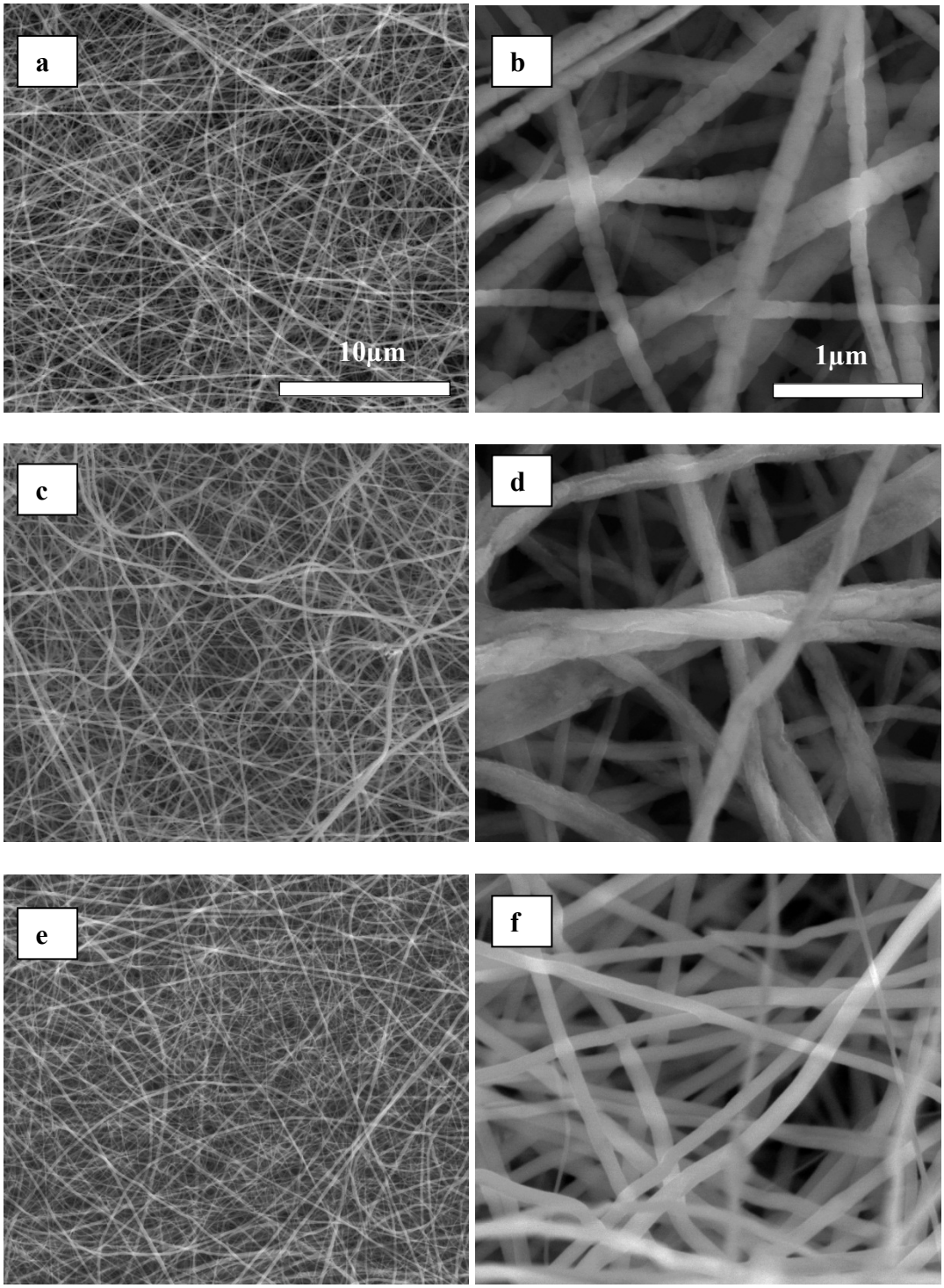

Figure 3-1. SEM images and analysis of the morphology of the electrospun nano-fiber silica-titania meshes produced with (a,b) 6% PVP TiO_2 (c,d) 10% PVP TiO_2 (e,f) silica-titania50/50

Figure 3-2 shows the diameter distribution of calcined fibers analyzed by image J. It confirms the observation of SEM images, which is 6%PVP titania fibers and 10%PVP titania-silica50/50 fibers have thinner diameter than 10%PVP titania fibers.

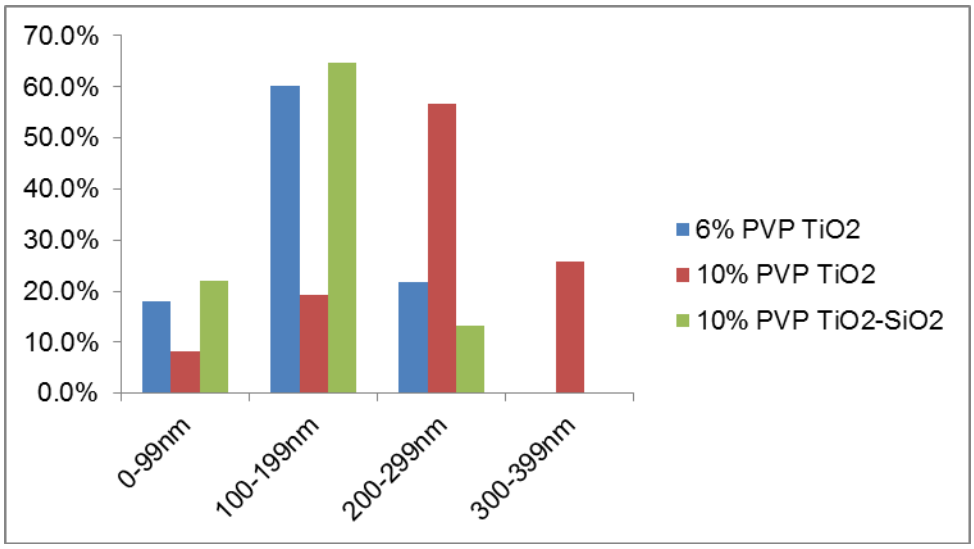

Figure 3-2. Histogram of diameter distribution of nano-fibers on the meshes

Chemical analysis by XPS (Table 1) showed no N, indicating PVP was removed thoroughly by the heat treatment. 6% PVP and 10% PVP titania fiber meshes were generally composed by Ti, O and small amount of silica as well. The titania-silica50/50 fiber mesh has Ti, Si and O, and the ratio of Ti to Si was 1:1, consistent with the initial molar ratio of TiP to TEOS. Typical XRD patterns of titania fibers and titania-silica50/50 fibers with heat treatment are shown in **Figure 3-3**. Two groups of titania fibers have similar spectra, which is presented in **Figure 3-3**a. The peaks of rutile and anatase crystal structures were found in the two groups of pure titania fibers. For titania-silica50/50 fibers, only the peaks of anatase were found and the peak intensity of hybrid fibers was also weaker than that of pure titania fibers.

Table 3-1. Elemental composition ± standard deviation (SD) of electrospun meshes analyzed by XPS

	Ti	Si	O	C
6%PVP-TiO_2	21.4±0.8	2.5±1.1	61.2±3.1	13.8±1.1
10%PVP-TiO_2	22.5±1.2	2.3±0.9	63.4±2.3	12.7±1.8
10%PVP-TiO_2-SiO_2	15.3±0.4	14.6±0.9	60.1±2.1	9.9±1.3

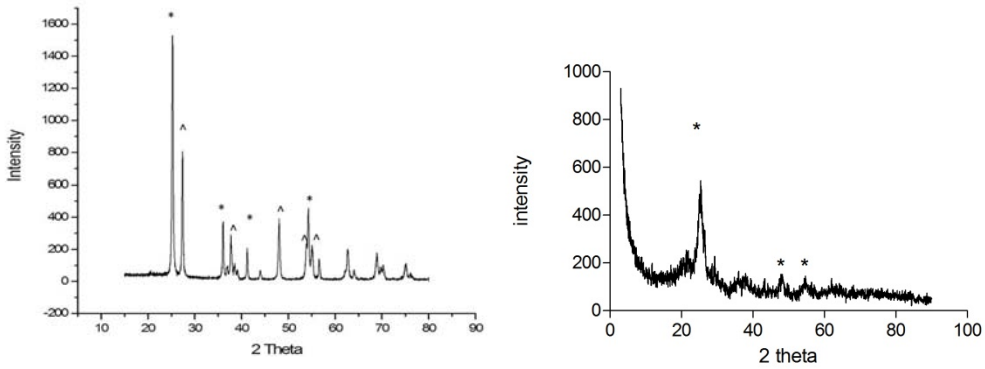

Figure 3-3. XRD spectra of (A) TiO_2 meshes and (B) silica-titania50/50 meshes. Respective rutile (^) and anatase (*) reference peaks are marked according to JCPDS database

In this study, pure titania and titania-silica50/50 ceramic fibrous meshes were made by electrospinning process and MSCs response on titania-silica fibers were evaluated. Factors which can influence the fiber diameter and fiber morphology of electrospun nanofibers were discussed in previous studies [1]. The concentration of starting polymer solution is the most commonly used method to adjust the electrospun fiber diameter. Generally, increasing polymer concentration is one of the major methods to increase electrospun fiber diameter [2]. For the pure ceramic electrospun fibers, which need heat treatment to remove the polymer component, the sol-gel content and calcination temperature can also contribute to fiber morphology [3]. When silica is added into the sol-gel system, even with the same concentration of starting polymer and same gel content, the fiber diameter is thinner than pure titania fibers. In addition, the additive of silica had influence on fiber surface morphology, too. The surface of titania-silica fiber is smoother than that of pure titania fiber. This result is further supported by XRD spectrum, which shows silica-titania has lower degree of crystallization under the same calcination temperature. After heating up to 700℃ for 3h, two groups of pure titania fibers formed rutile-anatase mixed crystals while silica-titania50/50 fibers formed not well-crystalized anatase crystals. Similar results were studied by heating the mixture of silica and titania nanoparticles [4], which shows the addition of silica affects crystal phase transformation of titania-silica particles. XPS results with the lack of N support the point that PVP was removed during calcination and the substrates are composed of silica and titania. The small amount of silica in titania fibers may be caused by calcining the fiber meshes on a silicon wafer.

3.1.3 Conclusion

In this study, submicron scale composite fibers titania-based ceramics with various compositions have been prepared by electrospinning. Pure ceramic fibers were obtained by heat treatment at 700℃ for 3h. SEM images showed the diameter and morphology of the

nanofibers were influenced by starting polymer concentration and sol-composition. The titania and titania-silica nanofibers have the average diameter around100~300nm. The fiber surface morphology and crystal phase was influenced by silica content.

3.2 Fabrication of Electrospun Silica-titania Nanofibers with Different Silica Content and Evaluation of The Morphology and Osteoinductive Properties

3.2.1 Introduction

A promising approach used for the regeneration of bone tissue involves seeding stem cells along with their differentiation-promoting growth factors onto porous, three-dimensional scaffolds [5]. The scaffold serves as an artificial extracellular matrix (ECM), which gives the cultured tissue both form and shape and maintains the native tissue contours. Fibrous biomaterials are one of the most promising types of scaffolds for tissue engineering due to their high porosity, high surface to volume ratio, and most importantly, the similarity to the natural extracellular matrix [6, 7]. Electrospinning provides a simple and versatile method for producing ECM-like fibrous structures from a rich variety of materials, including polymers and ceramics [8-14]. The morphology and properties of the nanofibers can be characteristically defined by modifying the concentration of polymer solution, solvent, applied electric field strength, and deposition distance [15-19].

Ceramic scaffolds have been considered as bone graft substitutes for bone regeneration applications because of their excellent biocompatibility and bioactive properties. It is also well known that titanium is widely used for implant applications because of its good mechanical properties and biocompatible oxide layer, titania. Similar to titania, silica-containing bioglass products can have beneficial osteoconductive functions. The silica-titania binary materials are widely studied for implant coatings [20-22], and it has been shown that ceramic coatings can enhance osteoblast maturation and osteo-differentiation of mesenchymal stem cells. In addition to the ceramic coatings, fibrous silica-titania materials have been fabricated and applied to various fields. [23-25] However, few studies have

investigated the effects of fibrous silica-titania ceramics of varying Ti:Si ratios on cell behavior.

Recent research has shown electrospun titania nanofibers have osteoionductive potential and the response of MG63 osteoblast-like cells can be regulated by manipulating nanofiber diameter and micro roughness [26]. Interestingly, surface roughness is not only affected by the fiber diameter, but also by the degree of crystallization and morphology of the fibers. Previous study showed that a different content of silica in silica-titania binary materials can influence the crystal phase of silica-titania nanoparticles [27]. But whether the crystallization degree of silica-titania materials also plays a role in cell response regulation is not known. In this study, the contributions of silica-titania nanofiber mesh properties to mesenchymal stem cell (MSC) response were evaluated by fabricating silica-titania electrospun nanofibers and modulating crystallization degree by changing the ratio of Ti/Si.

3.2.2. Materials and Methods

Fabrication and Characterization of Electrospun Silica-titania Fiber Meshes

Silica-titania nanofibrous meshes were prepared from a TiO_2 –SiO_2 mixed gel solution by hydrolyzing tetraethyl orthosilicate (TEOS) and titanium (IV) isopropoxide (TiP) in ethanol solution with acetic acid. The ratio of Ti/Si is shown in Table 3-1. In a typical procedure, 0.5ml sol was mixed with 0.5ml absolute ethanol, with 0.5ml glacial acetic acid used as catalyst. After stirring for 10 minutes, the solution was added to 1.5ml 10% PVP absolute ethanol solution, followed by magnetic stirring for 30 minutes. For the electrospinning setup, briefly, sol-PVP mixture was loaded in a plastic syringe with a flattened nozzle. Electrospinning proceeded with at 8kV, a 10cm collection distance and a 0.5ml/h feeding rate. The electrospun fibers were collected on a flat plate. Finally, the PVP was removed thoroughly by heating in air at 700°C for 3 hours.

Sample topography and cell morphology were examined by scanning electron microscopy (Hitachi S4800) using a 10 kV accelerating voltage. Fiber dimensions were evaluated using image analysis software (ImageJ, NIH software) from three samples per group; for each sample, three different fields of view were analyzed. Fiber diameter was evaluated from at least 270 fibers at 10,000X magnification.

The chemical composition of the scaffolds was examined by energy dispersive x-ray spectroscopy (Hitachi S4800 SEM/EDX) of at least two different samples per group with 3 locations per sample analyzed.

Surface roughness of the porous silica-titania meshes was evaluated using a laser confocal microscope (LEXT LCM, Olympus, Center Valley, PA). All LCM analyses were performed over a 644µm x 644µm area using a scan height step of 30nm, 20X objective, and a cutoff wavelength of 100µm. Three scans of at least two different samples per group were analyzed. The roughness parameters determined were mean surface roughness (R_a) and peak-to-valley ratio (Rz).

Additionally, crystal structure was determined by x-ray diffraction (XRD) and investigated by PANalytical XRD.

Cell Culture

MSCs were derived from the lower extremities of Wistar rats with approval of the animal ethics committee of Peking University Third Hospital. The adherent soft tissues of bones were cleaned, and epiphyses removed with scissors. The marrow was harvested by inserting a syringe needle (16-gauge) into each end of the bone and flushing repeatedly with phosphate buffered saline (PBS) supplemented with 100 U/ml penicillin and streptomycin into a 100mm culture dish. Cell suspension was obtained by drawing the marrow into a 20ml syringe through 22-gauge needles. The cells were centrifuged, counted, and seeded at a density of 1×10^6 in 8ml of α-MEM (Minimal Essential Medium) with 10% fetal bovine serum (FBS),

100 U/ml penicillin and streptomycin per 100mm culture dish, and cultured at 37°C in a 100% humidified atmosphere of 95% air and 5% CO_2. Non-adherent cells were removed at 3 days after seeding by changing the medium; thereafter, the medium was changed every 3 days. After 7 days of primary culture, when cell confluence was almost 80% of the dishes, the cell monolayers were digested by 0.25% trypsin/1mM EDTA for 3 minutes and cells of the 3rd to 5th passage were used for further analysis.

For cell culture on the fibrous meshes, MSCs were cultured in osteogenic media, containing Dulbecco's modified Eagle medium (DMEM) with 10% FBS, 1% penicillin and streptomycin, 100nM dexamethasone, 0.2mM ascorbic acid-2-phosphate and 10nM β-glycerol phosphate, at 37°C in 5% CO_2 and 100% humidity. Cells were grown on 12-well polystyrene tissue culture plates with cover glass as control and three different groups of the silica-titania meshes, at a density of 10,000cells/cm^2. MSCs were fed every 48 hours and harvested on day 6. Conditioned media were collected for assays and cell layers were washed twice with PBS, followed by two sequential incubations in 1ml of 0.25% trypsin/EDTA at 37°C for 10 minutes each time to release the cells from their substrate. Cells were then centrifuged at 2000rpm for 15 minutes, resuspended in 10 mL of saline solution and counted with a Z1 Coulter particle counter (Beckman Coulter, Brea, CA).

Biochemical Assays

Alkaline phosphatase (ALP) activity as well as osteocalcin (OCN) and osteopontin (OPN) secretion were measured using a quantitative enzyme-linked immunosorbent assay (ELISA). All the experiments were conducted strictly according to the instructions of the ELISA kits (ADL Inc., USA). The production of ALP, OCN and OPN were determined by absorbance measurement, using a microplate reader (BIO-RAD 550, Bio-Rad Laboratories Inc., USA). A set of standard samples were used to plot the standard curve of the absorbance. The ALP

activity, OCN and OPN secretion of the samples were calculated using the standard curve of the absorbance.

Statistical Analysis

Data from characterization of the silica-titania meshes are presented as the mean ± one standard deviation (SD) of all the measurements performed on different samples. Data from cell experiments are presented as mean ± standard error (SE) for six independent cultures. Data were evaluated by analysis of variance, and significant differences between groups were determined using Bonferroni's modification of the Student's t-test. A p value below 0.05 was considered to indicate a statistically-significant difference.

3.2.3 Results

The electrospinning process with TiP and TEOS in PVP was used to make relatively circular white scaffolds with an average diameter of 3.5cm. After the collected meshes were heated at 700˚C for three hours, the scaffolds became brittle and their diameter decreased to an average of 2.3cm. As the amount of titanium was increased, the scaffolds became more opaque.

Figure 3-4 a-c show SEM images of silica-titania hybrid nanofibers with different content of silica. The electrospun silica-titania fibers meshes had similar porous structures and fibrous diameters under magnification of 10,000X. The results of image analysis show silica-titania fibers were uniformly distributed with an average diameter between 100 to 300nm after heat treatment. By increasing content of titania, fibers had a slight increase in diameter.

Laser confocal microscope measurements (**Table 3-1**) revealed differences in the roughness of three groups of silica-titania meshes. The average roughness decreased as the silica content increased. Typical XRD patterns of silica-titania after 700ºC heat treatments were shown in **Figure 3-5.** The Ti:Si=3:7 group was amorphous, with only one broad peak around θ=22° corresponding to the (100) plane of amorphous phase of silica in the silica/titania composite fibers. This is the amorphous form of the silica crystalized phase (JCPDS 39-1425). With

increasing titania content, the anatase phase became more prominent. In the Ti:Si=7:3 group, each peak of titania was indexed and all of them were assigned to the tetragonal anatase. The peak values of the anatase phase were also consistent with reported values in the literature (JCPDS 21-1272). Chemical analysis by EDX (**Table 3-1**) show the fiber meshes containing Ti, Si and O elements, while N is not observed, indicating PVP was removed thoroughly by the heat treatment. Three groups of fiber meshes have molar ratios of Ti to Si of about 2:1, 1:1, 1:2, consisting with the initial molar ratio of TiP to TEOS.

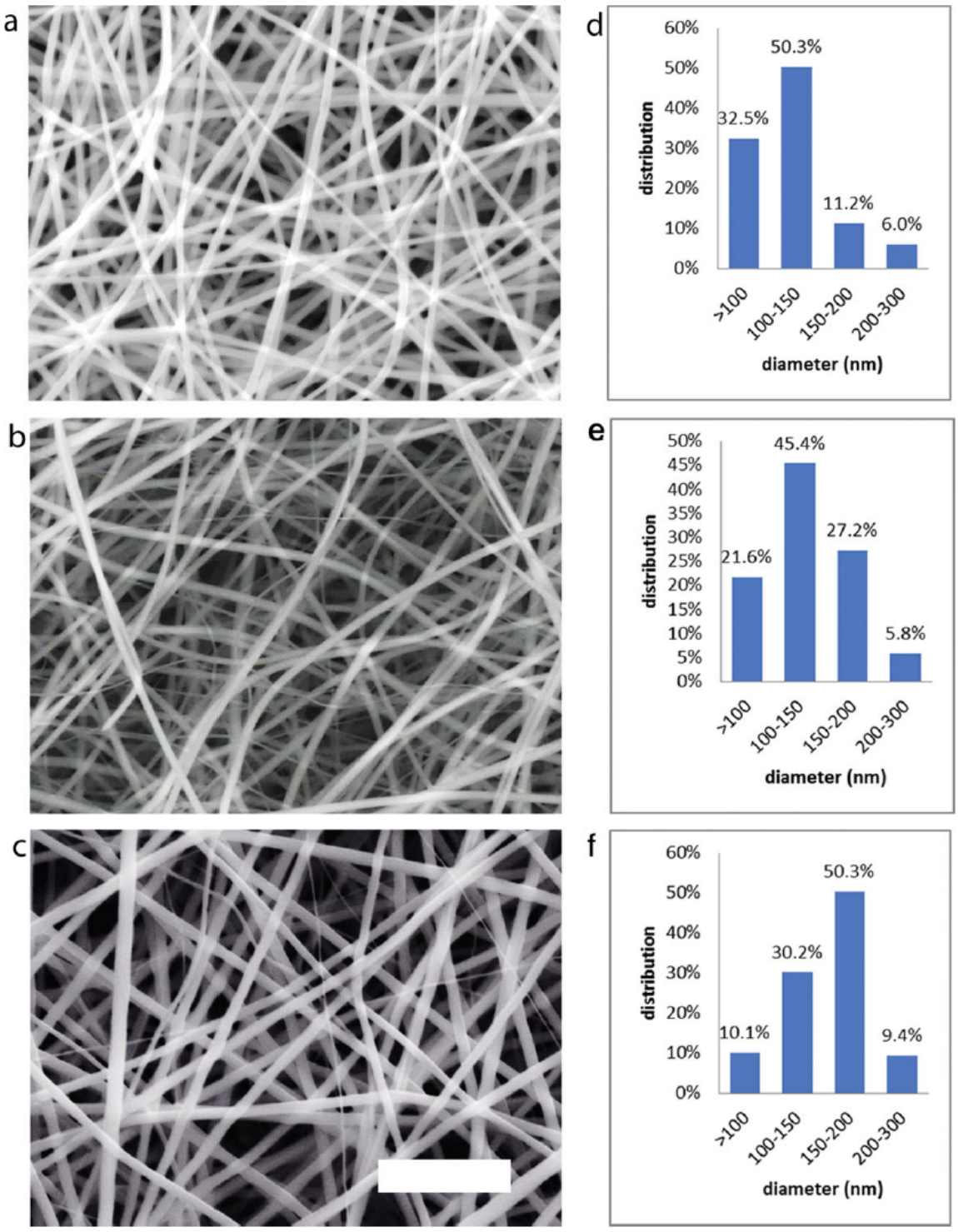

Figure 3-4. SEM images and analysis of the morphology of the electrospun nano-fiber silica-titania meshes produced with (a) Ti:Si=3:7 (b) Ti:Si=1:1 (c) Ti:Si=7:3, (d-f) histogram reveals thinner nano-fibers on the meshes with higher silica content compared to the meshes with lower silica content. The scale bar is 2µm

The cells of all the three mesh groups grew throughout the surfaces with similar morphology (**Figure 3-6**A showed the representative image of cell morphology). Cell number on all mesh groups was lower than that on glass. There was no difference between the Ti:Si=3:7 and the Ti:Si=1:1, while the Ti:Si=7:3 group had statistically lower cell numbers than the Ti:Si=3:7 group (**Figure 3-6**Ba). ALP activity was affected in the opposite way, with cells on the Ti:Si=7:3 group having the highest level of ALP enzymatic activity (**Figure 3-6**Bb). OCN levels were affected in a similar way to ALP activity. The Ti:Si=7:3 group had higher OCN levels when compared to the Ti:Si=3:7 and the Ti:Si=1:1 groups (**Figure 3-6**Bc). OPN levels were higher on the groups with higher Ti content, and OPN production on all mesh groups was significantly higher than the control group (**Figure 3-6**Bd).

Table 3-1. Elemental Composition and Surface Roughness ± standard deviation (SD) of titania-silica meshes

	Elemental Composition				Surface Roughness	
	Ti	Si	O	C	Sa(μm)	Sz(μm)
Ti:Si=3:7	14.38±1.26	27.22±2.33	56.38±1.02	2.02±0.99	0.50±0.01	14.79±1.82
Ti:Si=1:1	17.82±2.02	16.63±3.01	60.08±1.18	3.03±1.37	0.53±0.01	17.13±2.51
Ti:Si=7:3	26.42±3.56	14.08±2.27	58.70±2.01	0.99±0.52	0.77±0.02	25.64±3.08

Roughness of glass cover control: Sa= 0.35±0.01μm, Sz= 6.33±1.22μm

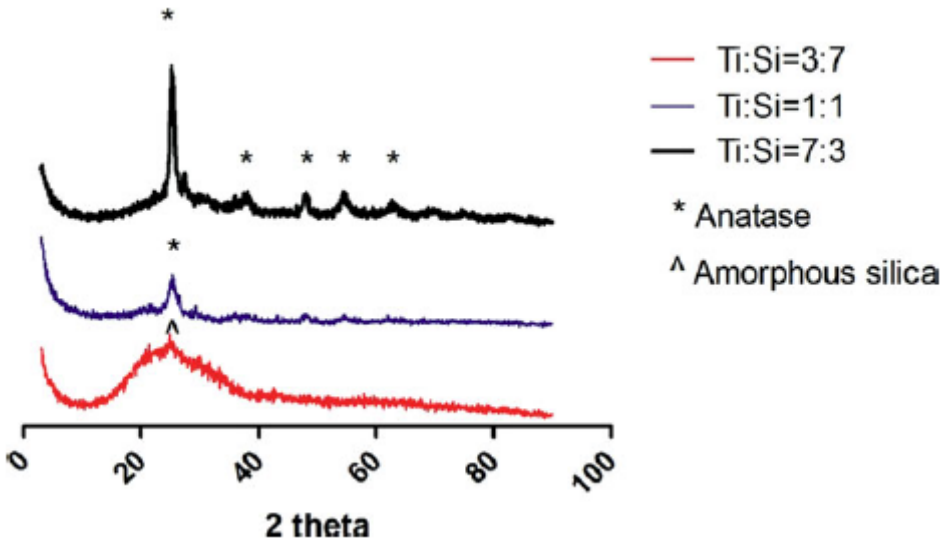

Figure 3-5. XRD spectra of three groups of nano-fiber meshes, and respective silica and anatase reference peaks (JCPDS database).

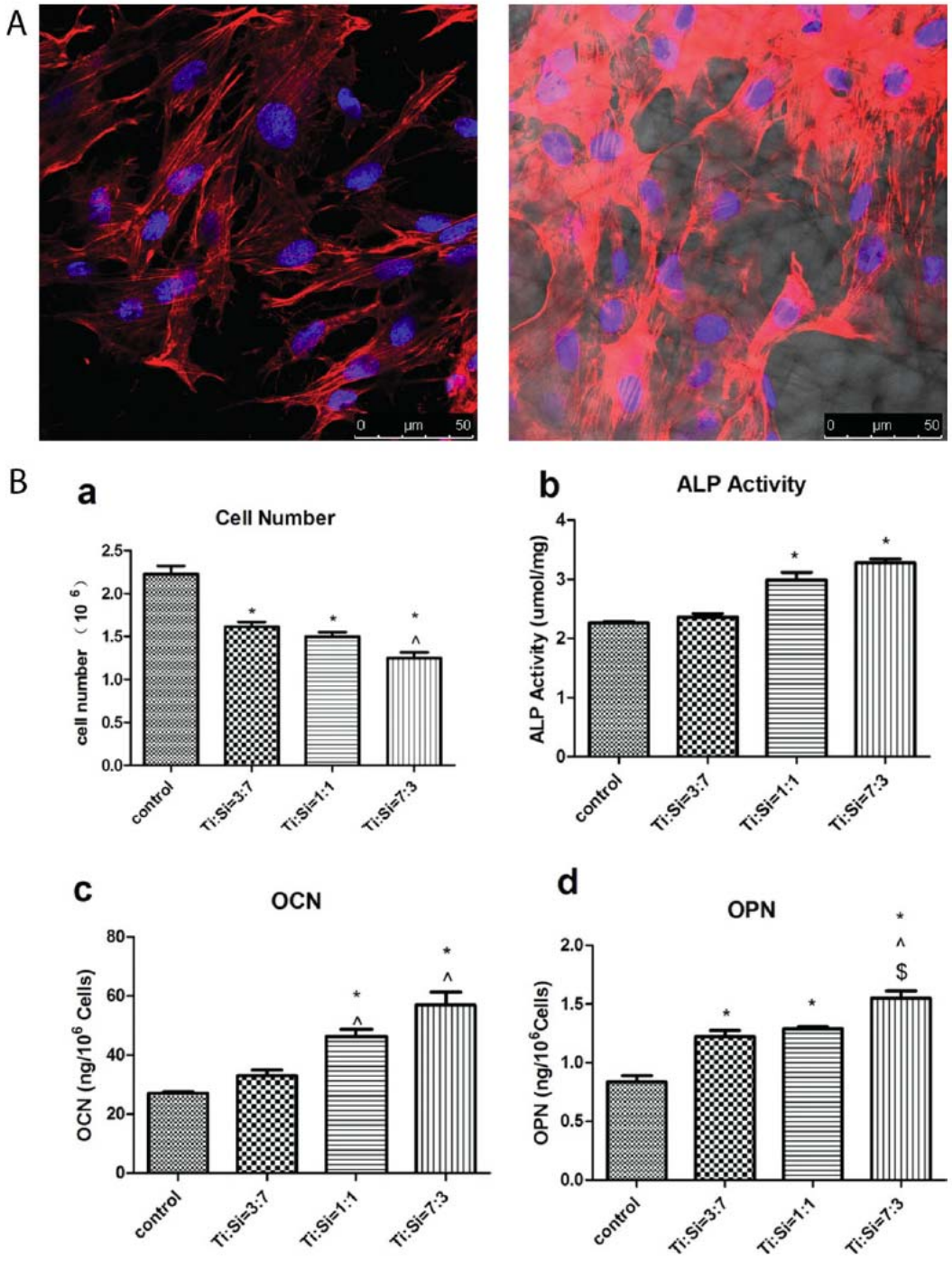

Figure 3-6. (A) Confocal Microscope images of the morphology of MSCs cultured on the nano-fiber silica-titania meshes. (B) Effects of structural properties of electrospun nano-fiber silica-titania meshes on MSCs osteogenic differentiation. (a) cell number, (b) ALP specific activity, (c) OCN, and (d) OPNlevels were measured. Data represented are the mean ± SE of six independent samples. * refers to a statistically-significant *p* value below 0.05 vs. control; ^ refers to a statistically-significant *p* value below 0.05 vs. Ti:Si=3:7; $ refers to a statistically-significant *p* value below 0.05 vs. Ti:Si=1:1

3.2.4 Discussion

In this study we created silica-titania hybrid meshes with different chemical compositions and crystal structures, which resulted in different surface roughness and nano-fiber diameter distribution. Factors which affect the morphology of inorganic electrospun nanofibers were shown by previous studies, including the concentration of polymer solution [27], the calcination temperature [38], the sol-gel content in polymer solution [29], and the ratio of the sol composition [30]. The image analysis of SEM images showed different fiber diameter distribution of three groups of silica-titania meshes. The titania content was directly related to the fiber diameter when PVP concentration is maintained. The thicker fiber diameter may be attributed to higher crystallization degree, which is supported by the XRD spectrum. The XRD spectrum showed that the Ti:Si=3:7 fibers were not well-crystallized and were composed mostly of amorphous silica and titania. With the increasing content of titania, under the same calcination temperature, a peak of crystallized anatase titania started to appear. In the Ti:Si=7:3 group, the anatase titania crystals were much better formed than in the Ti:Si=1:1 group. LCM measurements confirmed the difference in roughness among the three groups of meshes, where the Ti:Si=7:3 group was comparatively rougher than the other two groups. These results support previous observations that the surface roughness is affected by the fiber diameter distribution [26]. The EDX results showing the lack of N support the hypothesis that PVP was removed during calcination and the substrates were composed of silica and titania. Our results are in agreement with other studies on similar meshes made with 7% PVP after calcination at 700°C for 2 hours which have also found no additional weight loss measured by thermogravimetric analysis [31]. Cell morphology was found similar among the three groups of meshes, while cell number on the meshes was affected by the samples. All three groups of meshes had lower cell numbers than the glass control. However, differentiation of MSCs was stimulated compared to cultures on cover glass.

Alkaline phosphatase specific activity, which is an early marker of osteogenic differentiation, was significantly higher in the Ti:Si=1:1 and the Ti:Si=7:3 group when compared to the glass control. Osteocalcin, a late differentiation marker, had a similar trend with ALP activity, suggesting that MSCs were able to sense the different nanofibers, and thus, differentiation was enhanced on these samples. In addition, osteopontin, a highly phosphorylated sialoprotein that is a prominent component of the mineralized extracellular matrices of bones and teeth, also exhibited higher production on the electrospun substrates. Previous studies have shown that the surface roughness and morphology of substrates are considered to be modulators of cellular behavior. Many studies evaluating rough Ti/TiO_2 surfaces have reported the decreasing effect of surface roughness on cell number while promoting MSC differentiation toward osteoblasts [32-34]. These studies showed enhanced differentiation as evidenced by higher levels of alkaline phosphatase specific activity and osteocalcin compared to smooth surfaces using MG63s [34] and hMSCs [35]. In addition, three groups of electrospun substrates have variations in crystallinity, which has also been reported as a factor influencing cellular response. Studies on polymer crystallization [36] and bioglass crystallization [37] showed that crystallization degree can influence the surface nanotexture and cell response. Nevertheless, the results of those studies are inconsistent, and sometimes even contradictory. It has been shown that amorphous coating of calcium phosphate enhances bone formation [38], while some studies found the opposite results on similar materials [37,39]. In our study, higher crystallization of silica-titania binary materials enhanced MSC differentiation towards osteoblasts. Besides the differences in morphology, the substrates also have variations in chemical composition. Three groups of electrospun substrates all have elemental composition of Ti, Si and O, only with different Ti:Si ratios. According to the results, we found titania content was considered as an advantage for the cellular response. These results, together with the cell number, ALP, and OCN data suggest that surface

roughness combined with the degree of crystallization and titania content of TiO_2-SiO_2 meshes can synergistically drive the osteogenic differentiation process of MSCs.

3.2.5 Conclusion

In summary, we have evaluated the effect of silica content on the crystal phase and fiber diameter of silica-titania nanofiber meshes and the resulting osteoinductive effects of the meshes on MSCs. Factors of cell response such as cell number, differentiation, and local factor production were examined. The surface roughness, fiber diameter, and crystal phase of the meshes could be varied by only changing the ratio of sol composition. All silica-titania mesh groups supported MSC viability, as the cells grew throughout the entire surface. The silica-titania fibrous meshes enhanced the MSC osteogenic differentiation, as all experimental groups had higher levels of osteogenic differentiation markers when compared to the glass control. Cell morphology was similar in all three groups, while differentiation markers ALP, OCN, and the local factor OPN were all expressed at higher levels on the Ti:Si=7:3 group. These results indicate that cell response is sensitive to silica-titania substrates. In conclusion, this work demonstrates the potential of applying inorganic scaffolds with different physical parameters to drive cell differentiation and create an osteogenic environment for bone tissue engineering.

3.3 Effect of Structural Properties of Electrospun TiO_2 Nano-fibrous Meshes on their Osteogenic Potential

3.3.1 Introduction

The decade from 2001 to 2011 has been termed the "bone and joint decade", because it has been recognized that musculoskeletal injuries are the most reported health condition in the United States (US), with an associated cost close to 8% of the US gross domestic product in lost wages and healthcare related costs [40]. More than 25% of musculoskeletal injuries involve bone fractures, with many of these fractures not being able to heal by themselves, thus requiring some type of bone void filler that can promote bone regeneration and reduce healing time for the patient. With an aging population in developed countries and statistics showing, for example, that 1 in every 2 women over 50 years old will suffer an osteoporotic bone fracture [41], there is a pressing need to find reliable bone repair materials.

Tissue engineering offers a promising approach for repair and regeneration of damaged human tissue by mimicking the extracellular environment and taking advantage of the natural cues cells use to perform their role. A common methodology for bone tissue engineering is the fabrication of three-dimensional (3-D) porous scaffolds, which allow cells to invade the construct *in vitro* or *in vivo* and more closely mimic the native environment [42,43]. There are several methods to prepare porous scaffolds, such as freeze-drying and salt-leaching methods for polymer scaffolds [44], and replica methods used in ceramics [42,45]. Although discovered over 100 years ago [46], electrospinning has gained popularity recently as a simple and versatile method to produce fibrous structures from synthetic and natural polymers with nano- to micro-scale dimensions [46,47].

The electrospinning process has been extensively applied to create nano-fibrous scaffolds for cardiovascular [48], urologic [49] and bone tissue engineering applications [50], among others, using synthetic organic polymers such as poly(epsilon-caprolactone) (PCL)[51] and

poly(lactide-co-glycolide) (PLGA) [52]. Natural polymers such as collagen [53] and silk fibroin [54] have also been used in the electrospinning setup. Electrospun scaffolds have also been made using a composite of synthetic and natural polymers to take advantage of the mechanical properties of the former and the biological performance of the latter [55, 56]. These organic polymers can provide surfaces for cell attachment and growth, but it is often necessary to functionalize them, specifically for bone applications, with osteogenic molecules, such as hydroxyapatite (HA) [50] and growth factors like bone morphogenic proteins (BMP) [57] to promote cell differentiation.

Studies using solid substrate surfaces show that cell differentiation is sensitive to micro-scale and nano-scale topography [58-62]. When osteoblasts or mesenchymal stem cells (MSCs) are cultured on titanium substrates, which have an inherent TiO_2 passive oxide layer on the surface, they exhibit enhanced osteoblastic differentiation, particularly if the surface has both micro-scale and nano-scale features [63-65]. Whether surface structure also plays a role when cells are growing on nano-fibrous meshes is not known. The purpose of this study was to assess the contributions of nano-fiber dimensions and micro-scale pattern on cell response. To do this, pure TiO_2 nano-fibrous meshes were fabricated using electrospinning to have different surface micro-roughness and nano-fiber diameters.

3.3.2 Materials and Methods

Preparation of TiO_2 Scaffold

Titania nano-fibrous meshes were prepared from a TiO_2 gel solution prepared by hydrolysis of titanium(IV) isopropoxide (TiP) in poly(vinyl pyrrolidone) (PVP, $M_w \approx 300\ 000$) and acetic acid. Initially, 0.5 mL of TiP was mixed with 0.5 mL ethanol, with 0.5 mL acetic acid used as catalyst. After stirring for 10 minutes, the solution was added to 1.5 mL of 6% PVP or 10% PVP in ethanol solution, and magnetically stirred for 30 minutes. To produce electrospun nano-fiber meshes, 1 mL of such hybrid solution was loaded into a plastic

syringe with a blunt-ended stainless steel needle. The nano-fibers were spun using a feeding rate of 0.5 mL/h, a collection distance of 10 cm, and an applied voltage of 8 kV. To create a micro-scale pattern, the electrospun fibers were collected on a cross-hatched bronze net to imprint a pattern on the side of the mesh in contact with the collector. The PVP was removed from the fibers by heating in air at 700 °C for 3 hours.

Characterization of TiO_2 Scaffolds

Sample topography and cell morphology were examined by scanning electron microscopy (Ultra 60 FEG-SEM, Carl Zeiss SMT Ltd., Cambridge, UK) using a 5 kV accelerating voltage and 30 µm aperture. Fiber dimensions and pore sizes were evaluated using image analysis software (ImageJ, NIH software) from three images of at least two different samples. The chemical composition of the scaffolds was examined by energy dispersive x-ray spectroscopy (INCA EDX, Thermo Fisher Scientific, West Palm Beach, FL), with two different scaffolds per group analyzed in at least three different sites. Surface roughness of the porous TiO_2 meshes was evaluated using a laser confocal microscope (Lext LCM, Olympus, Center Valley, PA). LCM analyses were performed over a 644 µm x 644 µm area using a scan height step of 50 nm, a 20X objective, and a cutoff wavelength of 100 µm. Three scans each of at least two different samples per group were analyzed. The roughness parameters determined were mean surface roughness (S_a) and peak-to-valley height (S_z), and topographical images were also collected at the 20X magnification. Additionally, crystal structure x-ray diffraction (XRD) was investigated using 1.8 kW Cu Kα radiation, a 1° parallel plate collimator, a ¼ divergence slit, and a 0.04 rad soller slit (X'Pert PRO Alpha-1 diffractometer, PANalytical, Almelo, The Netherlands). Two samples per group were analyzed.

Cell Culture

MG63 cells (American Type Culture Collection, Rockville, MD) were cultured in Dulbecco's

Modification of Eagle's Medium (DMEM, cellgro® by Mediatech, Inc., Manassas, VA), containing 10% fetal bovine serum (Gibco, Carlsbad, CA) and 1% penicillin–streptomycin (Gibco), at 37°C in 5% CO_2 and 100% humidity. The MG63 cell line was originally derived from a human osteosarcoma and has been shown to exhibit many characteristics of pre-mature osteoblasts, making it an attractive model for *in vitro* studies [85-87]. Cells were grown on 24-well plate tissue culture polystyrene (TCPS) using a seeding density of 20,000 cells/well. Alternatively, cells were seeded onto two different formulations of the TiO_2 meshes (6% and 10% PVP), both on their flat and patterned sides. The meshes were slightly large to fit in a 24-well plate, so larger well-plates had to be used to avoid damage. Meshes were initially seeded in an untreated 6-well plate using a volume of 150 µL containing 20,000 cells to cover just the surface of the sample, and incubated for 4 hours to allow for initial cell attachment. Next, each well was brought up to a final volume of 2 mL and incubated for an additional 20 hours. After the first 24 hours, TiO_2 meshes were transferred to an untreated 12-well plate containing 1 mL of medium in each well. MG63 cells were fed every 48 hours until confluent on TCPS. Cells in all wells were then incubated with fresh media for 24 hours and harvested. Conditioned media were collected as described below. Cell layers were washed twice with DMEM, followed by two sequential incubations in 500 µL of 0.25% trypsin-EDTA (Gibco) for 10 minutes at 37°C to ensure all cells were released from their substrate. Cells were then centrifuged at 2000 rpm for 15 minutes, resuspended in 10 mL of saline solution and counted with a Z1 Coulter particle counter (Beckman Coulter, Brea, CA). Cells were centrifuged again at 2000 rpm for 15 minutes, the supernatant was decanted, and the cell pellets were resuspended in 500 µL of 0.05% Triton-X-100. Cells were lysed by sonication.

Biochemical Assays

Cell differentiation was evaluated as a function of alkaline phosphatase specific activity as an early differentiation marker, and osteocalcin content in the conditioned media as a late differentiation marker, as previously described [61]. Alkaline phosphatase specific activity was assayed as the release of *p*-nitrophenol from *p*-nitrophenylphosphate at pH 10.2 [88, 89] and values were normalized to the protein content, which was detected as colorimetric cuprous cations in a bicinchoninic reaction (BCA Protein Assay Kit, Pierce Biotechnology Inc., Rockford, IL, USA) at 570 nm (Microplate reader, BioRad Laboratories Inc., Hercules, CA, USA) [90]. Osteocalcin levels in the conditioned media were measured with a commercially available radioimmunoassay kit (Human Osteocalcin RIA Kit, Biomedical Technologies, Stoughton, MA) using a LS1500 gamma counter (Beckman Coulter, Brea, CA) as described previously [91]. The conditioned media were also assayed for protein levels of growth factors and cytokines, as described previously [92, 93]. Osteoprotegerin (OPG), a cytokine that works as a decoy receptor for receptor activator for nuclear factor κB ligand (RANKL) to inhibit osteoclastogenesis, was measured using an enzyme-linked immunosorbent assay (ELISA) kit (DY805 Osteoprotegerin DuoSet, R&D Systems, Minneapolis, MN). Vascular endothelial growth factor (VEGF), a growth factor involved in vasculogenesis and angiogenesis, was also measured using an enzyme-linked immunosorbent assay (ELISA) kit (DY293B VEGF DuoSet, R&D Systems).

3.3.3 Results

The process of electrospinning using the Ti (IV) isopropoxide and PVP mixture produced flexible, roughly-circular white meshes with an average diameter of 17 mm and less than 1 mm in thickness. After calcination at 700 °C for 3 hours, the meshes shrunk to an average diameter of 15 mm and became brittle. Laser confocal micrisopy (LCM) images **(Fig. 3-7)** showed topographical differences between the two sides of the 6% PVP (**Fig. 3-7 a, b**) and 10% PVP (**Fig. 3-7 c, d**) TiO_2 meshes. The surface of the meshes that was exposed to the

electrospinning setup was relatively flat, with fibers aligned randomly throughout the surface. In contrast, the surface of the mesh that was in contact with the cross-hatched bronze net used to collect the fibers retained the pattern stamped by the net, with bunches of aligned fibers forming ridges ranging from 13 to 26 μm in height. SEM images **(Fig. 3-8 a-d)** and image analysis **(Fig. 3-8 e, f)** revealed that the meshes were porous, with a similar average pore size of 1.44 ± 0.89 μm for 6% PVP scaffolds and 1.76 ± 1.00 μm for 10% PVP scaffolds. However, the higher magnification SEM images (**Fig. 3-8 b, d**) showed that changing the preparation from 6% to 10% PVP had an effect on the fiber diameter size, with the former having an average diameter of 184 ± 39 nm, and the latter a significantly larger average diameter of 343 ± 98 nm.

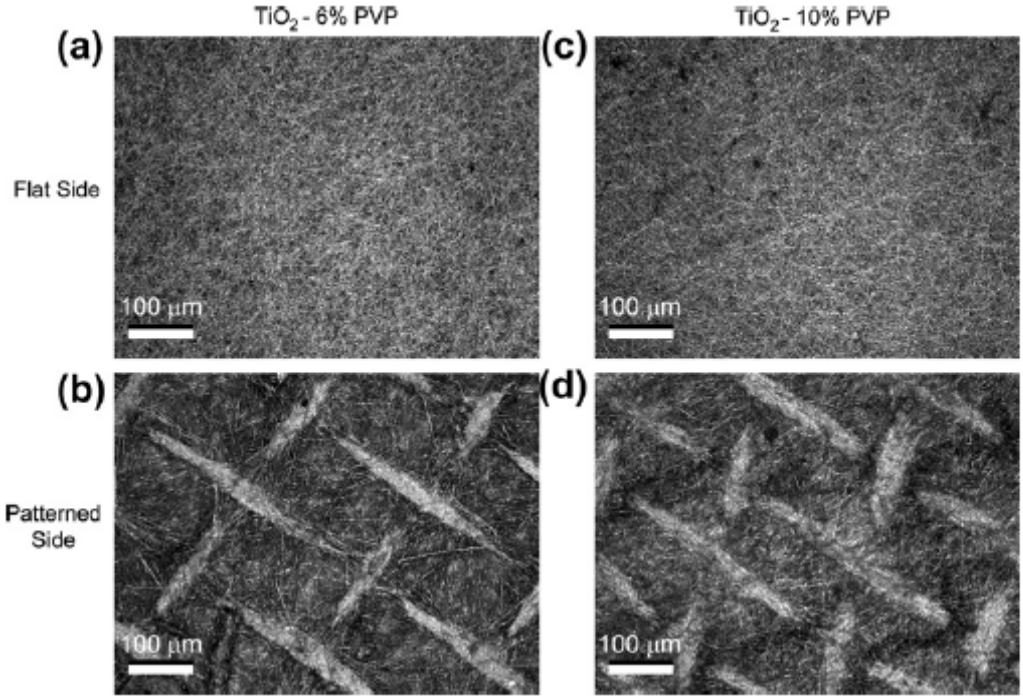

Figure 3-7. LCM images of both flat and patterned sides of the TiO2 meshes, made with 6% and 10% PVP. The nanofibers on the flat side of the meshes are randomly aligned, whereas the patterned side of the meshes has a clear cross-hatch pattern, with ridges of aligned nanofibers.

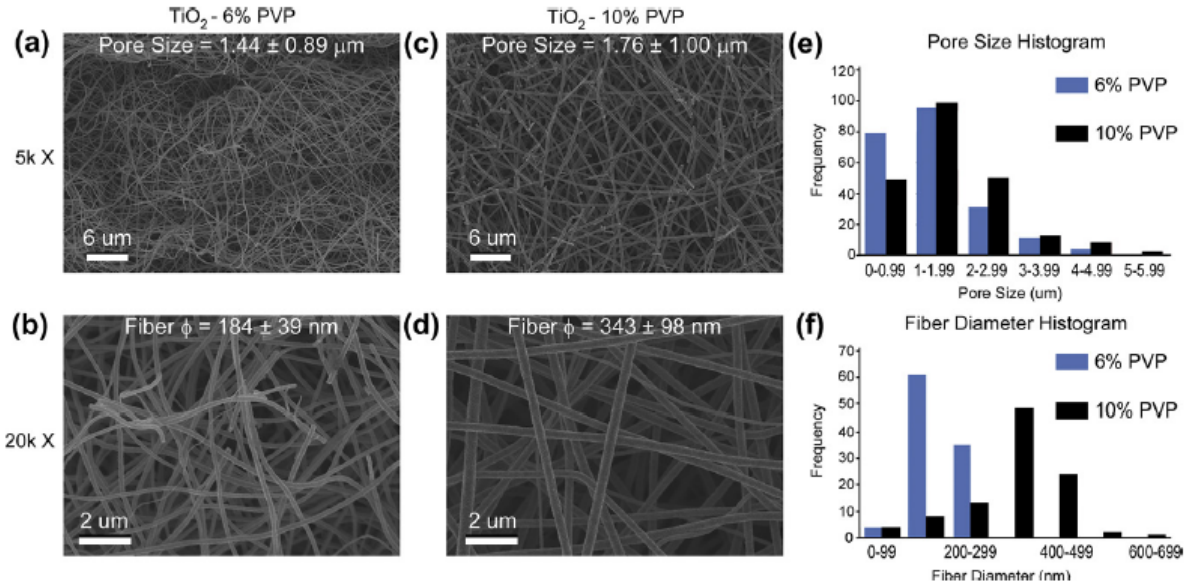

Figure 3-8. SEM images and analysis of the morphology of the electrospun nanofiber TiO2 meshes produced with (a,b) 6% or (c, d) 10% PVP. (e) Histograms at low magnification show similar pore sizes for both mesh formulations. However, (f) histograms at higher magnification reveal thinner nanofibers on the 6% PVP meshes compared to the 10% PVP.

LCM measurements **(Table 3-2)** revealed that the roughness of both 6% and 10% scaffolds was similar with their patterned side significantly rougher compared to the flat side. The X-ray diffraction (XRD) spectrum **(Figure 3-9)** of the nano-fibrous TiO_2 meshes presented main peaks for the rutile crystal structure. Chemical analysis by EDX **(Table 3-3)** showed that the initial PVP concentrations did not affect the final chemical composition after calcination, which included Ti and O as the major components with a molar ratio close to 1:2 consistent with the TiO_2 molecular formula. Small traces of Si and Ca were detected and no C from the PVP was found in the EDX spectra of all the samples.

Table 3-2. Surface roughness of TiO2 meshes measured by LCM.

Sample	Surface roughness (S_a, mean ± SD) (μm)	Peak-to-peak height (S_z, mean ± SD) (μm)
TiO_2–6% PVP (flat)	0.57 ± 0.02	12.06 ± 3.33
TiO_2–6% PVP (patterned)	2.68 ± 0.35	53.00 ± 14.44
TiO_2–10% PVP (flat)	0.61 ± 0.05	25.11 ± 7.33
TiO_2–10% PVP (patterned)	2.15 ± 0.57	62.71 ± 8.79

Table 3-3. Elemental composition of TiO2 meshes analyzed by EDX.

Sample	Concentration (mean at.% ± SD)			
	O	Ti	C	Si
TiO_2–6%PVP	61.1 ± 1.5	22.2 ± 2.0	11.8 ± 0.6	2.7 ± 1.2
TiO_2–10%PVP	63.7 ± 0.8	23.8 ± 0.8	8.94 ± 2.8	2.99 ± 2.2

Table 3-4. Surface elemental composition of TiO2 meshes analyzed by XPS.

Sample	Concentration (mean at.% ± SD)			
	O	Ti	Si	Ca
TiO_2–6% PVP	72.5 ± 2.0	27.4 ± 2.1	0.3 ± 0.0	–
TiO_2–10% PVP	73.9 ± 1.0	25.7 ± 1.1	0.3 ± 0.0	0.2 ± 0.0

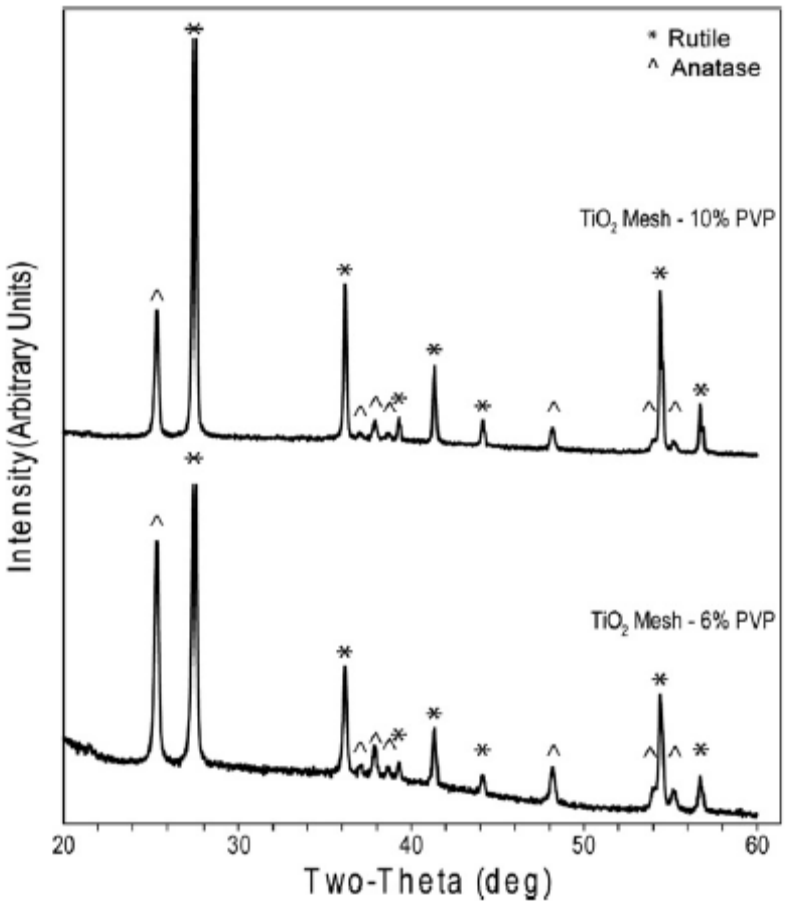

Figure 3-9. XRD spectra of 6% and 10% TiO2 nanofiber meshes.

Cell morphology was similar on flat **(Fig. 3-10)** and patterned **(Fig. 3-11)** sides of the TiO_2 meshes, regardless of the percent of PVP used during processing. The cells grew throughout the surface with elongated morphology and in some cases seemed to grow along some of the ridges of the patterned side and into the largest pores of both of the mesh. The response of the cells was sensitive to the micro- and nano-structure of the meshes **(Fig. 3-12)**. The number of cells on the patterned P6% and P10% groups were similar, but lower than the cell number of flat groups (Fig. 3-12 a). Cell numbers of all TiO_2 groups were lower than tissue culture polystyrene (TCPS). Alkaline phosphatase was affected in a similar manner, with cells on the patterned side of the meshes having lower levels of enzyme activity than cells on the flat side, regardless of the PVP preparation (Fig. 3-12 b). Osteocalcin levels were higher on the P10% group when compared to the F10% and P6% groups (Fig. 3-12 c). Osteocalcin levels were also higher on all TiO_2 meshes compared to TCPS. Osteoprotegerin (OPG) production was sensitive to both the micro-scale pattern of the surface and the size of the nano-fibers, as the levels were higher on the F10% group compared to F6%, and on both P6% and P10% groups compared to their flat sides (Fig. 3-12 d). Vascular endothelial growth factor (VEGF) production was higher on P6% and P10% groups compared to TCPS, with P10% being significantly higher than its flat counterpart F10% (Fig. 3-12 e).

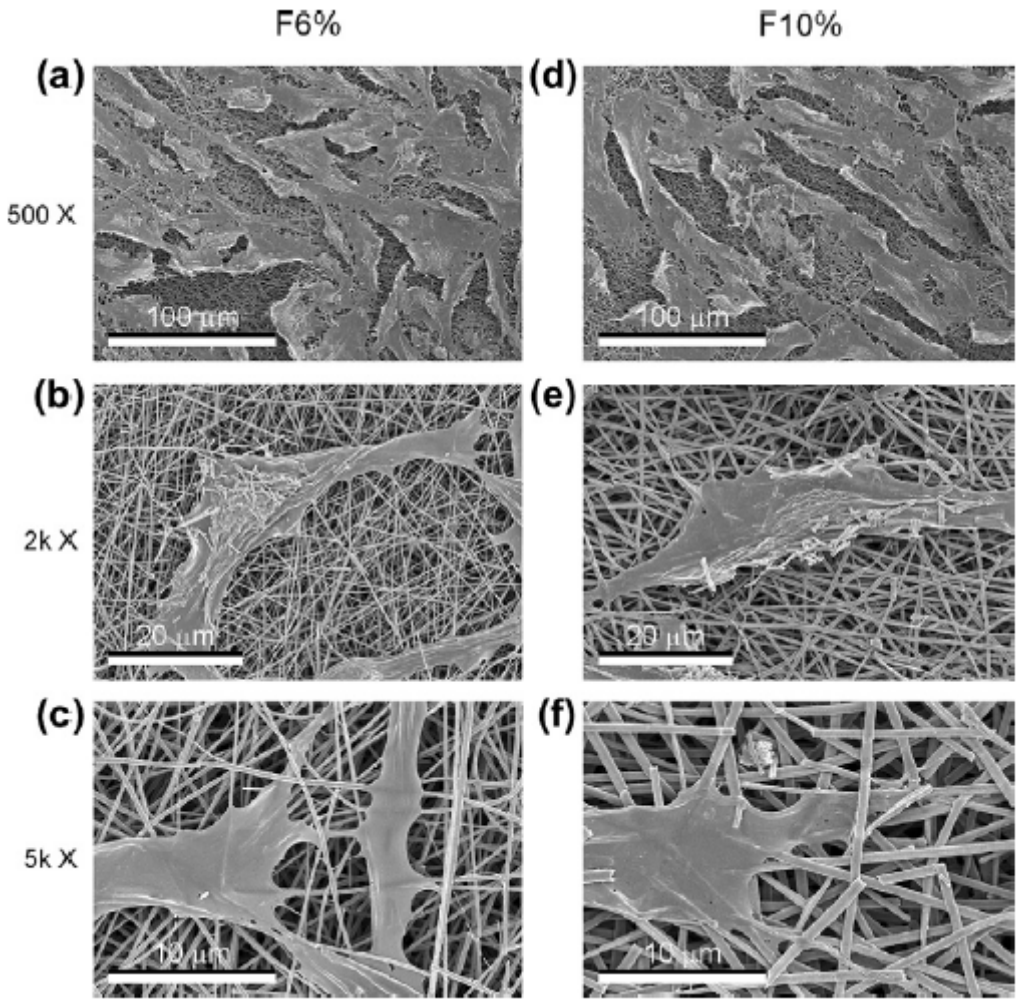

Figure 3-10. SEM images at different magnifications of the morphology of MG63 osteoblast-like cells cultured on the flat side of the nanofiber TiO2 meshes.

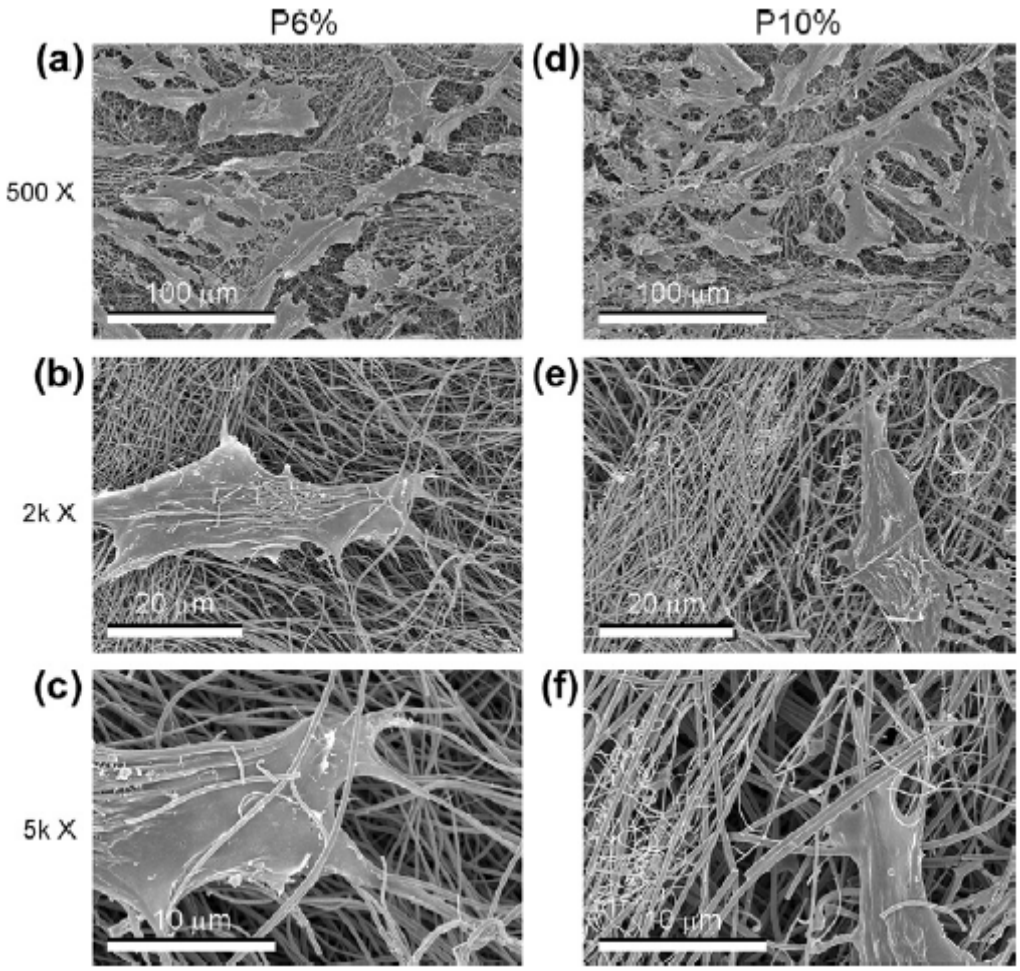

Figure 3-11. SEM images at different magnifications of the morphology of MG63 osteoblast-like cells cultured on the patterned side of the nanofiber TiO2 meshes.

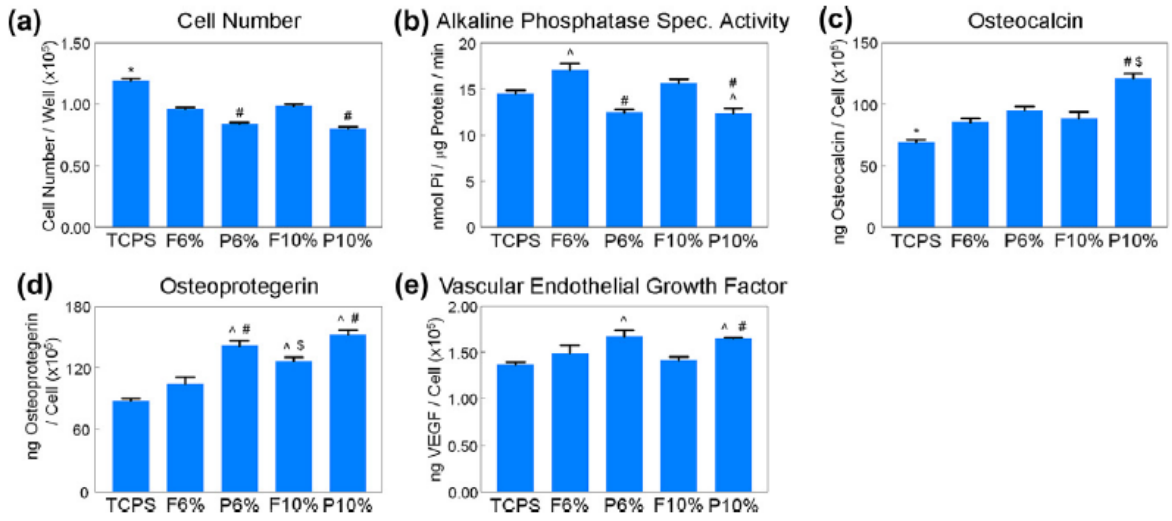

Figure 3-12. Effects of structural properties of electrospun nanofiber TiO2 meshes on osteoblast maturation. MG63 cells were plated on the flat or patterned side of both 6% and 10% PVP TiO2 meshes and grown to confluence. At confluence, (a) cell number, (b) ALP specific activity, (c) OCN, (d) OPG and (e) VEGF levels were measured. Data represented are the mean ± SE of six independent samples. ⁄Statistically significant p value below 0.05 vs. all TiO2 groups; ^statistically significant p value below 0.05 vs. TCPS; #statistically significant p value below 0.05 vs. flat side of the same formulation; $statistically significant p value below 0.05 vs. 6% PVP of the same side.

3.3.4 Discussion

In this study the electrospinning process was used to create pure TiO_2 meshes that had the same chemical composition and crystal structure, but different surface roughness and nano-fiber diameter. Differences in surface roughness were achieved by contrasting the side of each mesh that was exposed to the injection needle with the side that was in contact with the patterned bronze collector resulting in a cross-hatch pattern.

LCM measurements confirmed the difference in roughness between the two sides of the meshes, and showed that the patterned side was comparatively rougher than the flat side. These results using inorganic fiber meshes support previous observations showing that different collector patterns affect the topography and fiber alignment of polymeric electrospun meshes [66, 67].

By changing the PVP concentration of the starting solution from 6% to 10% PVP, the samples ended up with different average nano-fiber diameters. These results are consistent with previous studies on electrospun titania meshes [68-71], which showed that properties such as fiber diameter and pore size are dependent on electrospinning parameters such as PVP and titanium precursor concentrations, electric field strength, and solution feeding rate. Interestingly, these changes in surface roughness and fiber diameter were achieved without affecting the chemistry or the crystal structure of the substrates, thus emphasizing the effect of the structural variables of interest on cell response. In addition, the lack of C in the EDX spectra confirms that all PVP was removed during calcination and the substrates are, indeed, mainly composed of TiO_2.

Cell morphology was not sensitive to differences in micro-scale structure or nano-fiber diameter. However, cultures grew throughout the entire surface and interacted very closely with the nano-fibers. Even on the samples imprinted with the cross-hatch pattern, no major effects on cell morphology were observed, although a few cells did align with some of the

ridges. Previous studies on electrospun polymeric scaffolds reported preferential attachment of cells along patterned and aligned nano-fibers during early culture time points, but not after cells reach a larger percentage of confluence [72-80]. It is possible that during earlier time points in our study, cells alignment with the ridges of the cross-hatch pattern might have been more evident, although this was not evaluated in this study.

In the present study, the average pore size of the meshes was smaller than the size of the cells, so it was not possible for them to be incorporated into the mesh. However, cells still tried to migrate within the largest pores, as evidenced by single nano-fibers covering parts of their cell extensions. Previously, non-woven electrospun scaffolds seeded with human MSCs have been shown to support proliferation with even distribution inside the scaffolds after culture in a dynamic flow bioreactor, and to promote neo-vascularization within the scaffolds in a nude mouse subcutaneous model [81-87]. Conversely, it has been recently reported that most conventional electrospinning collecting systems result in tightly packed layers of nano-fibers that hinder cell infiltration [88]. The same group developed a new "focused, low-density, uncompressed nanofiber" (FLUF) collection system that results in loosely packed scaffolds with large pores that allow improved infiltration of cells.

Cell number on the TiO_2 meshes was affected by the surface roughness of the samples and not necessarily by the size of the nano-fibers. The rough side of both 6% and 10% PVP meshes had lower cell numbers than their smooth side. The effect of surface roughness on cell number has been previously reported by our lab and others for Ti/TiO_2 surfaces that promote osteoblast differentiation [72, 89-91]. The concept of decreased cell number on rougher surfaces that enhance osteoblast maturation has been explained as a transcriptionally regulated transition between cell proliferation and differentiation [92, 93]. In contrast, other groups have found higher cell numbers with an increase in nano-roughness [94], micro-roughness [95, 96] or a combination of both [73]. Our results are also in agreement with other

studies on electrospun polymeric scaffolds, which have found no effects on osteoblast proliferation due to nano-fiber alignment [79, 84] nor nano-fiber diameter [97].

Maturation of osteoblasts was controlled by a combination of surface roughness and fiber diameter on the TiO_2 meshes, or in other words a combination of micro-roughness and nano-topography created by the nano-fibers. Alkaline phosphatase specific activity, which is a marker of osteoblast differentiation expressed during early stages, was lower on the rough side of the 6% and 10% TiO_2 meshes and higher on the flat side of the 6% PVP meshes compared to TCPS. Osteocalcin, a late differentiation marker, was significantly higher on the rough side of 10% PVP meshes compared to all other groups, suggesting that osteoblast were able to sense the combination of micro- and nano-topography and, thus, differentiation was enhanced on these samples. Osteocalcin production was also dependent on the chemistry of the substrate, as levels on all TiO_2 meshes were higher than on TCPS. Many studies evaluating rough Ti/TiO_2 surfaces have reported enhanced differentiation as evidenced by higher levels of alkaline phosphatase specific activity and osteocalcin compared to smooth surfaces using MG63s [98] and hMSCs [61]. Our results are in agreement with other studies that have also found lower levels of alkaline phosphatase specific activity with associated higher production of osteocalcin on micro-rough surfaces [98, 99] or combined micro- and nano-rough surfaces that mimic bone structural hierarchy [68], suggesting a more mature osteoblastic phenotype. These results are attributed to the biphasic profile of alkaline phosphatase specific activity, with an earlier peak and subsequent downregulation in production that precedes the step-like upregulation of osteocalcin once the osteoblasts reach a certain stage of maturity [93]. Only few studies have looked at these differentiation markers on polymeric electrospun meshes, with no clear effect from nano-fiber alignment [84] or diameter [97].

In addition, local factors OPG and VEGF were also sensitive to the combination of surface roughness and nano-fiber diameter. OPG production was higher on the smooth side of the 10% meshes compared to the 6% meshes, favoring the larger nano-fiber diameter on flat substrates. However, the highest levels of OPG were found on the rough side of the 6% and 10% meshes compared to their smooth side. VEGF production had the highest levels on the rough side of both meshes compared to TCPS, with the 10% PVP mesh also having higher levels compared to its smooth counterpart. Overall, our results show enhanced osteoblast maturation and local factor production on rougher TiO_2 porous meshes with larger nano-fiber diameter of around 340 nm (*i.e.*, 10% PVP TiO_2 meshes). These results together with the cell number, ALP and OCN data suggest that surface roughness of porous TiO_2 substrates in combination with the nano-topography created by the fibers can drive the maturation process of osteoblasts on these surfaces.

3.3.5 Conclusions

In this study, we have evaluated the effect of porous and nano-fibrous TiO_2 meshes on the proliferation, differentiation, and local factor production of osteoblasts. The surface roughness and fiber diameter of the meshes could be varied without affecting their chemistry or crystal structure, emphasizing the effect of the structural parameters on cell response. The different TiO_2 mesh groups supported osteoblast viability, as the cells grew throughout the entire surfaces. The TiO_2 chemistry seemed to enhance osteoblast maturation, as all experimental groups had decreased proliferation and higher levels of differentiation markers compared to TCPS. Although cell morphology was similar on all TiO_2 mesh groups, cell response was sensitive to the substrate. Moreover, proliferation, differentiation and local factor production were regulated by different structural aspects of the meshes. Osteoblast proliferation was controlled by surface micro-roughness, whereas differentiation and local factor production were affected by both surface micro-scale pattern and nano-fiber diameter,

indicating that osteoblasts are sensitive to both the micro-roughness and the nano-topography created by the TiO_2 nano-fibers. Finally, the combination of micro-roughness with the nano-topography created by the larger nano-fibers enhanced osteoblast differentiation and local factor production, indicating that there might be a lower-limit threshold in the size of the nano-fibers that could be sensed by the osteoblasts to differentiate and generate an osteogenic environment. In conclusion, inorganic scaffold structural cues can be used to drive cell differentiation and create an osteogenic environment without the use of exogenous factors and, thus, structural parameters should be carefully considered when designing a scaffold for tissue engineering applications.

3.4 References

1. Jayesh Doshi, Darrell H. Reneker, Electrospinning process and applications of electrospun fibers. Journal of Electrostatics. 1995;35(2-3):151-160
2. Won Keun Son, Ji Ho Youk, Taek Seung Lee, Won Ho Park. The effects of solution properties and polyelectrolyte on electrospinning of ultrafine poly(ethylene oxide) fibers. Polymer. 2004;45(9):2959-2966
3. Bin Ding, Hakyong Kim, Chulki Kim, Myungseob Khil and Soojin Park, Morphology and crystalline phase study of electrospun TiO_2–SiO_2 nanofibres. *Nanotechnology, 2003;*14:532
4. Chang H., Kim S.H., Jang H.D., Cho S.W., Effect of SiO2 nanoparticles on the phase transformation of TiO2 in micron-sized porous TiO2–SiO2 mixed particles. Materials Letters. 2011, 65: 3272–3274
5. Yoshimoto H., Shin Y.M., Tera H., Vacanti J.P.. A biodegradable nanofiber scaffold by electrospinning and its potential for bone tissue engineering. Biomaterials. 2003, 24, 12: 2077-2082
6. Wei G., Ma P. Structure and properties of nano-hydroxyapatite/polymer composite scaffolds for bone tissue engineering. Biomaterials. 2004,25,19: 4749-4757
7. Tuzlakoglu K., Bolgen N., Salgado A. J., Gomes M. E., Piskin E. and Reis R. L.. Nano- and micro-fiber combined scaffolds: A new architecture for bone tissue engineering. Journal of Materials Science: Materials in Medicine. 2005, 16, 12: 1099-1104
8. Formhals A., Process and Apparatus for Preparing Artificial Threads. Us 1975504. 1934
9. Li M, Mondrinos MJ, Gandhi MR, Ko FK, Weiss AS, Lelkes PI. Electrospun protein fibers as matrices for tissue engineering. Biomaterials 2005, 26:5999–6008.
10. Wutticharoenmongkol P, Pavasant P, Supaphol P. Osteoblastic phenotype expression of MC3T3-E1 cultured on electrospun polycaprolactone fiber mats filled with hydroxyapatite nanoparticles. Biomacromolecules 2007, 8:2602–10.
11. Xin X, Hussain M, Mao JJ. Continuing differentiation of human mesenchymal stem cells and induced chondrogenic and osteogenic lineages in electrospun PLGA nanofiber scaffold. Biomaterials 2007, 28:316–25.
12. Chiu JB, Liu C, Hsiao BS, Chu B, Hadjiargyrou M. Functionalization of poly(L-lactide) nanofibrous scaffolds with bioactive collagen molecules. J Biomed Mater Res 2007, 83A:1117–27.
13. Shao C, Kim HY, Gong J, Ding B, Lee DR, Park SJ. Fiber mats of poly(vinyl alcohol)/silica composite via electrospinning. Mater Letters 2003, 57:1579–84.
14. Wu Y, Hench LL, Du J, Choy K-L, Guo J. Preparation of hydroxyapatite fibers by electrospinning technique. J Am Ceram Soc 2004, 87:1988–91.
15. Kim HW, Kim HE. Nanofiber generation of hydroxyapatite and fluor-hydroxyapatite bioceramics. J Biomed Res Part B 2006, 77B: 323–8.
16. Il-Doo Kim, Avner Rothschild, Byong Hong Lee, Dong Young Kim, Seong Mu Jo, and Harry L. Tuller, Ultrasensitive Chemiresistors Based on Electrospun TiO2 Nanofibers, nanoletters, 2006, 6(9): 2009-2013

17. Won Keun Son, Donghwan Cho, Won Ho Park, Direct electrospinning of ultrafine titania fibres in the absence of polymer additives and formation of pure anatase titania fibres at low temperature, nanotechnology, 2006, 17: 439-443
18. Eric Formo, Eric Lee, Dean Campbell, Younan Xia Functionalization of Electrospun TiO_2 Nanofibers with Pt Nanoparticles and Nanowires for Catalytic Applications, nanoletters, 2008, 8(2): 668-672
19. Sung Wook Lee, Young Un Kim, Sung-Seen Choi, Tae Young Park, Yong Lak Joo, Seung Goo Lee, Preparation of SiO2/TiO2 composite fibers by sol–gel reaction and electrospinning, materials letters, 2007, 61: 889-893
20. Young-Mi Kang a, Kyoung-Hwa Kim b, Yang-Jo Seol b, Sang-Hoon Rhee Evaluations of osteogenic and osteoconductive properties of a non-woven silica gel fabric made by the electrospinning method, Acta Biomaterialia 2009, 5: 462-469
21. Li P., Ohtsuki C., Kokubo T., Nakanishi K., Soga N., Groot K. The role of hydrated silica, titania, and alumina in inducing apatite on implants. Journal of Biomedical Materials Research 1994, 28, 1: 7-15
22. Dieudonn S.C., Dolder J., Ruijter J.E., Paldan H., Peltola T., van't Hof M.A., Happonen R.P., Jansen J.A. Osteoblast differentiation of bone marrow stromal cells cultured on silica gel and sol–gel-derived titania. Biomaterials. 2002, 23,14: 3041-3051
23. Kim P., Kim H., Joo J., Kim W., Song I.K., Yi J. Preparation and application of nanoporous carbon templated by silica particle for use as a catalyst support for direct methanol fuel cell. Journal of Power Sources 2005, 145, 2: 139-146
24. Ann M. Diskin, Robert H. Cunningham, R.Mark Ormerod The oxidative chemistry of methane over supported nickel catalysts. Catalysis Today. 1998, 46:147-154
25. Baglio V., Blasi A., AricòA. S., Antonucci V., Antonucci P.L., Trakanprapai C. , Esposito V., Licoccia S., and Traversa E. Composite Mesoporous Titania Nafion-Based Membranes for Direct Methanol Fuel Cell Operation at High TemperatureJ. Electrochem. Soc., 2005, 152, 7: A1373-A1377
26. Wang X., Gittens R.A., Song R., Tannenbaum R., Olivares-Navarrete R., Schwartz Z., Chen H., Boyan B.D. Effects of structural properties of electrospun TiO_2 nanofiber meshes on their osteogenic potential. Acta Biomaterialia. 2012, 8,2:878-885
27. Chang H., Kim S.H., Jang H.D., Cho S.W., Effect of SiO2 nanoparticles on the phase transformation of TiO2 in micron-sized porous TiO2–SiO2 mixed particles. Materials Letters. 2011, 65: 3272–3274
28. Li D, Xia YN. Fabrication of titania nanofibers by electrospinning. Nano Lett 2003;3(4):555-560.
29. Ding B., Kim H., Kim C., Khil M., Park S. Morphology and crystalline phase study of electrospun TiO2–SiO2 nanofibres. Nanotechnology 2003,14:532–537
30. Lee S.W., Kim Y.U., Choi S., Park T.Y, Joo Y.L., Lee S.G. Preparation of SiO2/TiO2 composite fibers by sol–gel reaction and electrospinning. Materials Letters 2007,61: 889–893
31. Park S-J, Chase GG, Jeong K-U, Kim HY. Mechanical properties of titania nanofiber mats fabricated by electrospinning of sol–gel precursor. J Sol-Gel Sci Technol 2010;54(2):188-194.

32. Zhao G, Zinger O, Schwartz Z, Wieland M, Landolt D, Boyan BD. Osteoblast-like cells are sensitive to submicron-scale surface structure. Clin Oral Implants Res 2006;17(3):258-264.
33. Kim MJ, Kim CW, Lim YJ, Heo SJ. Microrough titanium surface affects biologic response in MG63 osteoblast-like cells. J Biomed Mater Res A 2006;79(4):1023-1032
34. Zinger O, Zhao G, Schwartz Z, Simpson J, Wieland M, Landolt D, et al. Differential regulation of osteoblasts by substrate microstructural features. Biomaterials 2005;26(14):1837-1847.
35. Olivares-Navarrete R, Hyzy SL, Hutton DL, Erdman CP, Wieland M, Boyan BD, et al. Direct and indirect effects of microstructured titanium substrates on the induction of mesenchymal stem cell differentiation towards the osteoblast lineage. Biomaterials 2010;31(10):2728-2735
36. Newell R. Washburn, Kenneth M. Yamada, Carl G. Simon Jr. Scott B. Kennedy, Eric J. Amis, High-throughput investigation of osteoblast response to polymer crystallinity: influence of nanometer-scale roughness on proliferation. Biomaterials 2004; 25 1215–1224
37. M.C. Siebers, X.F. Walboomers, S.C.G. Leeuwenburgh, J.G.C. Wolke, J.A. Jansen, The influence of the crystallinity of electrostatic spray deposition-derived coatings on osteoblast-like cell behavior, *in vitro.* J Biomed Mater Res 2006; 78A: 258–267
38. Gross KA, Berndt CC, Goldschlag DD, Iacono VJ. *In vitro* changes of hydroxyapatite coatings. Int J Oral Maxillofac Implants 1997;12:589–597.
39. P. J. ter Brugge, J. G. C. Wolke, J. A. Jansen, Effect of calcium phosphate coating crystallinity and implant surface roughness on differentiation of rat bone marrow cells, Inc. J Biomed Mater Res 2002; 60: 70–78.
40. Jacobs JJ, Andersson GBJ, Bell JE, Weinstein SL, Dormans JP, Gnatz SM, et al. The burden of musculoskeletal diseases in the United States. Rosemont, IL: AAOS; 2008.
41. Agrawal CM, Attawia M, Borden MD, Boyan BD, Bruder SP, Bucholz RW, et al. Bone graft substitutes. Rosemont, IL: ASTM–AAOS; 2003.
42. Hing KA. Bioceramic bone graft substitutes: influence of porosity and chemistry. Int J Appl Ceram Technol 2005;2:184–99.
43. Lutolf MP, Hubbell JA. Synthetic biomaterials as instructive extracellular microenvironments for morphogenesis in tissue engineering. Nat Biotechnol 2005;23:47–55.
44. Heijkants RGJC, Van Tienen TG, De Groot JH, Pennings AJ, Buma P, Veth RPH, et al. Preparation of a polyurethane scaffold for tissue engineering made by a combination of salt leaching and freeze-drying of dioxane. J Mater Sci 2006;41:2423–8.
45. Miao XG, Tan DM, Li J, Xiao Y, Crawford R. Mechanical and biological properties of hydroxyapatite/tricalcium phosphate scaffolds coated with poly(lactic-coglycolic acid). Acta Biomater 2008;4:638–45.
46. Sill TJ, von Recum HA. Electro spinning: applications in drug delivery and tissue engineering. Biomaterials 2008;29:1989–2006.
47. Huang ZM, Zhang YZ, Kotaki M, Ramakrishna S. A review on polymer nanofibers by electrospinning and their applications in nanocomposites. Compos Sci Technol 2003;63:2223–53.

48. Stitzel J, Liu J, Lee SJ, Komura M, Berry J, Soker S, et al. Controlled fabrication of a biological vascular substitute. Biomaterials 2006;27:1088–94.
49. McManus M, Boland E, Sell S, Bowen W, Koo H, Simpson D, et al. Electrospun nanofibre fibrinogen for urinary tract tissue reconstruction. Biomed Mater 2007;2:257–62.
50. Venugopal JR, Low S, Choon AT, Kumar AB, Ramakrishna S. Nanobioengineered electrospun composite nanofibers and osteoblasts for bone regeneration. Artif Organs 2008;32:388–97.
51. Yoshimoto H, Shin YM, Terai H, Vacanti JP. A biodegradable nanofiber scaffold by electrospinning and its potential for bone tissue engineering. Biomaterials 2003;24:2077–82.
52. Li WJ, Laurencin CT, Caterson EJ, Tuan RS, Ko FK. Electrospun nanofibrous structure: a novel scaffold for tissue engineering. J Biomed Mater Res 2002;60:613–21.
53. Matthews JA, Wnek GE, Simpson DG, Bowlin GL. Electrospinning of collagen nanofibers. Biomacromolecules 2002;3:232–8.
54. Jin HJ, Chen JS, Karageorgiou V, Altman GH, Kaplan DL. Human bone marrow stromal cell responses on electrospun silk fibroin mats. Biomaterials 2004;25:1039–47.
55. Bhattarai N, Edmondson D, Veiseh O, Matsen FA, Zhang MQ. Electrospun chitosan-based nanofibers and their cellular compatibility. Biomaterials 2005;26:6176–84.
56. Zhang YZ, Ouyang HW, Lim CT, Ramakrishna S, Huang ZM. Electrospinning of gelatin fibers and gelatin/PCL composite fibrous scaffolds. J Biomed Mater Res B Appl Biomater 2005;72B:156–65.
57. Wagner WR, Hong Y, Huber A, Takanari K, Amoroso NJ, Hashizume R, et al. Mechanical properties and in vivo behavior of a biodegradable synthetic polymer microfiber extracellular matrix hydrogel biohybrid scaffold. Biomaterials 2011;32:3387–94.
58. Li CM, Vepari C, Jin HJ, Kim HJ, Kaplan DL. Electrospun silk–BMP-2 scaffolds for bone tissue engineering. Biomaterials 2006;27:3115–24.
59. Gao Y, Cao WL, Wang XY, Gong YD, Tian JM, Zhao NM, et al. Characterization and osteoblast-like cell compatibility of porous scaffolds: bovine hydroxyapatite and novel hydroxyapatite artificial bone. J Mater Sci Mater Med 2006;17:815–23.
60. Stein GS, Zhang Y, Hassan MQ, Li ZY, Stein JL, Lian JB, et al. Intricate gene regulatory networks of helix–loop–helix (HLH) proteins support regulation of bone-tissue related genes during osteoblast differentiation. J Cell Biochem 2008;105:487–96.
61. Olivares-Navarrete R, Hyzy SL, Hutton DL, Erdman CP, Wieland M, Boyan BD, et al. Direct and indirect effects of microstructured titanium substrates on the induction of mesenchymal stem cell differentiation towards the osteoblast lineage. Biomaterials 2010;31:2728–35.
62. Mendonca G, Mendonca DBS, Aragao FJL, Cooper LF. Advancing dental implant surface technology – from micron- to nanotopography. Biomaterials 2008;29:3822–35.
63. Mendonca G, Mendonca DBS, Simoes LGP, Araujo AL, Leite ER, Duarte WR, et al. The effects of implant surface nanoscale features on osteoblast-specific gene expression. Biomaterials 2009;30:4053–62.
64. Biggs MJP, Richards RG, Dalby MJ. Nanotopographical modification: a regulator of

cellular function through focal adhesions. Nanomedicine 2010;6:619–33.
65. Curtis ASG, Gadegaard N, Dalby MJ, Riehle MO, Wilkinson CDW, Aitchison G. Cells react to nanoscale order and symmetry in their surroundings. IEEE Trans NanoBiosci 2004;3:61–5.
66. Mendonca G, Mendonca DBS, Aragao FJL, Cooper LF. The combination of micron and nanotopography by H2SO4/H2O2 treatment and its effects on osteoblast-specific gene expression of hMSCs. J Biomed Mater Res A 2010;94A:169–79.
67. Kubo K, Tsukimura N, Iwasa F, Ueno T, Saruwatari L, Aita H, et al. Cellular behavior on TiO2 nanonodular structures in a micro-to-nanoscale hierarchy model. Biomaterials 2009;30:5319–29.
68. Gittens RA, McLachlan T, Olivares-Navarrete R, Cai Y, Berner S, Tannenbaum R, et al. The effects of combined micron-/submicron-scale surface roughness and nanoscale features on cell proliferation and differentiation. Biomaterials 2011;32:3395–403.
69. Franceschi RT, James WM, Zerlauth G. 1-Alpha,25-dihydroxyvitamin-D3 specific regulation of growth, morphology, and fibronectin in a human osteo-sarcoma cell-line. J Cell Physiol 1985;123:401–9.
70. Lajeunesse D, Kiebzak GM, Frondoza C, Sacktor B. Regulation of osteocalcin secretion by human primary bone-cells and by the human osteosarcoma cellline Mg-63. Bone Miner 1991;14:237–50.
71. Kieswetter K, Schwartz Z, Hummert TW, Cochran DL, Simpson J, Dean DD, et al. Surface roughness modulates the local production of growth factors and cytokines by osteoblast-like MG-63 cells. J Biomed Mater Res 1996;32:55–63.
72. Bretaudiere JP, Spillman T. Alkaline Phosphatases. Weinheim: Verlag Chemica; 1984.
73. Martin JY, Schwartz Z, Hummert TW, Schraub DM, Simpson J, Lankford J, et al. Effect of titanium surface-roughness on proliferation, differentiation, and protein-synthesis of human osteoblast-like cells (mg63). J Biomed Mater Res 1995;29:389–401.
74. Smith PK, Krohn RI, Hermanson GT, Mallia AK, Gartner FH, Provenzano MD, et al. Measurement of protein using bicinchoninic acid. Anal Biochem 1985;150:76–85.
75. Gundberg CM, Hauschka PV, Lian JB, Gallop PM. Osteocalcin – isolation,characterization, and detection. Methods Enzymol 1984;107:516–44.
76. Simonet WS, Lacey DL, Dunstan CR, Kelley M, Chang MS, Luthy R, et al. Osteoprotegerin: a novel secreted protein involved in the regulation of bone density. Cell 1997;89:309–19.
77. Raines AL, Olivares-Navarrete R, Wieland M, Cochran DL, Schwartz Z, Boyan BD. Regulation of angiogenesis during osseointegration by titanium surface microstructure and energy. Biomaterials 2010;31:4909–17.
78. Li D, Ouyang G, McCann JT, Xia YN. Collecting electrospun nanofibers with patterned electrodes. Nano Lett 2005;5:913–6.
79. Wang YZ, Wang GX, Chen L, Li H, Yin TY, Wang BC, et al. Electrospun nanofiber meshes with tailored architectures and patterns as potential tissueengineering scaffolds. Biofabrication 2009;1.
80. Li D, Xia YN. Fabrication of titania nanofibers by electrospinning. Nano Lett 2003;3:555–60.
81. Park S-J, Chase GG, Jeong K-U, Kim HY. Mechanical properties of titania nanofiber

mats fabricated by electrospinning of sol–gel precursor. J Sol–Gel Sci Technol 2010;54:188–94.
82. Rupp F, Scheideler L, Olshanska N, deWild M, Wieland M, Geis-Gerstorfer J. Enhancing surface free energy and hydrophilicity through chemical modification of microstructured titanium implant surfaces. J Biomed Mater Res A 2006;76A:323–34.
83. Massaro C, Rotolo P, De Riccardis F, Milella E, Napoli A, Wieland M, et al. Comparative investigation of the surface properties of commercial titanium dental implants. Part I. Chemical composition. J Mater Sci Mater Med 2002;13:535–48.
84. Ma J, He X, Jabbari E. Osteogenic differentiation of marrow stromal cells on random and aligned electrospun poly(l-lactide) nanofibers. Ann Biomed Eng 2010;39:14–25.
85. Meinel AJ, Kubow KE, Klotzsch E, Garcia-Fuentes M, Smith ML, Vogel V, et al. Optimization strategies for electrospun silk fibroin tissue engineering scaffolds. Biomaterials 2009;30:3058–67.
86. Murugan R, Ramakrishna S. Design strategies of tissue engineering scaffolds with controlled fiber orientation. Tissue eng 2007;13:1845–66.
87. Srouji S, Kizhner T, Suss-Tobi E, Livne E, Zussman E. 3-D nanofibrous electrospun multilayered construct is an alternative ECM mimicking scaffold. J Mater Sci Mater Med 2008;19:1249–55.
88. Blakeney BA, Tambralli A, Anderson JM, Andukuri A, Lim D-J, Dean DR, et al. Cell infiltration and growth in a low density, uncompressed three-dimensional electrospun nanofibrous scaffold. Biomaterials 2011;32:1583–90.
89. Wall I, Donos N, Carlqvist K, Jones F, Brett P. Modified titanium surfaces promote accelerated osteogenic differentiation of mesenchymal stromal cells in vitro. Bone 2009;45:17–26.
90. Zhao G, Zinger O, Schwartz Z, Wieland M, Landolt D, Boyan BD. Osteoblast-like cells are sensitive to submicron-scale surface structure. Clin Oral Implants Res 2006;17:258–64.
91. Kim MJ, Kim CW, Lim YJ, Heo SJ. Microrough titanium surface affects biologic response in MG63 osteoblast-like cells. J Biomed Mater Res A 2006;79:1023–32.
92. Stein GS, Lian JB, Stein JL, VanWijnen AJ, Montecino M. Transcriptional control of osteoblast growth and differentiation. Physiol Rev 1996;76:593–629.
93. Lian JB, Stein GS. Concepts of osteoblast growth and differentiation – basis for modulation of bone cell-development and tissue formation. Crit Rev Oral Biol Med 1992;3:269–305.
94. Han P, Ji WP, Zhao CL, Zhang XN, Jiang Y. Improved osteoblast proliferation, differentiation and mineralization on nanophase Ti6Al4V. Chin Med J (Engl) 2011;124:273–9.
95. Kubies D, Himmlova L, Riedel T, Chanova E, Balik K, Douderova M, et al. The interaction of osteoblasts with bone-implant materials. 1. The effect of physicochemical surface properties of implant materials. Physiol Res 2011;60:95–111.
96. Brett PM, Harle J, Salih V, Mihoc R, Olsen I, Jones FH, et al. Roughness response genes in osteoblasts. Bone 2004;35:124–33.
97. Badami A, Kreke M, Thompson M, Riffle J, Goldstein A. Effect of fiber diameter on spreading, proliferation, and differentiation of osteoblastic cells on electrospun

poly(lactic acid) substrates. Biomaterials 2006;27:596–606.
98. Zinger O, Zhao G, Schwartz Z, Simpson J, Wieland M, Landolt D, et al. Differential regulation of osteoblasts by substrate microstructural features. Biomaterials 2005;26:1837–47.
99. Zhao G, Raines AL, Wieland M, Schwartz Z, Boyan BD. Requirement for both micron- and submicron scale structure for synergistic responses of osteoblasts to substrate surface energy and topography. Biomaterials 2007;28:2821–9

Chapter 4. Three-dimensional titanium scaffolds promote osteoblast maturation and integrin α2β1 mediated mechanism

4.1 Introduction

Titanium and its alloys are the most commonly used materials for implants in dental and orthopedic applications because of their mechanical properties (*e.g.,* weight-to-strength ratio) and good biological performance [1, 2, 3]. Hierarchy surface roughness of metallic implants, such as those made from titanium, play an important role in osseointegration. Osseointegration of implants is critical for successful bone regeneration and healing in dental and orthopedic applications [4]. To enhance bone integration, micro-roughness has become a standard feature required for advanced osteogenic responses [5-7]. Nano-featured titanium surfaces also increase ALP activity and upregulate gene expression of the bone-related proteins [8, 9]. Compared to surface modification, 3D porous scaffolds allow for bone to grow into the component providing enhanced fixation and produces a system which enables stresses to be transferred from the implant to the bone [10].

Numerous investigations into porous materials started in 1930's [11, 12], including polymers, ceramics and metals [13, 14]. For bone tissue engineering, porous ceramics scaffolds, such as hydroxyapatite and calcium phosphatate were well studied and proven to have great biocompatibilities and bioactivities [15, 16]. However, the disadvantages of ceramics are also obvious. The poor mechanical properties limit the applications of porous ceramic materials for load bearing implants, so metals are still preferred for orthopedic load bearing applications. Galante *et al*. [17] pioneered the development of fiber-metal leading to its clinical use as a porous coating in hip and knee arthroplasty. In the last twenty years, a variety of porous coatings and materials have also been used to obtain biological fixation of porous implants and bone. The most common metallic materials include sintered Ti and beads, diffusion-bonded Ti, fiber metal and plasma-sprayed Ti, among others [7, 18, 19].

Recently, a new series of highly porous metals have been developed and applied in orthopedic surgery, such as porous tantalum and titanium foams made by various techniques [10, 20].

Clinical and histological evidence from retrieved implants clearly demonstrate that these porous surfaces enhance bone tissue in-growth and are effective in supplementing the stability of the implants by biological fixation [14, 21-23]. Boblyn *et al.* [24] used highly porous tantalum as implants and characterized the mechanical properties and bone ingrowth in dogs. The results show bone ingrowth increased from 13% at two weeks to 42~53% at 4 weeks. V.K. Balla *et al.* [10] also used porous tantalum structures to study the biological properties *in vitro*. A human fetal osteoblast cell line was used for the cell viability and proliferation assay. Previous studies have focused on the fabrication of porous metal implants and the influence of these implants on pre-osteoblast cells [25]. However, the osteoblast responses including other differentiation marker and local growth factors production on 3D porous scaffold has not been clearly investigated yet, especially for the combined effect of 3D feature with the surface roughness on osteoblasts have not been characterized. In this study, MG63 cells were selected as the major immature osteoblast model. MG63 cells are human osteosarcoma-derived osteoblast-like cells. This cell line has been well characterized and exhibits numerous osteoblastic traits that are typical of a comparatively immature osteoblast. Normal human osteoblasts were also used to confirm the results.

Osteoblasts interact with substrate via integrin binding to extracellular matrix proteins. Integrin expression is also substrate sensitive [26-28]. For instance, osteoblasts express primarily α5β1 when grow on TCPS, but they shift to express α2β1 when grown on Ti and Ti6Al4V alloy. Our previous study showed that the β1 subunit and α2β1 heterodimer play critical roles in osteoblast-response to microscale surface structure and surface energy of Ti substrate [29, 30]. However, whether β1 and α2β1 integrin also contribute to osteoblast

maturation on 3D Ti scaffolds is not known. In this study, wild type MG63 cells and integrin β1/α2β1 MG63 knockdown cells were seeded on Ti surfaces and 3D Ti scaffolds, and cell maturation and the role of integrin β1 and α2 were investigated.

4.2. Materials and Methods

4.2.1 Fabrication and characterization of 3D Ti scaffolds

Single orderly oriented titanium wire meshes (Xinxing Ti company, Anping, Hebei, China) were cut by laser cutter and the scaffolds were prepared by compressing four layers together. Briefly, four layers of single titanium wire meshes were placed together, pouched by hydraulic press using 5 tons pressure. The scaffold has the diameter of 15mm and thickness of 450~500μm. PT grade 2 titanium discs (Institute Straumann AG, Waldenburg Switzerland) were used as 2D surface control. To create the rough texture of 2D surface and 3D scaffold, 98% sulfate acid and 60% nitrite acid (ratio 1:1) mixture was used to etch the titanium surface. PT discs and 3D scaffolds were placed in the acid mixture, reacting in boiling water bath for 45 min. After acid etching, PT discs, acid etch PT discs, 3D scaffolds, acid etched 3D scaffolds were cleaned using standard procedure in our previous study [31]. Briefly, Ti disks were cleaned by sonication in 2% Micro-90 detergent (International Product Corporation, Burlington, NJ) in distilled, ultrapure water for 2 x 15 min followed by two 15 min rinses in ultrapure water. Samples were rinsed 2 x 15 min in sequential ultrasonic baths of reagent grade acetone, isopropanol, and ethanol. After cleaning, disks were rinsed with ultrapure water three times for 10 min in a sonicated bath. Cleaned disks were packed in self-sealed sterilization pouches (Cardinal Health, Dublin, OH) and autoclaved.

Sample morphology was characterized by scanning electron microscopy (SEM, Ultra 60 FEG-SEM, Carl Zeiss SMT Ltd., Cambridge, UK) using a 5 kV accelerating voltage and 30 μm aperture.

The chemical composition of the scaffolds and discs was examined by X-ray photoelectron spectroscopy (XPS; Thermo K-Alpha XPS, thermo Fisher Scientific, West Palm Beach, FL). The instrument was equipped with a mono chromatic Al Kα X-ray source (hv=1468.6eV) and spectra were collected using an X-ray spot size of 100 μm and a pass energy of 200 eV, with 1 eV increments, at 55° takeoff angle.

3D structure and surface roughness of the scaffolds was evaluated using laser confocal Microscopy (LCM; Lext LCM, Olympus, Center Vally, PA). LCM analysis was performed over a 100μm x 100um area using a scan height step of 30n and a cutoff wavelength of 100μm. Three scans of each sample and at least two different samples per group were analyzed.

4.2.2 Cell culture

Human Osteosarcoma-derived osteoblast-like cells (MG63) were obtained from the American Type Culture Collection (Rockvill, MD). MG63 cell line was a well characterized pre-mature osteoblast cell culture model for assessing responses to Ti surface structures [32, 33]. The construction and selection of transfected integrin β1 silenced (shITGβ1) and integrin α2β1 co-silenced (shITG α2β1) MG63 cells were described in our previous studies [29, 30]. The stable transfected MG63 cells were stored at -80°C. In this experiment, the stored cells were thawed and cultured until confluence on T-75 flask before plating on the scaffolds. Wild type, shITG β1, shITGα2β1 MG63 cells and normal human osteoblast cells (Lonza Group, Ltd, US) were cultured in Dulbecco's modified Eagle's medium (DMEM; Cellgro by Mediatech, Inc., Manassas, VA) containing 10% Fetal bovine serum (Gibco, Carlsbad, CA) and 1% penicillin-streptomycin (Gibco) at 37℃ in 5% CO_2 atmosphere and 100% humidity. For the control groups, cells were grown on 24-wells plate tissue culture polystyrene (TCPS) using a seeding density of 20,000 cells per well in 1ml full media. For the experimental groups, cells were seeded on PT, acid etched PT substrate, and 3D Ti, acid etched 3D Ti in

untreated 24-well plate of the same density as TCPS control. Cells were fed 24 hours after plating and every 48 hours until confluent on the TCPS. At confluence on TCPS, cells were fed with fresh media for 24 hours and harvested. Conditioned media were collected for ELISAs. Cell layers were washed twice with PBS, followed by 3 times 10 min incubation in 500µl of 0.25% trypsin-ethylenediaminetetraacetic acid (Gibco) at 37℃ to release the cell from surface and scaffolds. Cell suspensions were centriguged at 2000 rpm for 15min, resuspended in 10ml of saline solution and counted with a Z1 Coulter particle counter (Beckman Coulter, Brea, CA). After counting, cell suspensions were centrifuged again at 2000 rpm for 15 min, the cell pellets were resuspended in 500µl of 0.05% triton-X-100 and lysed by sonication.

To further study the continuous proliferation and differentiation potential in long time culture, cells were cultured on TCPS, PT and 3D Ti scaffolds for longer period of time. When cells reached confluence on TCPS, the day was marked as Day 0, then the cells were continued culturing for 2, 6, 8, 10, 12 days. At Day 2 (Day 6~12), cells were fed with fresh media for 24 hours and harvested using the same protocol.

4.2.3 Biochemical assays

Cell morphology was characterized by scanning electron microscopy (SEM, Ultra 60 FEG-SEM, Carl Zeiss SMT Ltd., Cambridge, UK) using a 5 kV accelerating voltage and 30 µm aperture.

MG63 cell maturation was evaluated by examining the alkaline phosphatase activity (ALP activity) and osteocalcin (OCN) content. ALP activity is an early differentiation maker of osteoblast, which was measured by determining p-nitrophenol (pNP) release from p-nitrophenylphosphate (pNPP) at pH 10.2 in the cell lysate and normalized to total protein content (Micro BCA Protein Assay kit, Pierce Biotechnology Inc., Rockford, IL, USA). OCN levels were measured a radioimmunoassay kit (Human OsteocalsinRIA kit, Biomedical

Technologies, Stoughton, MA). Protein levels of growth factors and cytokine were also assayed of the conditioned media as described previously [34]. Osteoprotegerin (OPG), which reduces the production of osteoclasts, by inhibiting the differentiation of osteoclast precursors, was measured using an enzyme-linked immunosorbent assay (ELISA) kit (DY805 Osteoprotegerin DuoSet, R&D Systems, Minneapolis, MN). Vascular endothelial growth factor (VEGF), a growth factor involved in vasculogenesis, was also measured using an ELISA kit (DY293B, VEGF DuoSet, R&D Systems, Minneapolis, MN). Osteocalcin, OPG and VEGF production were further normalized by the total cell number.

4.2.4. Statistical analysis

Data from characterization of the Ti scaffolds are presented as the mean ± one standard deviation (SD) of the measurements of chemical composition and surface roughness performed on four different groups of samples. Data from cell experiments are presented as mean ± standard error (SE) for six independent cultures. All experiments were repeated at least twice to ensure validity of the observations and the representative results from an individual experiment is shown. Data were evaluated by analysis of variance, and significant differences between groups were determined using Bonferroni's modification of Student's t-test. A p value below 0.05 was considered to indicate a statistically significant difference.

4.3. Results

4.3.1 Scaffold Preparation

The laser-cut Ti single layers produced circular meshes with an average diameter of 15 mm and a thickness of 200 μm. After compressing four layers together, the scaffolds had an average diameter of 15 mm and thickness of 500~550μm. Laser confocal microscope (LCM) images showed topographical structure of 3D titanium scaffolds (Fig. 1A). The average wire diameter and pore side length were around 150 μm and the pores were interconnected. SEM

images showed the surface morphology of the titanium wire of 3D scaffolds before and after acid etching (Fig. 1B-1E). The roughness was quantitatively measured by LCM (Table 1). The result showed that after 45 min acid etching, the surface roughness increased by 200nm in average.

Chemical analysis by XPS showed O and Ti as the main chemical species in all the groups. A small amount of Ca was detected in the 3D group, but after acid treatment, no Ca was detected. An increased amount of carbon contamination was also observed on both acid etching groups, as the percentage of carbon on the surfaces was significantly higher than non-etched surfaces (Table 1).

4.3.2 Cell Morphology and Proliferation

Cell morphology on 3D scaffolds was observed at confluence on TCPS and 12 days after confluence. At confluence on TCPS (about 5-6 days in culture), the cells on 3D scaffolds have two different morphologies (Fig. 2A, 2B). Elongated morphology was observed on the titanium wire, while in crossing space of two (or more) wires, the cells anchored to the wires and formed canopy-like morphology. Similar cell morphology was observed on acid etched 3D scaffolds (Fig. 2C, 2D). After 12 more days of culture, cells expanded across the whole top surface of scaffold (Fig. 2E). Cells were also observed from the bottom view of the scaffold (Fig. 2F).

4.3.3 MG63 Cell and Human Osteoblast Behavior at confluence on TCPS (day 0)

When the cells were confluent on TCPS (usually takes 5-6 days), the day was marked as day 0. The number of cells on scaffolds was significantly lower than those on PT and acid PT surfaces (Fig. 3A). The production of osteo-differentiation markers, ALP activity (Fig. 3B) and OCN (Fig. 3C) were found increased on the 3D and acid 3D scaffold group. The local growth factor, OPG and VEGF production (Fig. 3D, 3E) were affected in a similar manner, with cells on the 3D and acid 3D scaffold having significant higher levels than the 2D

surfaces. The effect of surface roughness on MG63 maturation was not as obvious, but the increased roughness did have a positive effect on MG63 maturation, as significant higher ALP activity level was observed with the acid 3D group and the highest production value of OCN, OPG and VEGF were all obtained from the acid 3D group. Normal human osteoblasts were affected by the 3D structure in a similar manner: cell number was lower and ALP activity and OCN level were significantly higher on the 3D scaffolds compared to 2D scaffolds (Fig. 4A-4C)

4.3.4 Roles of Integrin β1 and α2β1

Figures 5A-5E shows the cellular responses of wild type MG63 and silenced integrin β1 (shITGβ1) and α2β1 (shITGα2β1) MG63 on 3D scaffolds. All of the cells (WT, shITGβ1 and shITGα2β1) numbers on 3D and acid 3D scaffolds were lower than those on Ti surfaces (Fig 5A). When compared to the wild type MG63 cells, β1 silencing increased cell number on rougher surfaces (acid PT) and 3D/acid 3D scaffolds, but not on PT surfaces; α2β1 silenced cells had the highest cell number on scaffolds in comparison to the other two cell types of the same groups. The effects of integrin-silencing on osteoblast differentiation were also surface dependent. On PT surfaces, integrin-silencing didn't have significant effect in the production of all growth factors. On acid PT surfaces, ALP activities and OPG were reduced because of the integrin-silencing. On both 3D and acid 3D groups, both of the two differentiation markers, ALP activities and OCN, and local growth factors (OPG and VEGF) production in integrin knockdown MG63 cells were significantly lower than those of wild type MG63 cells. α2β1 silenced cells on 3D scaffolds had the lowest OCN, OPG, and VEGF compared to the wild type and β1 silenced cells. The enhanced ALP activities and VEGF production on 3D and acid 3D scaffolds of wild type MG63 cells were completely abolished by β1-silencing and OCN and OPG productions, the 3D structural effects on MG63 cells were partially

blocked by β1-silencing. α2β1 silencing completely blocked all the structural effect of 3D scaffolds.

4.3.5 MG63 Cell behavior during time

Cell number on the 3D scaffolds was lower in the early stage of culture time, and cell number continued to increase with time. In contrast, cell numbers on PT peaked after 8 days post confluence (Fig. 6A). Increased ALP activities were observed on 3D scaffolds in the early and late stage of culture. OCN production was five to eight fold higher at confluence and at 2 days post confluence when cells numbers were lower compared to cells on PT and TCPS. OCN production was two to three folds higher at later time points when the cells show a high proliferation rate (Fig. 6B, 6C). The local growth factors OPG and VEGF were affected by the 3D scaffold in a similar way (Fig. 6D, 6E)

Table 4-1. Elemental Composition and Surface Roughness ± standard deviation (SD)

	Elemental Composition				**Surface Roughness**
	Ti	O	C	Ca	Sa(μm)
PT	18.7±6.3	49.6±8.7	31.5±4.2	-	0.43±0.02
AcidPT	16.3±6.1	41.9±7.7	42.9±5.8	-	0.63±0.02
3D	19.8±6.6	52.1±9.0	19.6±7.8	3.0±2.2	0.60±0.02
Acid3D	18.4±5.8	45.7±9.9	35.2±6.4	-	0.83±0.03

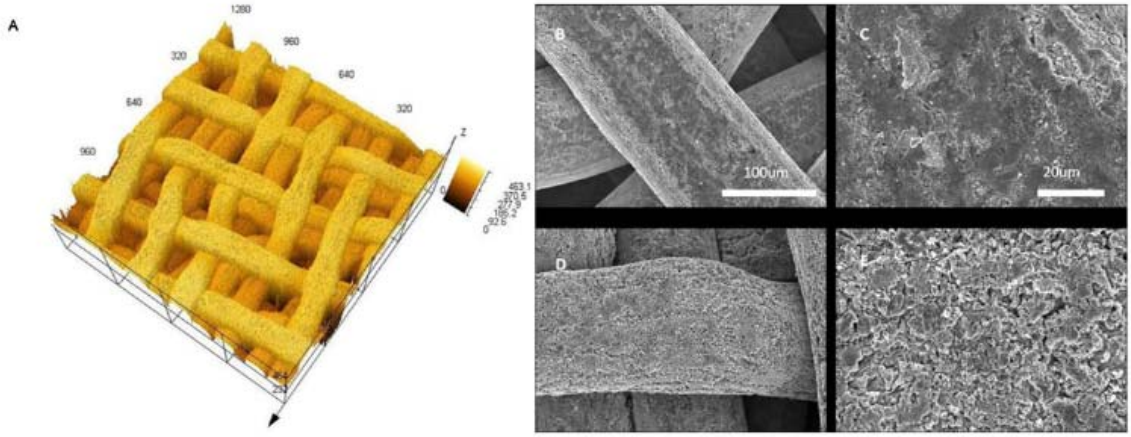

Figure 4-1 LCM and SEM imagens of 3D titanium scaffolds. A: the LCM image of 3D scaffold, which has interconnected porous structure. B-E: the surface structure of un-etched (B.C) and acid-etched (D,E) titanium wire. Increased surface roughness were observed on acid-etched surfaces.

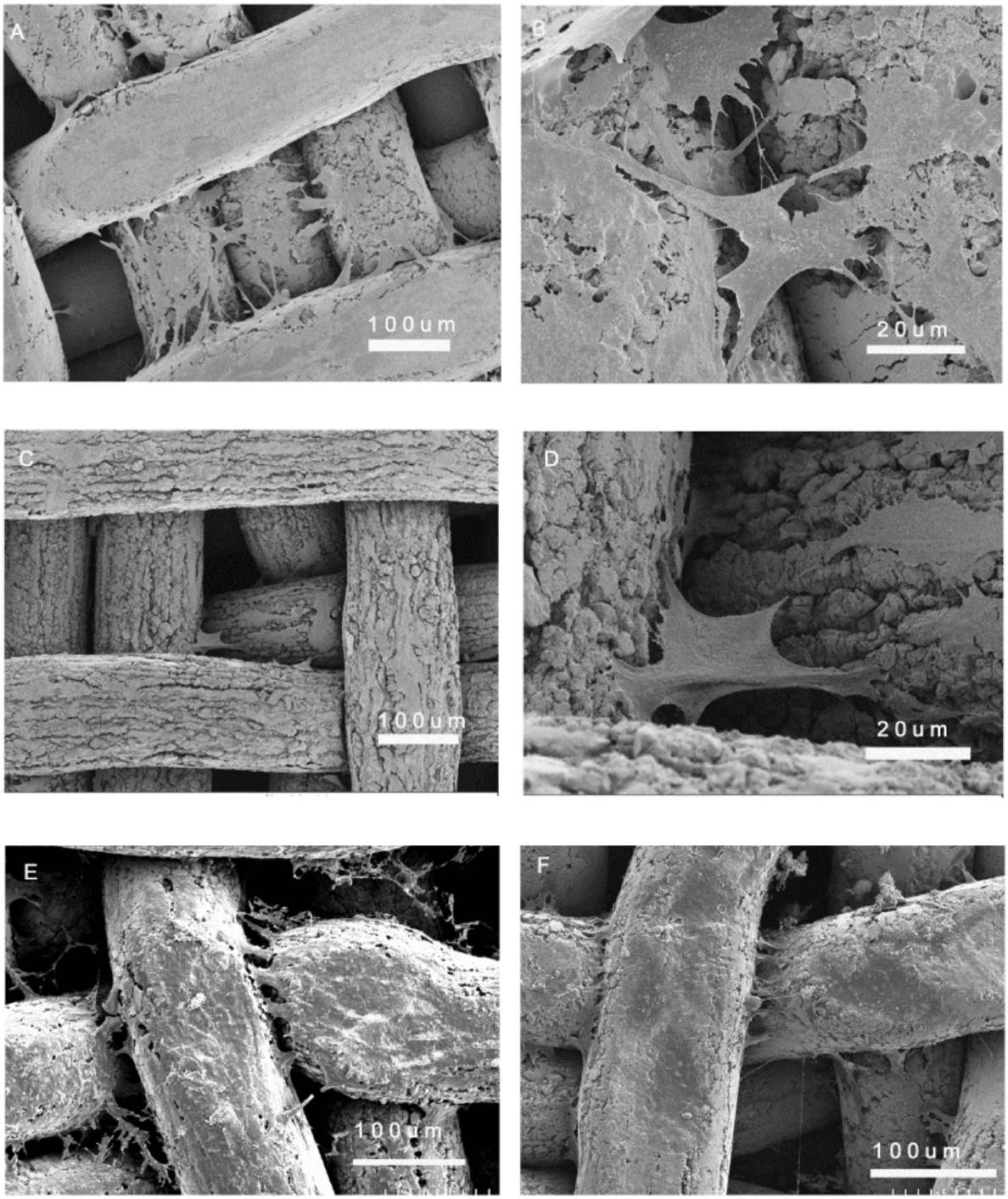

Figure 4-2. SEM images at different magnifications of the morphology of MG63 osteoblast-like cells cultured for 6 days on the 3D scaffolds (A,B) and acid-etched 3D scaffolds (C,D) and for 18 days on the top surface (E) and bottom surface (F) of 3D scaffolds.

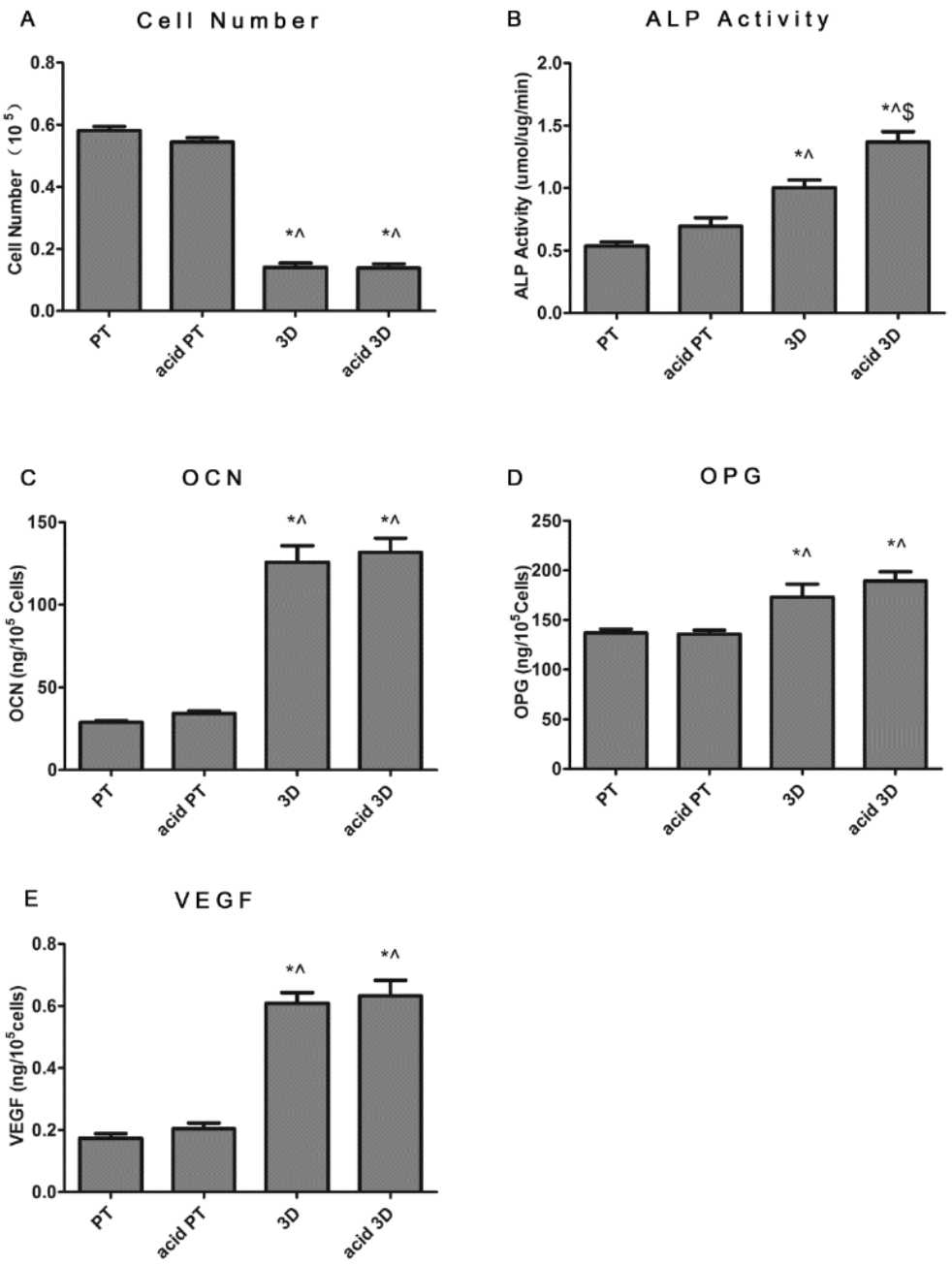

Figure 4-3. Effects of structural properties of 3D scaffolds combined with surface roughness modificationon MG63 maturation. MG63 cells were plated on the PT, acid PT, 3D and acid 3D scaffolds and harvested at confluence on TCPS. (a) Cell number, (b) ALP specific activity, (c) OCN, (d) OPG, and (e) VEGF levels were measured. Data represented are the mean ± SE of six independent samples. * refers to a statistically-significant *p* value below 0.05 vs. PT; ^ refers to a statistically-significant *p* value below 0.05 vs. acid PT; $ refers to a statistically-significant *p* value below 0.05 vs. 3D.

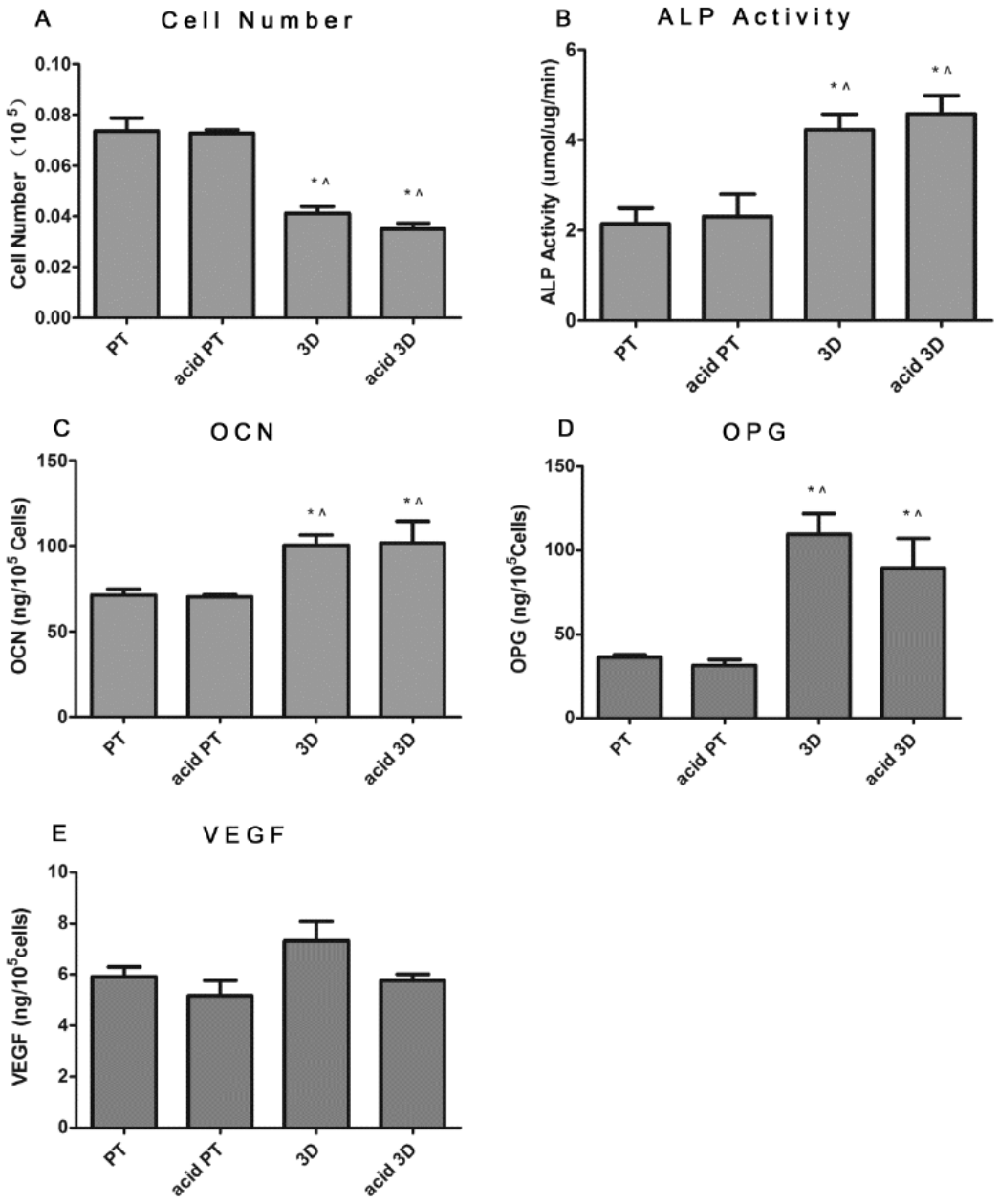

Figure 4-4. Effects of structural properties of 3D microstructure combinedwith surface roughnessmodification on normal human osteoblast maturation. Normal human osteoblastswere platedand harvested at confluence on TCPS. (a) Cell number, (b) ALP specific activity, (c) OCN, (d) OPG, and (e) VEGF levels were measured. Data represented are the mean ± SE of six independent samples. * refers to a statistically-significant *p* value below 0.05 vs. PT; ^ refers to a statistically-significant *p* value below 0.05 vs. acid PT.

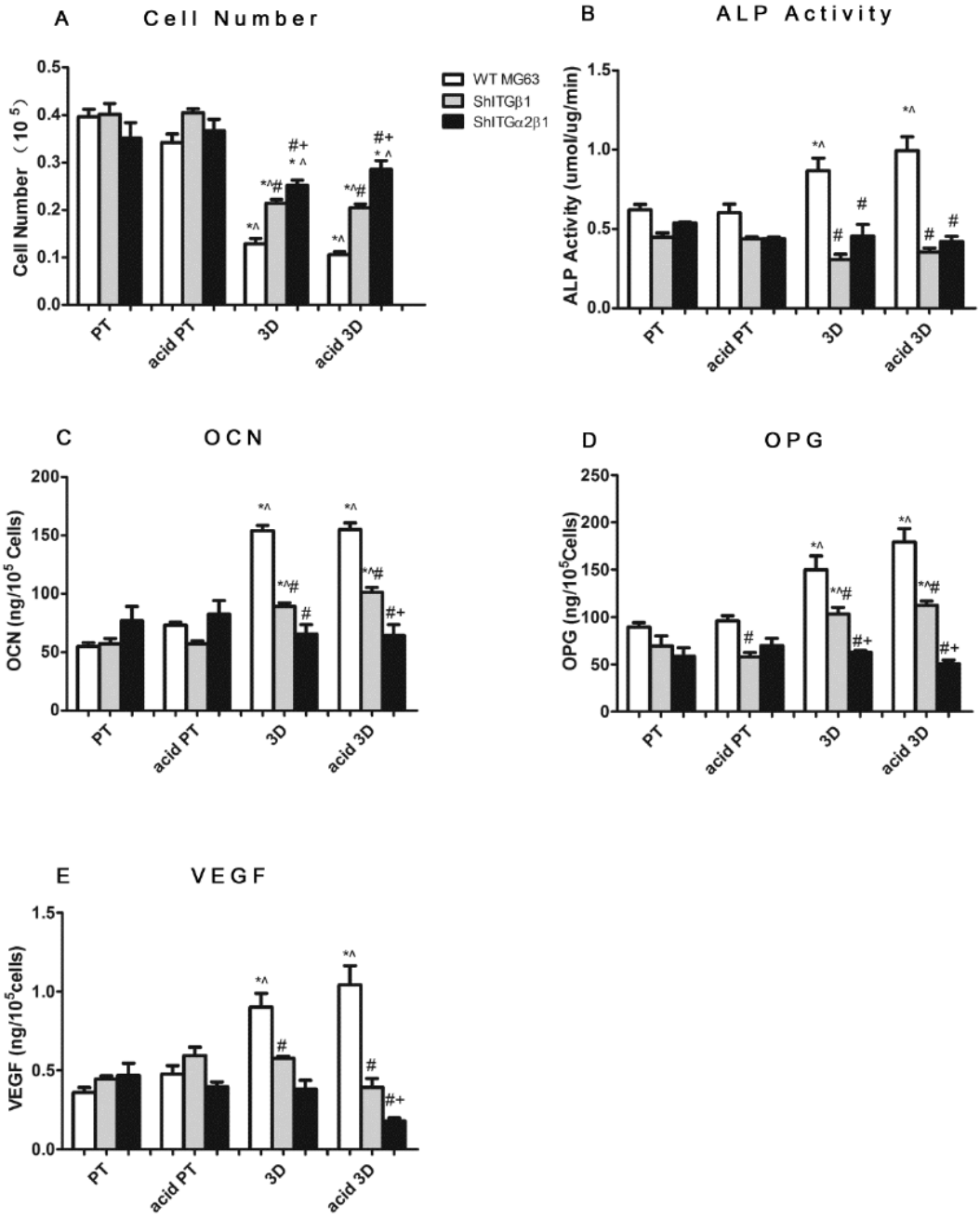

Figure 4-5. Role of integrin β1 and α2 on osteoblast maturation on 3D scaffolds. MG63 cells were plated and harvested at confluence on TCPS. (a) Cell number, (b) ALP specific activity, (c) OCN, (d) OPG, and (e) VEGF levels were measured. Data represented are the mean ± SE of six independent samples. * refers to a statistically-significant *p* value below 0.05 vs. PT among the same cell type; ^ refers to a statistically-significant *p* value below 0.05 vs. acid PT among the same cell type; # refers to a statistically-significant *p* value below 0.05 vs. WT MG63; + refers to a statistically-significant *p* value below 0.05 vs. shITGβ1 MG63

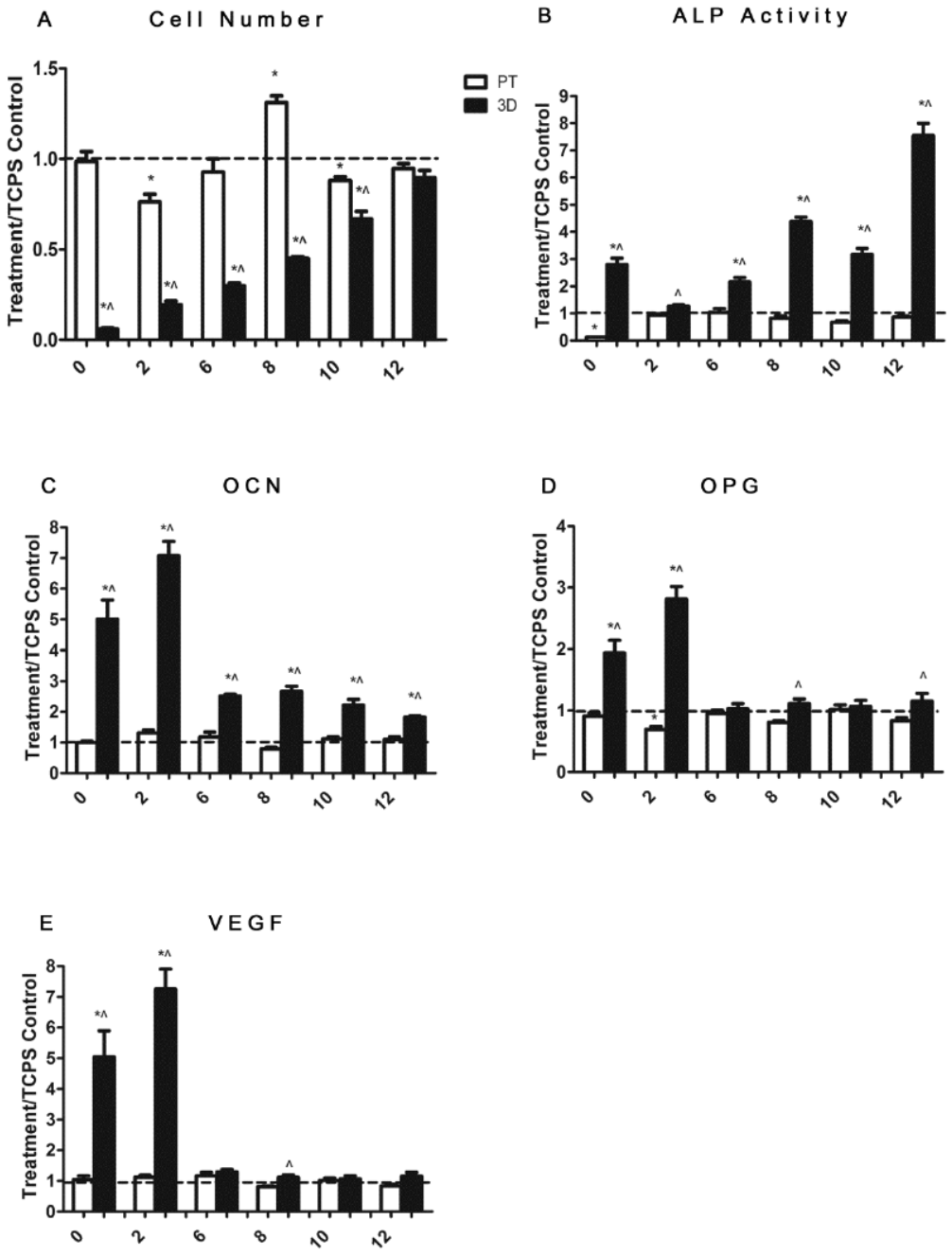

Figure 4-6. . Effects of structural properties of 3D scaffoldsonMG63 cells during culture time. MG63were platedand theday when cellsgetconfluence on TCPSis marked as 0. (a) Cell number, (b) ALP specific activity, (c) OCN, (d) OPG, and (e) VEGF levels were measured. Data represented are the mean ± SE of six independent samples. * refers to a statistically-significant *p* value below 0.05 vs. TCPS base line; ^ refers to a statistically-significant *p* value below 0.05 vs. PT at the same time point.

4.4. Discussion

In the present study, a simple 3D scaffold model with interconnected porous structure with or without surface roughness modification was developed to evaluate the proliferation and maturation of osteoblast-like MG63 cells and human osteoblasts. The role of integrin α2 and β1 during the maturation process was also determined. As expected, SEM images and confocal laser microscopy measurements confirm the roughness increased by 200nm (Sa) after acid etching. XPS analysis showed that the major elements of titanium discs and scaffolds were Ti, O and C. Trace calcium was detected on the non-etched 3D scaffolds might be due to the manufacture process of titanium meshes and the calcium was removed by acid etching confirmed the trace calcium was only on the very surface of the scaffold. Carbon contamination was increased by acid etching in this study. These findings are consistent with previous studies and can be explained by the fact that acid etching increases surface oxidation and roughness, which results in more carbon trapping [35].

The initial osteoblast growth on 3D scaffolds compared to PT surfaces was measured by cell number of MG63 and normal human osteoblasts. Since it is hard to directly observe cells on Ti discs and scaffolds, we use TCPS as observing control, and cells were normally harvested at confluence on TCPS. [8, 32, 34] At confluence on TCPS (about 5~6 days), there were much fewer cells on the scaffolds than on the surfaces. This could be attributed to the interconnected porous structures of the 3D scaffolds, which may let the cells penetrate through the pores without attaching to the wire surfaces. When the initial attaching density is low, there are also a low number of cell-cell contacts to form colonies. This could result in low proliferation rate [36]. Although cell counts were smaller on 3D scaffolds, the maturation of MG63 and human osteoblasts were promoted. This finding is consistent with the previous theory that the proliferation and differentiation are negatively correlated. [8, 37, 38] The surface roughness effects were not as significant as the 3D structural effects. Previous studies

showed titanium discs with micro-rough surfaces can enhance osteoblast maturation and osseointegration [32, 39]. Normally, the rough surfaces were made by sand blasting and HF etching [40], with 1~2μm average roughness increase compared to the smooth surfaces. In this study, the acid etching process increased surface roughness by only 200nm, which is moderate in comparison to the rough Ti surfaces in previous study. The cell responses showed that a 200nm increase of roughness could not make a significant increase in OCN, OPG and VEGF production. However, we can still observe significantly higher ALP activities. The greatest amount of local growth factor appeared in the acid 3D group too. This fact indicates that micro-roughness in 3D environment has an additive effect on osteoblast maturation.

Previously, we have shown that α2 and β1 are required for osteoblast differentiation on titanium surfaces with micro-roughness [29, 30]. In addition, the role of the different heterodimer α5β1 and α2β1 in the osteoblast maturation process was also studied in our group, and we found that the α2β1 heterodimer, which is the collagen binding receptor, plays a critical role in osteoblast maturation on rough titanium surfaces. In the present study we confirmed the role of integrins in osteoblast response to 3D scaffolds. Both of the differentiation markers ALP activities and OCN, as well as the local growth factor OPG and VEGF, descended in both of the integrin silencing groups. Moreover, the structural effects of the 3D scaffolds, which induce an enhancement of osteoblast maturation, were partially blocked by β1 silencing and totally blocked by α2β1-silencing. The results showed that without the α2β1 heterodimer signaling, MG63 cells exhibited more proliferation phenotype than differentiation. This is the first time we find integrin α2β1 also plays an important role in the osteoblast maturation on 3D titanium scaffolds.

In this study we have found that initial proliferation on 3D scaffolds was low, which can be caused by fewer attachments when the cells were seeded. To further determine cell

proliferation on 3D scaffolds, we did the time course study by culturing the cells on PT and 3D scaffolds until 12 days after confluence on TCPS. The cell number showed that although low proliferation was found on 3D scaffolds in the early stage of culture (confluence on TCPS), cells continued proliferating for the next 12 days. In contract, on PT surfaces the cell number peaked 8 days post confluence and a significant decrease occurred after, which is consistent with previous research showing a decrease of DNA content in osteoblasts cultured on TCPS and polished Ti surface after 9 days of culture [25]. These results indicate that 3D structures, which have higher surface area, can support cell proliferation in long term cultures. The osteoblast differentiation markers ALP activities and OCN had higher levels on 3D scaffolds than those on PT through the entire culture time. Osteocalcin which is the late osteoblast differentiation marker, had 5-7 fold higher level on 3D scaffolds in the early stage of culture then went back to 2-3 folds in the later stage, revealing that the osteoblast maturation is much faster on 3D scaffolds and the enhancement effects of 3D structures could last for a considerable period of time. Similar effects of 3D structures on MG63 cell response were also found in OPG and VEGF. ALP activities level fluctuated on 3D scaffolds can be attributed to the biphasic nature of ALP, which has been shown before to increase in early stage of osteoblast differentiation followed by a decrease when some mature osteoblasts start producing osteocalcin [41], and with the proliferation continued on 3D scaffolds, ALP activities went up and down alternately. At 12 day post-confluence, ALP activity was still significantly higher on 3D scaffolds than that on PT, indicating further differentiation potential. Taken together of these results, 3D porous scaffolds provide osteoblasts a more robust environment to commence differentiation in early stage of culture and to continue support differentiation in long time course.

4.5 Conclusion

In this study, we have evaluated the effect of porous 3D Ti scaffolds on osteoblast maturation and the critical role of integrin β1 and α2β1 in the maturation process. MG63 osteoblast-like cells and human osteoblasts were sensitive to the 3D structure, and the 3D structures enhanced osteoblast maturation, as all 3D groups had lower cell numbers and higher levels of differentiation markers compared to PT Ti discs. Moreover, cell number, differentiation and local factor production were also regulated by surface roughness, as the acid etched 3D scaffolds had the lowest cell number and highest ALP activity. The silencing of integrin β1 partially abolished and α2β1 completely abolished the structural effects of 3D structures and surface roughness, indicating that integrin β1 subunit and α2β1 heterodimer play a critical role during the maturation of MG63 cells. The time course study showed the fact that osteoblasts on 3D scaffold maturate faster than those on surfaces, as higher osteocalcin and local growth factors production started in the early stage of culturing time. The osteocalcin showed 5 to 7 folds higher than control in the earlier time point then went back to 2 to 3 folds. ALP activities went up and down alternately and 12 day post-confluence, ALP activity was still significantly higher on 3D scaffolds than that on PT, indicating further differentiation potential. Overall, our study shows that 3D scaffolds can be used as promising designs of bone implants and bone regeneration scaffolds for clinical and tissue engineering applications.

4.6 References

1. Vanzillotta, P.S., M.S. Sader, I.N. Bastos, and G.D. Soares, *Improvement of in vitro titanium bioactivity by three different surface treatments.* Dental Materials, 2006. **22**(3): p. 275-282.
2. Vannoort, R., *Titanium - the Implant Material of Today.* Journal of Materials Science, 1987. **22**(11): p. 3801-3811.
3. Kokubo, T. and S. Yamaguchi, *Bioactive Ti Metal and its Alloys Prepared by Chemical Treatments: State-of-the-Art and Future Trends.* Advanced Engineering Materials, 2010. **12**(11): p. B579-B591.
4. Legeros, R.Z. and R.G. Craig, *Strategies to Affect Bone Remodeling - Osteointegration.* Journal of Bone and Mineral Research, 1993. **8**: p. S583-S596.
5. Liu, X.Y., P.K. Chu, and C.X. Ding, *Surface modification of titanium, titanium alloys, and related materials for biomedical applications.* Materials Science & Engineering R-Reports, 2004. **47**(3-4): p. 49-121.
6. Zhao, G., Z. Schwartz, M. Wieland, F. Rupp, J. Geis-Gerstorfer, D.L. Cochran, and B.D. Boyan, *High surface energy enhances cell response to titanium substrate microstructure.* Journal of Biomedical Materials Research Part A, 2005. **74A**(1): p. 49-58.
7. He, P., J.C. Feng, B.G. Zhang, and Y.Y. Qian, *Microstructure and strength of diffusion-bonded joints of TiAl base alloy to steel.* Materials Characterization, 2002. **48**(5): p. 401-406.
8. Gittens, R.A., T. McLachlan, R. Olivares-Navarrete, Y. Cai, S. Berner, R. Tannenbaum, Z. Schwartz, K.H. Sandhage, and B.D. Boyan, *The effects of combined micron-/submicron-scale surface roughness and nanoscale features on cell proliferation and differentiation.* Biomaterials, 2011. **32**(13): p. 3395-3403.
9. Annunziata, M., A. Oliva, A. Buosciolo, M. Giordano, A. Guida, and L. Guida, *Bone marrow mesenchymal stem cell response to nano-structured oxidized and turned titanium surfaces.* Clinical Oral Implants Research, 2012. **23**(6): p. 733-740.
10. Balla, V.K., S. Bodhak, S. Bose, and A. Bandyopadhyay, *Porous tantalum structures for bone implants: Fabrication, mechanical and in vitro biological properties.* Acta Biomaterialia, 2010. **6**(8): p. 3349-3359.
11. Seitz, F., *On the Porosity Observed in the Kirkendall Effect.* Acta Metallurgica, 1953. **1**(3): p. 355-369.
12. He, Y., Y. Jiang, N.P. Xu, J. Zou, B.Y. Huang, C.T. Liu, and P.K. Liaw, *Fabrication of Ti-Al micro/nanometer-sized porous alloys through the Kirkendall effect.* Advanced Materials, 2007. **19**(16): p. 2102-+.
13. Spector, M., *Characteristics of Tissue-Growth into Proplast and Porous Polyethylene Implants in Bone - Reply.* Journal of Biomedical Materials Research, 1979. **13**(6): p. 991-992.
14. Stevens, B., Y.Z. Yang, A. MohandaS, B. Stucker, and K.T. Nguyen, *A review of materials, fabrication to enhance bone regeneration in methods, and strategies used engineered bone tissues.* Journal of Biomedical Materials Research Part B-Applied Biomaterials, 2008. **85B**(2): p. 573-582.
15. Fu, Q., E. Saiz, M.N. Rahaman, and A.P. Tomsia, *Bioactive glass scaffolds for bone tissue engineering: state of the art and future perspectives.* Materials Science & Engineering C-Materials for Biological Applications, 2011. **31**(7): p. 1245-1256.
16. Okumura, T., Y. Gonda, K. Ioku, M. Kamitakahara, T. Okuda, I. Yonezawa, H. Kurosawa, I. Asahina, and T. Ikeda, *Behavior of beta-tricalcium phosphate granules*

composed of rod-shaped particles in the rat tibia. Journal of the Ceramic Society of Japan, 2011. **119**(1386): p. 101-104.
17. Galante, J. and W. Rostoker, *Fiber metal composites in the fixation of skeletal prosthesis.* Journal of Biomedical Materials Research, 1973. **7**(3): p. 43-61.
18. Li, C., W. Qi, and K. Muneharu, *Improved high temperature tensile properties of Ti-6Al-4V alloy by plasma sprayed coating.* Advanced Welding and Micro Joining / Packaging for the 21st Century, 2008. **580-582**: p. 547-550.
19. Espana, F.A., V.K. Balla, S. Bose, and A. Bandyopadhyay, *Design and fabrication of CoCrMo alloy based novel structures for load bearing implants using laser engineered net shaping.* Materials Science & Engineering C-Materials for Biological Applications, 2010. **30**(1): p. 50-57.
20. Fukuda, A., M. Takemoto, T. Saito, S. Fujibayashi, M. Neo, D.K. Pattanayak, T. Matsushita, K. Sasaki, N. Nishida, T. Kokubo, and T. Nakamura, *Osteoinduction of porous Ti implants with a channel structure fabricated by selective laser melting.* Acta Biomaterialia, 2011. **7**(5): p. 2327-2336.
21. Cook, S.D., K.A. Thomas, J.E. Dalton, T.K. Volkman, T.S. Whitecloud, and J.F. Kay, *Hydroxylapatite Coating of Porous Implants Improves Bone Ingrowth and Interface Attachment Strength.* Journal of Biomedical Materials Research, 1992. **26**(8): p. 989-1001.
22. Chaudhari, A., A. Braem, J. Vleugels, J.A. Martens, I. Naert, M.V. Cardoso, and J. Duyck, *Bone Tissue Response to Porous and Functionalized Titanium and Silica Based Coatings.* PLoS ONE, 2011. **6**(9): p. e24186.
23. Fujibayashi, S., M. Takemoto, M. Neo, T. Matsushita, T. Kokubo, K. Doi, T. Ito, A. Shimizu, and T. Nakamura, *A novel synthetic material for spinal fusion: a prospective clinical trial of porous bioactive titanium metal for lumbar interbody fusion.* European Spine Journal, 2011. **20**(9): p. 1486-1495.
24. Bobyn, J.D., G.J. Stackpool, S.A. Hacking, M. Tanzer, and J.J. Krygier, *Characteristics of bone ingrowth and interface mechanics of a new porous tantalum biomaterial.* Journal of Bone & Joint Surgery, British Volume, 1999. **81-B**(5): p. 907-914.
25. St-Pierre, J.P., M. Gauthier, L.P. Lefebvre, and M. Tabrizian, *Three-dimensional growth of differentiating MC3T3-E1 pre-osteoblasts on porous titanium scaffolds.* Biomaterials, 2005. **26**(35): p. 7319-7328.
26. Gronthos, S., K. Stewart, S.E. Graves, S. Hay, and P.J. Simmons, *Integrin expression and function on human osteoblast-like cells.* Journal of Bone and Mineral Research, 1997. **12**(8): p. 1189-1197.
27. Boyan, B.D., C.H. Lohmann, D.D. Dean, V.L. Sylvia, D.L. Cochran, and Z. Schwartz, *Mechanisms involved in osteoblast response to implant surface morphology.* Annual Review of Materials Research, 2001. **31**: p. 357-371.
28. Garcia, A.J., M.D. Vega, and D. Boettiger, *Modulation of cell proliferation and differentiation through substrate-dependent changes in fibronectin conformation.* Molecular Biology of the Cell, 1999. **10**(3): p. 785-798.
29. Wang, L.P., G. Zhao, R. Olivares-Navarrete, B.F. Bell, M. Wieland, D.L. Cochran, Z. Schwartz, and B.D. Boyan, *Integrin beta(1) silencing in osteoblasts alters substrate-dependent responses to 1,25-dihydroxy vitamin D-3.* Biomaterials, 2006. **27**(20): p. 3716-3725.
30. Olivares-Navarrete, R., P. Raz, G. Zhao, J. Chen, M. Wieland, D.L. Cochran, R.A. Chaudhri, A. Ornoy, B.D. Boyan, and Z. Schwartz, *Integrin alpha 2 beta 1 plays a critical role in osteoblast response to micron-scale surface structure and surface*

energy of titanium substrates. Proceedings of the National Academy of Sciences of the United States of America, 2008. **105**(41): p. 15767-15772.
31. Park, J.H., R. Olivares-Navarrete, R.E. Baier, A.E. Meyer, R. Tannenbaum, B.D. Boyan, and Z. Schwartz, *Effect of cleaning and sterilization on titanium implant surface properties and cellular response.* Acta Biomaterialia, 2012. **8**(5): p. 1966-1975.
32. Boyan, B.D., R. Batzer, K. Kieswetter, Y. Liu, D.L. Cochran, S. Szmuckler-Moncler, D.D. Dean, and Z. Schwartz, *Titanium surface roughness alters responsiveness of MG63 osteoblast-like cells to 1 alpha,25-(OH)(2)D-3.* Journal of Biomedical Materials Research, 1998. **39**(1): p. 77-85.
33. Schwartz, Z., P. Raz, G. Zhao, Y. Barak, M. Tauber, H. Yao, and B.D. Boyan, *Effect of Micrometer-Scale Roughness of the Surface of Ti6Al4V Pedicle Screws in Vitro and in Vivo.* Journal of Bone and Joint Surgery-American Volume, 2008. **90A**(11): p. 2485-2498.
34. Wang, X.K., R.A. Gittens, R. Song, R. Tannenbaum, R. Olivares-Navarrete, Z. Schwartz, H.F. Chen, and B.D. Boyan, *Effects of structural properties of electrospun TiO2 nanofiber meshes on their osteogenic potential.* Acta Biomaterialia, 2012. **8**(2): p. 878-885.
35. Le Guehennec, L., M.A. Lopez-Heredia, B. Enkel, P. Weiss, Y. Amouriq, and P. Layrolle, *Osteoblastic cell behaviour on different titanium implant surfaces.* Acta Biomaterialia, 2008. **4**(3): p. 535-543.
36. Heng, B.C., P.P. Bezerra, P.R. Preiser, S.K.A. Law, Y. Xia, F. Boey, and S.S. Venkatraman, *Effect of cell-seeding density on the proliferation and gene expression profile of human umbilical vein endothelial cells within ex vivo culture.* Cytotherapy, 2011. **13**(5): p. 606-617.
37. Lohmann, C.H., Z. Schwartz, Y. Liu, H. Guerkov, D.D. Dean, B. Simon, and B.D. Boyan, *Pulsed electromagnetic field stimulation of MG63 osteoblast-like cells affects differentiation and local factor production.* Journal of Orthopaedic Research, 2000. **18**(4): p. 637-646.
38. Lan, M.A., C.A. Gersbach, K.E. Michael, B.G. Keselowsky, and A.J. Garcia, *Myoblast proliferation and differentiation on fibronectin-coated self assembled monolayers presenting different surface chemistries.* Biomaterials, 2005. **26**(22): p. 4523-4531.
39. Hakki, S.S., S.B. Bozkurt, E.E. Hakki, P. Korkusuz, N. Purali, N. Koc, M. Timucin, A. Ozturk, and F. Korkusuz, *Osteogenic differentiation of MC3T3-E1 cells on different titanium surfaces.* Biomedical Materials, 2012. **7**(4).
40. Sahafi, A., A. Peutzfeldt, E. Asmussen, and K. Gotfredsen, *Bond strength of resin cement to dentin and to surface-treated posts of titanium alloy, glass fiber, and zirconia.* Journal of Adhesive Dentistry, 2003. **5**(2): p. 153-162.
41. Lian, J.B. and G.S. Stein, *Concepts of Osteoblast Growth and Differentiation - Basis for Modulation of Bone Cell-Development and Tissue Formation.* Critical Reviews in Oral Biology & Medicine, 1992. **3**(3): p. 269-305.

Chapter 5. Summary

5.1 Fabrication of Hydroxyapatite Nanoparticles and Functional Peptide Modified Polycaprolactone Electrospun Meshes and Thermal Polymerized Alginate Hydrogels

Biodegradable polymers are considered to be an ideal choice for tissue engineering scaffolds. For bone repair and regeneration specifically, PCL has been widely used because of its slow degradability, good biocompatibility, and superior rheological and viscoelastic properties. The design and preparation of nanoscale fine structures have attracted great attention because of their potential unique properties and applications. In this study, electrospinning technique was used to fabricate nano to micro scale PCL fibers. Fiber diameter was adjusted by the solution concentration and solvent polarity and the mesh morphology was altered by different collectors. To further enhance the biocompatibility, hydroxyapatite nanocrystals were used as the filler, and the functional peptides were conjugated to the PCL surface to promote the cell affinity. Besides PCL electrospun fibers, alginate was modified with glycidyl methacrylate (GMA) to produce an alginate-GMA (AA-GMA) macromonomer, which polymerized at physiological temperature when using APS as an initiator and TEMED as a catalyst. AA-GMA hydrogels exhibited a three-dimensional porous structure with an average pore size ranging from 50-150μm, and the pore size increased with deceasing macromonomer gel content. Muscle injection *in vivo* showed the AA-GMA solution mixed with initiator could form a hydrogel *in situ* and exhibited a mild inflammatory response. Human endothelial cells (HUVECs) were encapsulated in the AA-GMA hydrogels *in situ* at body temperature. Cell viability remained good at low and high macromonomer concentrations and cells proliferated well in the hydrogels.

5.2 Fabrication of Electrospun titania-based nanofiber meshes and evaluations of the morphology and osteogenic potential

Ceramic scaffolds have been considered as bone graft substitutes for bone regeneration applications because of their excellent biocompatibility and bioactive properties. It is also

well known that titanium is widely used for implant applications because of its good mechanical properties and biocompatible oxide layer, titania. Similar to titania, silica-containing bioglass products can have beneficial osteoconductive functions. In the first study, we have evaluated the effect of silica content on the crystal phase and fiber diameter of silica-titania nanofiber meshes and the resulting osteoinductive effects of the meshes on MSCs. The surface roughness, fiber diameter, and crystal phase of the meshes could be varied by only changing the ratio of sol composition. All silica-titania mesh groups supported MSC viability, as the cells grew throughout the entire surface. The silica-titania fibrous meshes enhanced the MSC osteogenic differentiation, as all experimental groups had higher levels of osteogenic differentiation markers when compared to the glass control. These results indicate that cell response is sensitive to silica-titania substrates. In the second study, we eliminated the effect of different chemistry and crystal type, and only focused on the micro-scale and nano-scale surface roughness. We have evaluated the effect of porous and nano-fibrous TiO_2 meshes on the proliferation, differentiation, and local factor production of osteoblasts. The surface roughness and fiber diameter of the meshes could be varied without affecting their chemistry or crystal structure, emphasizing the effect of the structural parameters on cell response. The different TiO_2 mesh groups supported osteoblast viability. Although cell morphology was similar on all TiO_2 mesh groups, cell response was sensitive to the substrate. Osteoblast proliferation was controlled by surface micro-roughness, whereas differentiation and local factor production were affected by both surface micro-scale pattern and nano-fiber diameter, indicating that osteoblasts are sensitive to both the micro-roughness and the nano-topography created by the TiO_2 nano-fibers. Finally, the combination of micro-roughness with the nano-topography created by the larger nano-fibers enhanced osteoblast differentiation and local factor production, indicating that there might be a lower-limit threshold in the size of the nano-fibers that could be sensed by the osteoblasts to differentiate and generate an osteogenic

environment. In conclusion, inorganic scaffold structural cues can be used to drive cell differentiation and create an osteogenic environment without the use of exogenous factors and, thus, structural parameters should be carefully considered when designing a scaffold for tissue engineering applications.

5.3 Three-dimensional titanium scaffolds promote osteoblast maturation and integrin α2β1 mediated mechanism

Titanium and its alloys are the most commonly used materials for implants in dental and orthopedic applications because of their mechanical properties and good biological performance. To enhance the osseointegration, implants with rough surfaces have become the current standard. Compared to rough surfaces, 3D porous scaffolds allow for bone to grow into the component providing enhanced fixation and produces a system which enables stresses to be transferred from the implant to the bone. In this study, we have evaluated the effect of porous 3D Ti scaffolds on osteoblast maturation and the critical role of integrin β1 and α2β1 in the maturation process. MG63 osteoblast-like cells and human osteoblasts were sensitive to the 3D structure, and the 3D structures enhanced osteoblast maturation, as all 3D groups had lower cell numbers and higher levels of differentiation markers compared to PT Ti discs. Moreover, cell number, differentiation and local factor production were also regulated by surface roughness, as the acid etched 3D scaffolds had the lowest cell number and highest ALP activity. The silencing of integrin β1 partially abolished and α2β1 completely abolished the structural effects of 3D structures and surface roughness, indicating that integrin β1 subunit and α2β1 heterodimer play a critical role during the maturation of MG63 cells. The time course study showed the fact that osteoblasts on 3D scaffold maturate faster than those on surfaces, as higher osteocalcin and local growth factors production started in the early stage of culturing time. The osteocalcin showed 5 to 7 folds higher than control in the earlier time point then went back to 2 to 3 folds. ALP activities went up and

down alternately and 12 day post-confluence, ALP activity was still significantly higher on 3D scaffolds than that on PT, indicating further differentiation potential.

5.4 Conclusion

In this dissertation, we first focused on the polymer materials to construct scaffolds for tissue engineering, including electrospun fibrous scaffolds and thermal-crosslinked hydrogel. The electrospun fiber morphology was adjusted by altering the concentration, solvent and collector patterns, and the biocompatibility was further enhanced by bioactive ceramic additive and functional peptide conjugation. The importance of these modifications was shown by cell and animal studies. Thermal crosslinked alginate hydrogel was synthesized by adding methacrylic group. The biocompatibility of the hydrogel was evaluated by HUVEC cell encapsulation.

Second, we moved on to study pure ceramic scaffolds, titania-silica binary materials and pure titania respectively. Both of the materials supported cell growth and osteoblast differentiation. For the titania-silica binary materials, the increase of titania content increased crystallization degree and both the chemistry change and different crystallization seemed to affect MSC differentiation toward osteoblast, as titania-silia7-3 group had highest level of differentiation markers compared to control. In the second study we focused on the structural cue by using pure titania material to fabricate four different meshes with different micro and nano surface roughness. We found fibrous meshes with higher micro roughness and relatively higher nanofiber diameter had the most promising results, indicating micro roughness and nano fiber diameter synergistically affect osteoblast maturation.

Third, in clinical application, especially load-bearing application, metallic materials are the most widely used materials. We designed a novel titanium 3D porous scaffold with surface roughness modification on the titanium wires, to study the osteogenic effect of this type of scaffold. We found a significant increase of the osteogenic markers on 3D scaffolds

compared to the 2D surfaces, and the surface modification had an additive effect on ALP activity. The mechanism which drives cells to see the structural difference was evaluated by integrin silencing. The silencing of integrin β1 partially abolished and α2β1 completely abolished the structural effects of 3D structures and surface roughness, indicating that integrin β1 subunit and α2β1 heterodimer play a critical role during the maturation of MG63 cells.

In summary, we've fabricated different type of tissue engineering scaffolds and carefully evaluate the parameters of these scaffolds which affect cell response. Overall, our study shows that 3D scaffolds can be used as promising designs of bone implants and bone regeneration scaffolds for clinical and tissue engineering applications.

List of Publication

Peer Reviewed Articles:

1. **Wang X.**, Zhu J., Yin L., Liu S., Zhang X., Ao Y., Chen H., Fabrication of electrospun titania-silica nanofiers with different silica content and evaluation of the morphology and osteoinductive properties. Journal of Biomedical Materials Research, Part A, Jul 2012. Doi: 10.1002/jbm.a.34293
2. **Wang X**., Zhu J., Yin L., Liu S., Zhang X., Ao Y., Chen H., Evaluation of the morphology and osteogenic potential of titania-based electrospun nanofibers. Journal of Nanomaterials, 2012. Doi: 10.1155/2012/959578
3. **Wang X**., Gittens R.A., Song R., Tannenbaum R., Olivares-Navarrete R., Schwartz Z., Chen H., Boyan B.D. Effects of structural properties of electrospun TiO_2 nanofiber meshes on their osteogenic potential. Acta Biomaterialia. 2012, 8,2:878-885
4. Shao, Z., X. Zhang, Y. Pi Y., **Wang X.,** Jia Z., Zhu J., Dai L., Chen W., Yin L., Chen H., Zhou C., Ao Y., Polycaprolactone electrospun mesh conjugated with an MSC affinity peptide for MSC homing in vivo. Biomaterials, 2012. 33, 12: 3375-3387.
5. **Wang, X**., Xia C., Zhang Z., Deng Xu., Wei S., Zheng G., Chen H. Direct Growth of Human Enamel-Like Calcium Phosphate Microstructures on Human Tooth. Journal of Nanoscience and Nanotechnology, 2009. 9, 2: 1361-1364(4)

In progress:

Wang X., Gittens R.A., Olivares-Navarrete R., Schwartz Z., Chen H., Boyan B.D., Three-dimensional titanium scaffolds promote osteoblast maturation and integrin α2β1 mediated mechanism, in preparation.

Wang X., Hao T., Qu J., Wang C., Chen H., Characterization of Thermal Polymerizable Alginate-GMA Hydrogel for *in situ* Cell Encapsulation, in preparation

Peer Reviewed Abstracts:

1. **Wang X**, Yun S, Fang J, Chen H: Fabrication of Microporous 3-D Scaffolds with Electrospun Nanofibers, The 2008 Asian Conference on Nanoscience and Nanotechnology (AsiaNANO2008), Singapore, 2008
2. Gittens R., **Wang X.**, Song R., Schwartz Z., Chen H., Boyan B., Fabrication of TiO2 nano-fiber meshes by electrospinning and evaluation of their osteoblast differentiation potential, Society of Biomaterials, 2010, Oral report
3. **Wang X.**, Gittens R., Song R., Tannenbau R., Olivares-Navarrete R., Schwartz Z., Chen H., Boyan B., Effectiveness of Structural Properties of Electrospun TiO_2 Nano-fiber Meshes on their Osteogenic Potential, 9th World Biomaterials Congress, Poster session
4. **Wang X.**, Gittens R., Schwartz Z., Chen H., Boyan B., Osteogenic Potential of 3-Dimensional Titanium Scaffold on Osteoblast Maturation, Biomedical Engineering Society, 2012, Oral report
5. **Wang X.**, Gittens R., Schwartz Z., Chen H., Boyan B., Three Dimensional Porous Titanium Scaffolds enhance osteoblast differentiation and local factor production, Orthopaedic Research Society, 2013, Poster session
6. **Wang X.**, Gittens R., Schwartz Z., Chen H., Boyan B., Three Dimensional Titanium Scaffold Promotes Human Osteoblast Maturation., International Association for Dental Research IADR Annual Meeting, Poster session

VITA

XIAOKUN WANG

XIAOKUN was born in Dalian, China. She attended high school in Dalian, Liaoning. Then went to Peking University for college, received a B.A. in Chemistry in 2007. She started her graduate school also in PKU in the Department of Biomedical Engineering before she came to Georgia Tech. In 2009, the joint PhD program started among Peking University, Georgia Tech and Emory University, and she was one of the first group of students enrolled in this program. In 2011, she came to Georgia Tech to complete the last part of her thesis. When she is not working on her research, Miss WANG enjoys watching movie and playing with her scientific cats Noggin and Gremlin.